THE EASTERN MASSACHUSETTS SEA BREEZE STUDY

by

Jennifer E. Thorp
B.S., Plymouth State University, 2007

THESIS

Submitted to Plymouth State University
in Partial Fulfillment of

the Requirements for the Degree of

Master of Science
in

Applied Meteorology

May, 2009

This thesis has been examined and approved.

_____

Thesis Director, Dr. Samuel T. K. Miller
Professor of Meteorology
Department of Atmospheric Science & Chemistry
Plymouth State University / Plymouth, NH

_____

Mr. Dan St. Jean
Science and Operations Officer
National Weather Service, Gray / Portland, ME

_____

Dr. Barry Keim
Louisiana State Climatologist
Department of Geography and Anthropology
Louisiana State University / Baton Rouge, LA

_____

Date

DEDICATION

This thesis is dedicated to my family, boyfriend, and friends who supported me through my college career and helped me pursue my dreams.

ACKNOWLEDGEMENTS

I would like to acknowledge the support of several individuals who helped me obtain archived data and gave me the technical know-how I needed to complete this study. A special thanks to Brendon Hoch (Plymouth State University), Dr. Samuel T. K. Miller (Plymouth State University), Scott Reynolds (CWSU Nashua, NH), and Plymouth State University graduate students and faculty. Without their time, knowledge, and patience, this project would not have been possible.

TABLE OF CONTENTS

LIST OF TABLES

LIST OF FIGURES

ABSTRACT

THE EASTERN MASSACHUSETTS SEA BREEZE STUDY

by

Jennifer E. Thorp

B.S., Plymouth State University, 2007

This study investigates many different aspects of the sea breeze at Logan Airport in Boston, Massachusetts (KBOS) and along the Massachusetts coastline. Part of the study adapts the method of predicting sea breeze events developed by Miller and Keim (2003) for Portsmouth, New Hampshire (KPSM) to KBOS. A nearly ten-year dataset of hourly KBOS surface observations (1998-2007) was used to identify 879 days when the sea breeze occurred or was likely to occur at the airport. These days were classified as sea breeze, marginal, or non-sea breeze events. Sea breeze events were further classified into fast and slow transitions, with a fast transition identified by a wind shift taking one hour or less to develop, and a slow transition identified by a wind shift taking two hours or more to develop. Marginal events were events that had a duration of 1 hour or less, no clear start or finish, or were interrupted by periods of "calm" or "light and variable" winds. Non-events were events in which the background conditions for a sea breeze to occur existed, but a sea breeze did not develop.

Times of onset and event durations for the sea breeze events (fast, slow, and marginal) were calculated and used to create seasonal statistics by event type. It was

found that seasonal variation did occur with both characteristics, but was more evident in the time of onset. Slow events occurred earliest in the day overall, while marginal events occurred a bit later, and fast events occurred the latest. Slow events had the longest duration overall, while marginal events, by definition, had the shortest duration. Seasonally, similar results were found for both characteristics with a few variations.

United States surface analyses for each event at the time of onset (or average time of onset, 1500 UTC, for non-events) were classified using the seven synoptic classes developed by Miller and Keim (2003), and statistics were developed to evaluate the distribution of synoptic classes amongst the different types of events and various seasons. Composite surface analyses of the different synoptic classes and types of events were then developed. There were significant differences between the composites of each event type within a synoptic class.

Wind vector plots, created from surface observations using Barnes analysis, were used to identify the position of the sea breeze front as the sea breeze airmass penetrated inland. The depth and shape of this front was examined by synoptic class. The prevailing synoptic scale flow was found to limit penetration in expected areas along the coastline.

Mesoscale calculations were used to determine the critical balance of the cross-shore temperature gradient (dT/dx) versus the cross-shore geostrophic wind component (u_G) at the surface necessary for the occurrence and non-occurrence of the sea breeze. It was found that by stratifying the events by synoptic classes, a smaller transition area (containing both sea breeze and non-sea breeze events) could be created. The method was taken further by adding a third variable, the 850 hPa geostrophic wind component. The

three dimensional plot showed a large transition area and future research may be able to reduce this area by breaking it down by synoptic class.

Finally, the effect of the sea breeze on convection was analyzed using radar reflectivity data from the Taunton, Massachusetts WSR-88D (KBOX) for 2002 through 2007 (562 events). Convection was present inland along the Massachusetts coastline for only 24 of the total 562 events (4%). This small occurrence results from a bias from the methodology used to develop the data set. However, when the sea breeze did occur convection developed or was affected by the sea breeze front.

CHAPTER 1

1. Introduction and Background

The sea breeze is a gravity current in which there is a landward flow of cool, moist marine air that develops when daytime heating results in a significant land-sea temperature difference (Miller *et al.*, 2003). Boston's General Edward Lawrence Logan International Airport is located on the shore of the Gulf of Maine, and is therefore significantly impacted by sea breezes. Unexpected changes in wind direction and speed can result in passenger delays, wasted fuel, and added expense. An effective method is needed to predict sea breeze events and behavior at Logan. Part of the goal for this study was to adapt the method of predicting sea breeze events developed by Miller and Keim (2003) to Logan Airport (KBOS). Many of the characteristics of the sea breeze at Boston were studied by Barbato (1978).

Barbato investigated the sea breeze circulation at Boston using a one-year dataset. Barbato found 40 sea breeze episodes in Boston during 1972. Explicit criteria were created to identify a sea breeze episode. The first criterion stated that there must be high pressure and anticyclonic flow in Boston. The second condition required that more than half the amount of possible sunshine for the day be received. The third and fourth criteria stipulated that the regional winds must be offshore prior to the event and that a sea breeze wind maximum must occur during the afternoon. The fifth criterion stated that a noticeable cooling in temperature at Logan Airport needed to be present just after the onset of the sea breeze. The final criterion asserted that the sea breeze must be ≥5 hrs in duration at Logan Airport.

In this study, standard synoptic data, upper air data, and Landsat-1 data were used to determine the various parameters of the Boston sea breeze. The upper air data came from the Massachusetts Institute of Technology (MIT) in Cambridge which deployed radiosondes twice a day between September 1971 and May 1973 at 1000 UTC and 1500 UTC. Onset was defined as the first time the wind was between 15° and 145° and the mean time of onset was 1500 UTC. The mean duration at Logan Airport was 8.1 hrs. The mean vertical depth of the sea breeze flow was 667 m with a range between 330 m and 1230 m.

Similar research was done by Miller and Keim (2003) and a one-year data-set for Portsmouth, New Hampshire for 2001 was utilized. The study defined three types of events: sea breeze event, marginal event, and non-sea breeze event. Sea breezes were defined as insolation-driven local onshore winds with marginal events representing weak sea breezes. Non-sea breeze events were those days when sufficient insolation was present but failed to produce a sea breeze at Portsmouth (Miller and Keim, 2003). Using the METARs from Portsmouth's Pease Air National Guard Base, 167 dates were identified as events. Surface analyses for each date were obtained and classified using a synoptic class system developed for the study. Using standard surface observations, a cross-shore geostrophic wind component (u_G) and a cross-shore potential temperature gradient ($\delta\theta/\delta x$) were calculated for the hour of onset. The study found that in the presence of stronger positive u_G value, a stronger negative value of $\delta\theta/\delta x$ was needed to develop a sea breeze.

An extensive look at the sea breeze was done by Miller *et* al. (2003) reviewing over 2500 years of sea breeze research. The study utilized a gridded wind vector analysis

for Portsmouth, NH using land and sea based observations to visualize the sea breeze flow. The observations were interpolated to the grid using a Barnes analysis scheme. The grouping of available data stations (particularly over land) allowed for a 10-km grid spacing. The rectangular grid was rotated 30° clockwise from north to make it shore parallel. The wind vectors created using this method were plotted allowing Miller *et al.* (2003) to analyze the location of the sea breeze front based on a shift in wind direction. The study looked at three case studies based on different synoptic scale surface flow regimes; northwesterly, southwesterly, and northeasterly. The focus of the case studies was to investigate the effect of the Coriolis force on the evolution of the sea breeze events.

McPherson (1970) also used gridded modeling to investigate the shape of inland penetration of the sea breeze front. This study sought to determine the effect of coastal irregularities on inland penetration. A three-dimensional model based off work done by Estoque (1961, 1962), was used to interpolate data to a 276 km by 56 km grid with a 4-km grid spacing integrated over an 18 hr time period. McPherson found that a bay located along an otherwise straight coastline caused the sea breeze front to bow landward compared to the straight portions of coastline to either side of the bay. This bowing creates a bulge in the sea breeze front that dampens out as the front progresses further inland.

The effect of grid spacing on the behavior of the sea breeze was studied by Colby. (2004) Colby used the Mesoscale Model (MM5) to simulate the sea breeze along the Massachusetts coastline and then compared the results to actual observations from 3 coastal weather stations and 3 inland weather stations. The results were also compared to

the NCEP Eta Model which uses a 22-km grid that is outputted onto a 40-km grid. Data from the Aviation Model (AVN) at 1200 UTC was used to set boundary and initial conditions for the MM5. The purpose of the study was to investigate the effect of using a nested grid to look at factors such as the time of onset, wind direction and speed, and the temperature and dew point. The nested grid was made up of three grids using a two-way interaction with the outer grid using a 36-km grid spacing, the middle grid using a 12-km grid spacing, and the innermost grid using a 4-km grid spacing. The model was run in 3 modes; the first mode used all three grids, the second used only the 36- and 12-km grids, and the third mode used just the 36-km grid. The model was used to simulate the sea breeze for 7 case studies. Colby found that the 4-km grid was both the best and the worst at forecasting the characteristics noted above at the given station locations. The 4-km grid performed the worst at forecasting the dew point in all 7 cases. The 36-km grid was able to develop the sea breeze but lacked detail. The 36-km and the Eta Model both were unable to resolve small scale rain showers that had actually developed while the 4-km grid produced these showers for one of the cases.

Another goal of the current study was to investigate the effect of the sea breeze on thunderstorms in Massachusetts. Little research exists concerning the sea breeze circulation's effect on convection in Massachusetts. Research has been done pertaining to this topic along coastal regions in warmer climate zones such as the Gulf of Mexico and India (Medlin and Croft, 1998, and Suresh, 2007).

Medlin and Croft (1998) used the WSR-88D radar data from Mobile, Alabama to investigate the interactions between large scale flow and the sea breeze circulation, as well as the effects of physiographic features such as elevation. The study found that

events that occurred in late spring and early summer had a stronger land-sea temperature differential which allowed for a deeper inland penetration, and therefore convection would occur farther inland. In late summer, the overall anticyclonic flow over the region is increased and the thermal gradient is reduced causing decreased inland penetration. The convective initiation occurs closer to the coastline where there is greater thermodynamic instability and more water vapor content in the lower troposphere. It was also found that Mobile Bay caused the sea breeze flow to diverge and move further inland. Most convective initiation occurred within 15 km of the coast. The initiation also occurred when thermodynamic instability and heating were at a maximum. Also, first cell development was either along a coastal boundary or near peaks in elevation (Medlin and Croft, 1998).

Research has also been done in Chennai, India using Doppler weather radar to determine many characteristics of the sea breeze. Radar data were used to identify the sea breeze front as well as the depth of the inland penetration of the sea breeze circulation, the speed of the propagation inland, the vertical depth of the sea breeze, and the occurrence of the convection along the front. The radar echoes appeared as a "thin line of enhanced reflectivity." This line is due to inhomogeneities in the refraction index. In regards to inland penetration, the study found that the most common depth was 10-20 km (34.6% of all cases) while distances less than 10 km came in second with 16% of all cases, and distances greater than 50 km came in a close third with 15.7% of all cases. Penetration depths of 20-30 km, 30-40 km, and 40-50 km, made up the remaining cases with fairly even distribution (Suresh, 2007).

An interesting characteristic of the sea breeze at Chennai was that sometimes the sea breeze would penetrate into the region north of the radar before the region to the south. Of the 248 days in the study, 57% of the time the sea breeze penetrated north first, 14% of the time the sea breeze penetrated south first, and the remaining 29% of the time the penetration was simultaneous on both sides of the radar. The reason for this behavior can be attributed to the land-use of these two regions. The area north of the radar is much more industrialized causing the necessary land-sea temperature differential to occur earlier. The southern region has more forests, vegetation, and parks. For Chennai, the study found that the depth of the sea breeze circulation ranged from less than 200 m to over 1000 m. The mean depth for the location varied between 490 and 765 m with the modal depth being between 400 and 600 m. This study found that the sea breeze moved inland at the slow pace of 4 km h^{-1} for the first 30 km and that between 30 to 80 km the speed increased to about 12-15 km h^{-1}. The speed of the sea breeze propagation is at its greatest at a height between 300 to 600 m (Suresh, 2007).

Figure 1.1: Map showing Chennai, India which is indicated by the purple circle.

Suresh (2007) also examined sea breeze-initiated convection. Overall, 37.1% of all cases showed no convection. Of the cases that did have convection, 7.3% had convection occurring within 50 km of the coastline, 31.4% had convection occurring between 50-100 km from the coast, and the remaining 24.2% noted convection at a distance greater than 100 km. (Suresh, 2007)

The initial goal of the current study was to develop a 9-year climatology of sea breeze occurrences at Logan International Airport (Fig. 1.2). The events were classified into four event type sub-categories and seven synoptic flow regimes. Statistics were generated in regards to the event type and the synoptic flow regime. As part of continuing research, more statistics were developed for the time of onset and the duration of the

event. The shape of the inland penetration of the sea breeze circulation was mapped using a vector analysis, similar to that of Miller *et al.* (2003). The mesoscale forcing for the events was examined using cross-shore temperature and geostrophic wind components. The study also includes an investigation into the effect of the sea breeze on convection in Massachusetts, by comparing cases where a sea breeze occurs to cases where a sea breeze does not occur.

It is hypothesized that behavior of the sea breeze (as revealed by the statistical results and vector analyses) will be similar to results of Miller and Keim (2003). The shape of the inland penetration is expected to vary with the different flow regimes; for example, with a southwesterly flow regime, the sea breeze should not penetrate as far inland along the coastline south of Boston as one associated with a northwesterly or northeasterly regime. As for convection, a significant connection between the sea breeze and thunderstorms is hypothesized. Results of other studies (Medlin and Croft, 1998 and Suresh, 2007) show that convection can be associated with the sea breeze in tropical and sub-tropical locations. Research has indicated this connection can occur at mid-latitudes, specifically in Maine (*See Appendix A*).

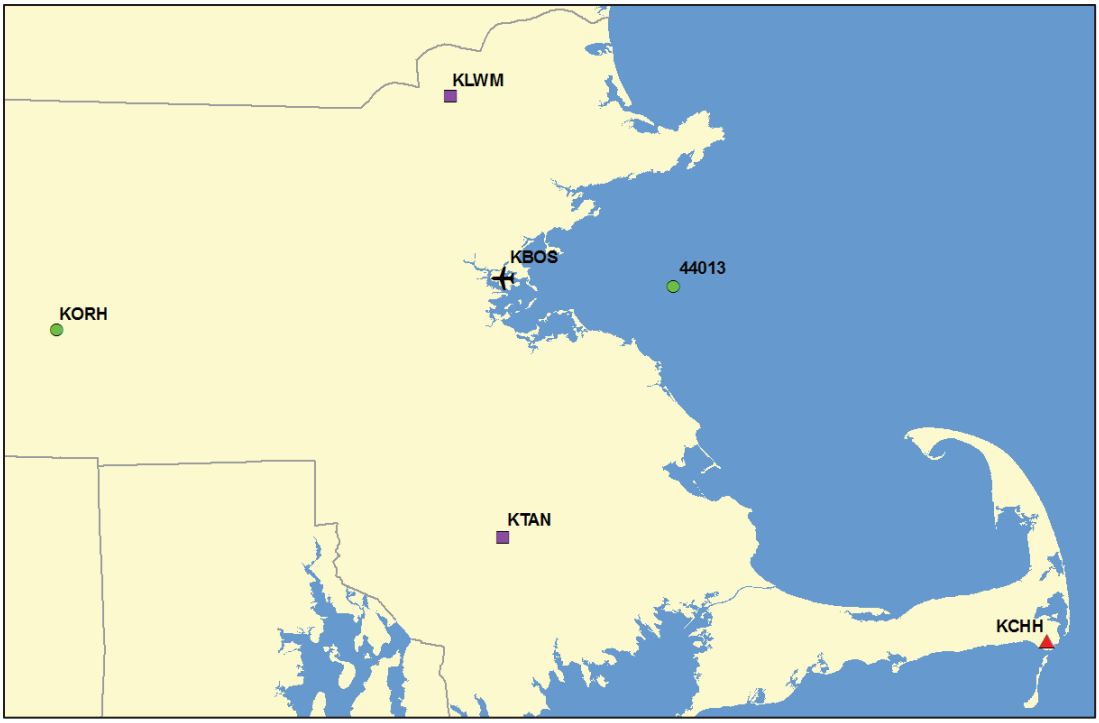

Figure 1.2: Map of Massachusetts showing the location of Logan Airport which is denoted by the airplane.

Results are separated into four chapters (chapters 3 through 6). The data and methodology for this study can be found in chapter two. Chapter three will focus on the results of the synoptic classes and inland penetration as a function of synoptic class. In chapter four, statistics for the time of onset and the duration of the event will be discussed. Chapter five contains results of the mesoscale calculations (cross-shore components). Finally, chapter six will include results of the convective analyses, and chapter seven will contain the summary and conclusions.

CHAPTER 2

2. Data and Methods

It was first necessary to define a sea breeze event at Logan International Airport. Using Miller and Keim (2003) as a reference, the following event types were defined for Logan:

1.) A *sea breeze event* occurs when the surface wind in the study area is from some westerly direction at the beginning of the day, then shifts to a direction between 10° and 190° midday, and then returns to some westerly direction at the end of the day. This wind shift must not be associated with a synoptic-pressure system. The cloud cover must remain less than "broken" (BKN). The exception to this rule is when the ceiling height is equal to or greater than 18,000 feet. It was decided that any cloud cover above 18,000 feet would be high cirrus clouds and not significantly diminish daytime heating. The final stipulation was that no precipitation could occur in the study area within six hours of the onset and the end of the event.

a.) A *fast transition* is when the wind shift to a direction between 10° and 190° occurs in an hour or less.

b.) A *slow transition* is when the wind shift to a direction between 10° and 190° occurs in two or more hours.

2.) A *non-sea breeze event* is an event in which the same conditions as a sea breeze event exist, except no wind shift is observed at Logan Airport.

3.) A *marginal event* is one in which a sea breeze event occurs but either is short lived (less than 2 hours), interrupted by periods of "calm" or "light and variable" winds, or has no clear start and/or finish.

These definitions were necessary to create a non-biased data set that could be used in this study. There were many days not included in this study where the sea breeze occurred and the cloud cover and/or precipitation criteria were not met.

After defining the different event types, a nearly ten-year data set (1998-2007) was obtained from the Plymouth State Weather Center (PSU Weather Center, 2008). METAR observations from KBOS were examined to identify dates when sea breeze events could occur based on the definitions noted above. The dates were then classified as fast, slow, marginal, or non-sea breeze events. There were 171 fast sea breeze events, 60 slow sea breeze events, 78 marginal events, and 570 non-sea breeze events for a total of 879 events over the nearly ten-year period (Tables 2.1 and 2.2).

Table 2.1: Summary of the data set used in this study by synoptic class.

Synoptic Class	*No. of cases*	*Percentage of total*
1	168	19.1
2	232	26.4
3	144	16.4
4	191	21.7
5	22	2.5
6	61	6.9
7	61	6.9
All	879	

Since this study was an expansion of previous research, the original 5-year dataset (2001-2005) was quality controlled (Thorp, 2007). An improvement was made to the time of onset for the slow sea breeze events. Originally, the time of onset was more

subjective and was chosen based on when it seemed like the wind was beginning to turn into the sea breeze. To make this study more objective, the time of onset was adjusted to be the time at which the wind direction was first within the 10° to 190° window.

Table 2.2: Summary of the data set used in this study by event type and synoptic class.

Synoptic Class	*Fast Transition SB*	*Slow Transition SB*	*Marginal Events*	*Non-sea breeze events*	*All Events*
1	42	14	26	86	168
2	36	11	8	177	232
3	4	2	6	132	144
4	53	7	23	108	191
5	0	0	0	22	22
6	13	21	11	16	61
7	23	5	4	29	61
All	171	60	78	570	879

a. Time of Onset and Event Duration

The hour of onset for each event was recorded during the initial parts of the study. This time is defined to be the first time that the wind direction was greater than 10° and less than 190°. The time of onset was used to create statistics by event type (fast, slow, and marginal only) and season. The seasons used were winter (December, January, February), spring (March, April, May), summer (June, July, August), and fall (September, October, November).

The duration of each event was the calculated difference between the time of onset and the end time of the event. The end time of the event was the first time the wind direction was greater than or equal to 190° and less than or equal to 10°. Hourly observations were used for this calculation. Event duration was stratified using the same method of statistics as the time of onset.

b. Synoptic Classification

The surface analysis for each date was obtained using the nearest analysis time prior to the time of onset (example, time of onset 1400 UTC, analysis time 1200 UTC). In the case of non-sea breeze events, the average time of the onset for sea breeze events was used, which is 1500 UTC. The surface analyses were obtained from the National Climatic Data Center's Service Records Retention System (NESDIS, 2008). The surface charts were then stratified into the synoptic classes defined by Miller and Keim (2003).

There were six synoptic classes and one miscellaneous class. Synoptic classes one, two, and three represent an overall northwesterly surface flow regime. Class one had anticyclonic flow, class two had neutral flow, and class three had cyclonic flow. Class four was anticyclonic southwesterly flow while class five was cyclonic southwesterly flow. Synoptic class six corresponded to northeasterly surface flow and synoptic class seven was the miscellaneous class (*Appendix B*).

Statistics were then generated for each event type and synoptic class to identify any trends and patterns. After creating statistics, the individual surface charts were used to create composite analyses for each event type and synoptic class (example, fast transition sea breeze synoptic class one). The composites were generated using the National Climatic Data Center's North American Regional Reanalysis composite website (ESRL PSD, 2008).

c. Inland Penetration

During the initial process of building the data set of events, information about the maximum sustained wind that occurred during the event was recorded including the time of occurrence, speed, and direction. The speed and direction were converted to u and v

components and the averages and standard deviations were calculated for the three major synoptic flow patterns. Northwesterly flow included synoptic classes one through three. Southwesterly only included synoptic class four since only non-events occurred with synoptic class five. The northeasterly flow was represented by synoptic class six.

The fast sea breeze events were used since they represent a stronger sea breeze flow. Dates were chosen at random based on the number of standard deviations from the mean. For one and two standard deviations, both the u and v component had to be within the same standard deviation. For three standard deviations, either the u or the v component needed to be within the third standard deviation. This was because there was never an occurrence of both components being three standard deviations from the mean.

Two dates were chosen from each standard deviation category resulting in six dates for each of synoptic class one, two, and four. Synoptic class three only included four dates which is the total number of events for that class. Of those four dates, one event was within two standard deviations while the remaining three were within one standard deviation. Since synoptic class six only had 14 events in total there was only one observation that fell within the three standard deviations range. A total of 27 events were used in this portion of the study.

To examine the depth of inland penetration, vector wind analyses were employed. These analyses were then created using a Barnes Analysis over a gridded area with the northwest corner at 43°N 71.75°W and a grid spacing of 5 km. The grid extends 180 km toward the east and 165 km toward the south from the northwest point (*See Appendix C*). Data from 40 different weather stations (both nautical and land based) were used to create these analysis (*See Appendix C*). The vector wind analyses were created using the hourly

wind speed and directional data which were converted to u and v wind components. The location of the sea breeze front was used to measure how far inland the sea breeze flow was extending from the coastline. An average mid-event plot was created for each of the classes by averaging the mid-event u and v components (interpolated values) of the chosen dates for each synoptic class.

d. Mesoscale Calculations

Mesoscale calculations were made for the cross-shore *in situ* temperature gradient (dT/dx) and geostrophic wind component (u_G) for all event types to determine a relationship between these variables and the occurrence or non-occurrence of a sea breeze at Logan Airport (*See Appendix D*). Calculations were performed using observations recorded at four neighboring stations to estimate both parameters for Logan, at either the time of onset (for sea breeze and marginal events), or the mean time of onset (1500 UTC, for non-sea breeze events). The station north of Boston was Lawrence, Massachusetts (KLWM) and the southerly station was Taunton, Massachusetts (KTAN) (Fig 2.1). Worcester, Massachusetts (KORH) was used as the western site and buoy 44013 was used as the eastern site (Fig 2.1).

The cross shore components were used to create a two-dimensional plot with dT/dx on the y-axis and u_G on the x-axis. A three-dimensional plot was also developed using the u_G component of the wind at 850 hPa. Sounding data from Chatham, MA (KCHH) were interpolated to the hour of onset using a simple linear equation (*See Appendix C*). Marginal events were not included in the three-dimensional plot and fast and slow sea breezes were grouped together. The sea breeze events were plotted in comparison to the non-sea breeze events.

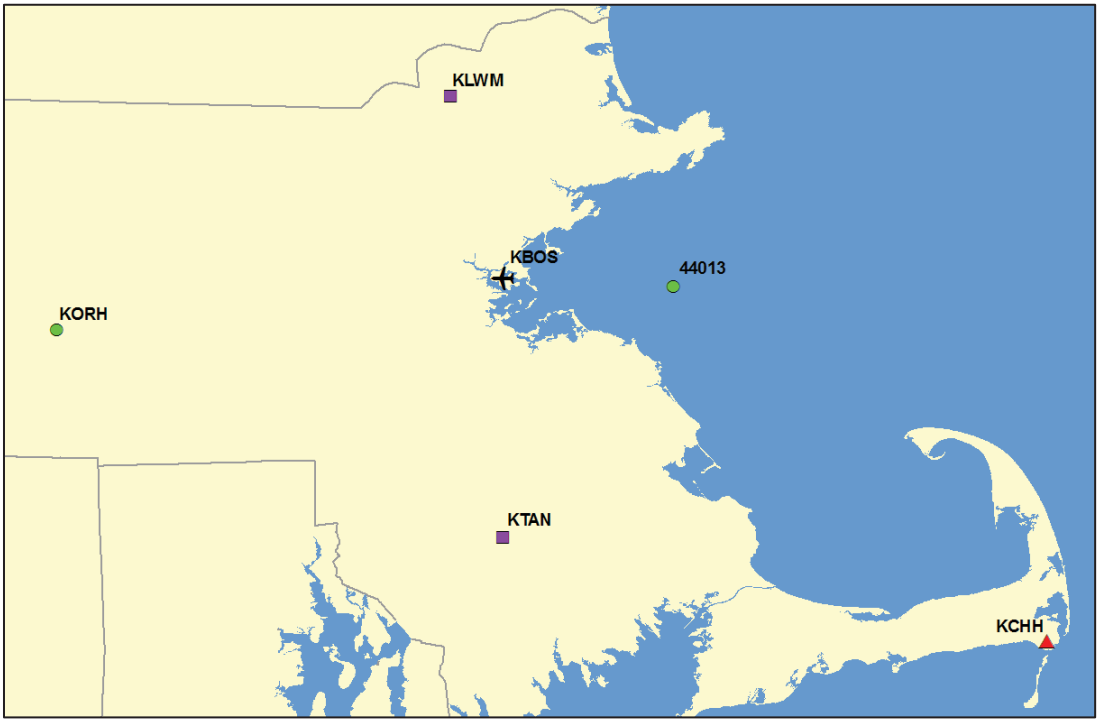

Figure 2.1: Map of Massachusetts showing the location of ASOS stations used for the cross shore component analyses. Purple squares represent stations used for uG and green circles represent stations used for dT/dx. The red triangle indicates the site used for sounding data in the three dimensional analysis. Logan Airport is denoted by the airplane.

e. Radar Analysis of Convection

Level II reflectivity data were obtained from the National Climatic Data Center (NCDC, 2008). Radar data from Taunton, MA (KBOX) were used for this part of the study. Each event and non-event date was queried and graphed showing data availability and the operational mode of the radar was produced (Fig. 2.2). If the radar was in precipitation mode at anytime between 1200 UTC and 2359 UTC the data were downloaded for further analysis. The 0.5° reflectivity data were then examined to determine whether convection was occurring in or entering into the coastal region in which the sea breeze front could exist. A threshold of greater than or equal to 30 dBZ was used to distinguish convective cells from non-convective cells (Bedka and Mecikalski, 2004).

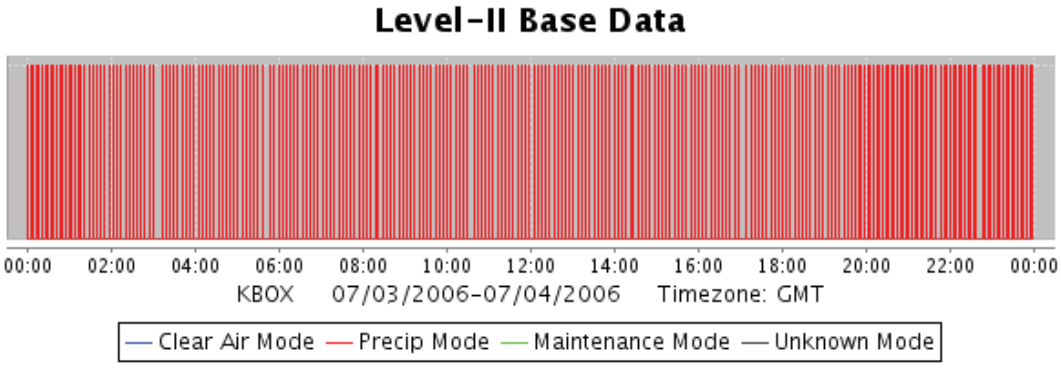

Figure 2.2: Example of the NCDC data availability graph.

Using this method for warm season months (April to September) from 2002 through 2007, 26 dates were chosen. Vector wind analyses were created using the same method described in the inland penetration section. The purpose of these analyses was to

locate the sea breeze front indicated by wind shift. This location can then be compared to the reflectivity data to determine whether convection was developing, weakening, or remaining the same along the sea breeze front.

CHAPTER 3

3. Time of Onset and Event Duration

a. Time of Onset

The time of onset for each event (fast, slow, and marginal) was recorded as described in the previous chapter. The possible times of onset for each event type were then plotted alongside the mean with an error bar of three standard deviations (Fig. 3.1). There were 171 fast sea breeze events, 60 slow sea breeze events, and 78 marginal sea breeze events. Only one data point (2300 UTC, slow events) does not fall within the range of the error bar. For the time of onset of 2300 UTC for slow events, there is only one observation of this time in the data set (shown in Fig. 3.2b).

A dual midday peak is evident for both slow and marginal events (Fig. 3.2b and 3.2c). There is a suggestion of this trend in the fast events at 1700 UTC (Fig. 3.2a), but it is not as strong a signal as with the slow and marginal events. It seems that the *weaker* the event, the *stronger* this signal is; the second peak is weaker than the first in both the fast and slow events and then equal to the first for the marginal events. Perhaps if another event type existed between marginal and non-events the second peak would be larger than the first. There is a third peak present for all events that occurs in the early evening. This peak gets increasingly later as one transitions from the fast events to the marginal events.

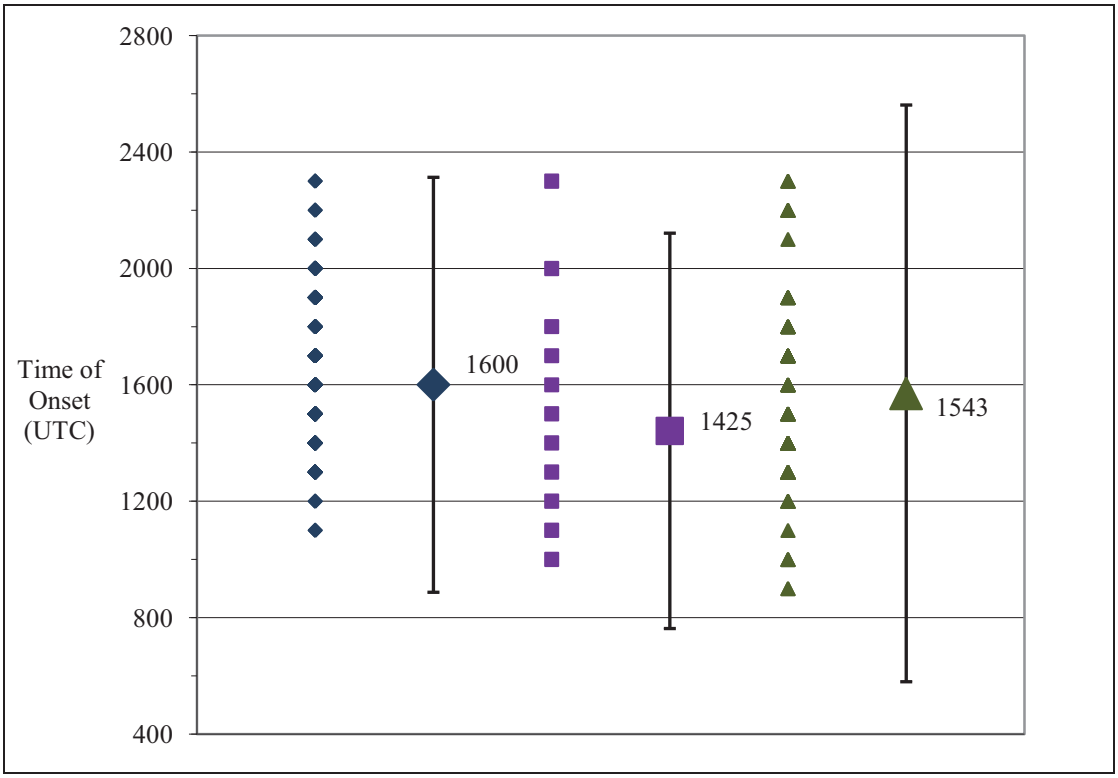

Figure 3.1: Plot of times of onset by event type alongside the mean with error bars of three standard deviations. The fast events are the blue diamond, the slow events are the purple square, and the marginal events are the green triangles.

a.)

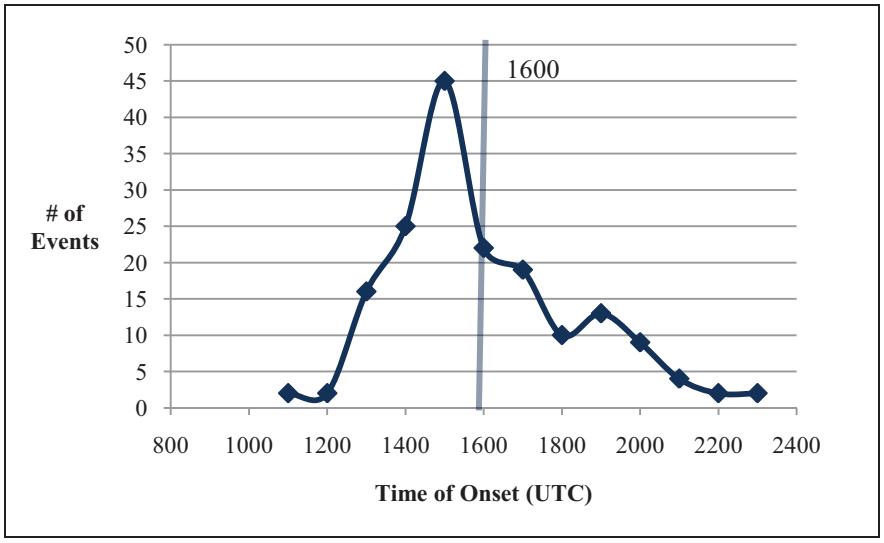

b.)

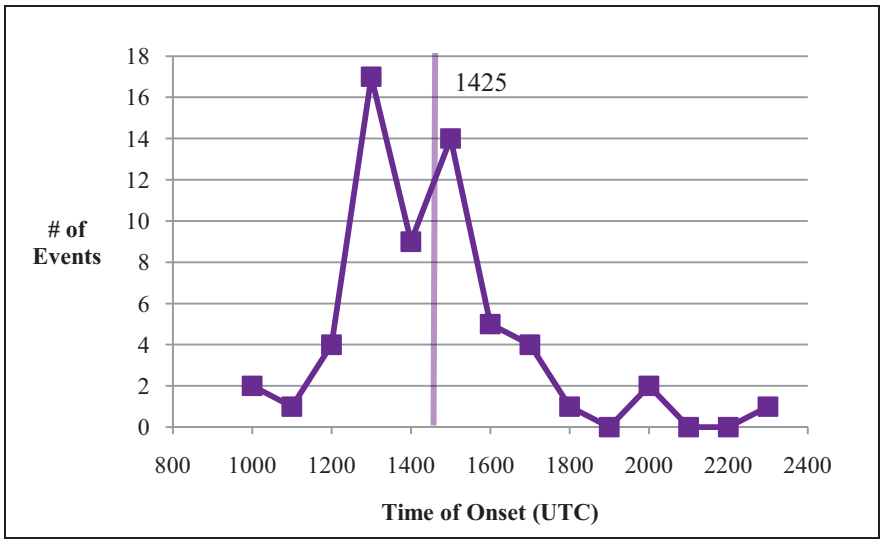

c.)

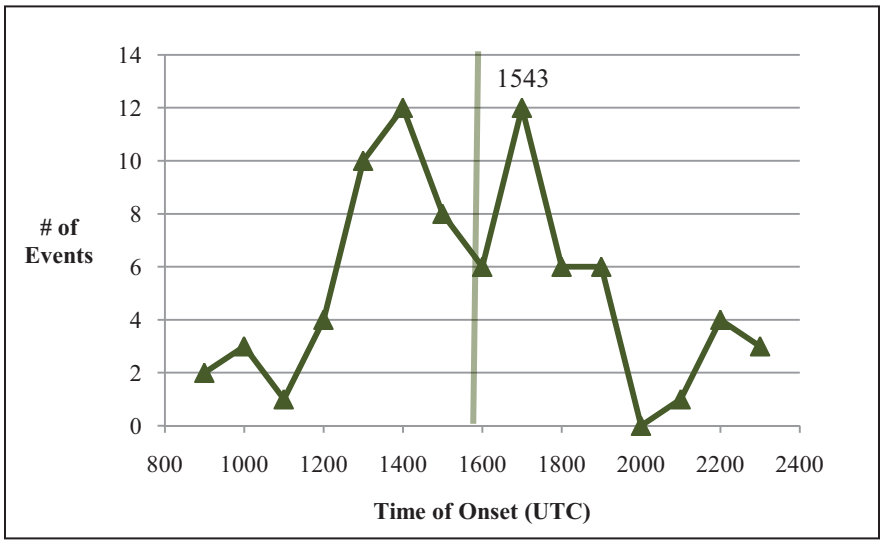

Figure 3.2: Time of onset distributions by event type. a.) fast, b.) slow, and c.) marginal. Vertical line indicates mean.

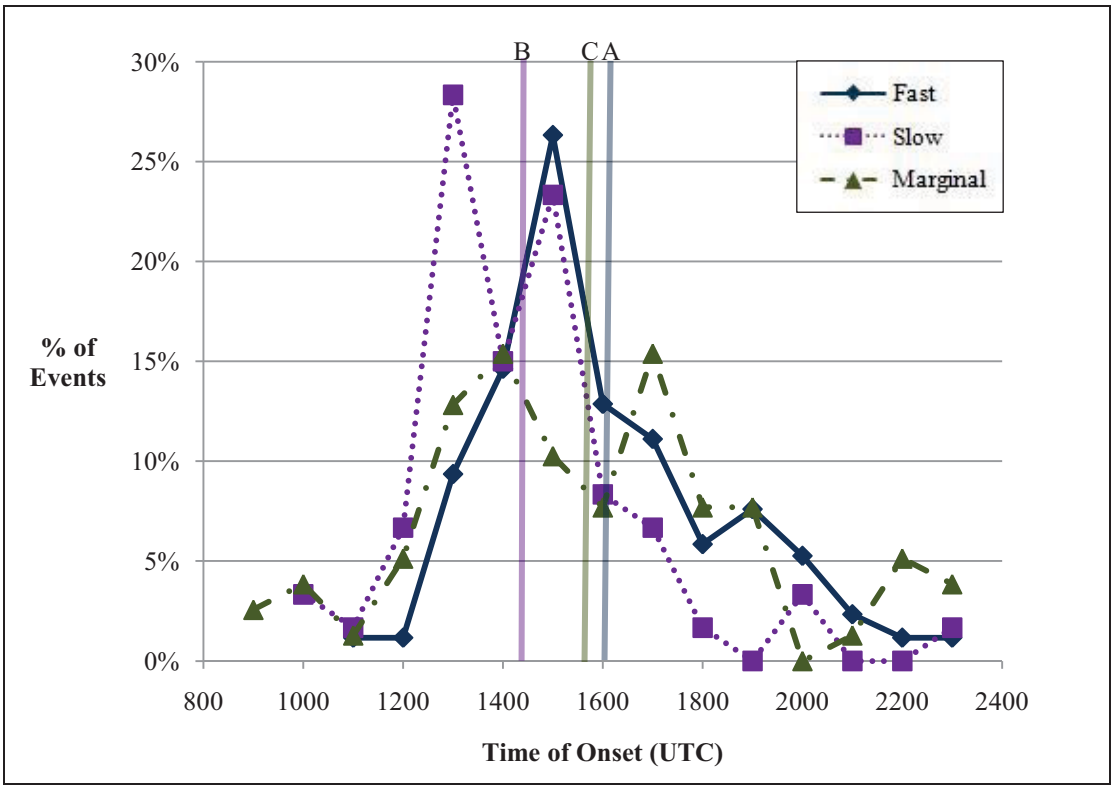

Figure 3.3: Time of onset distributions overlaid based on percentage of events. Line A is fast event mean, line B is slow event mean, and line C is marginal event mean.

Figure 3.3 shows all of the event types as an overlay. The position of each event type's mean time of onset shows slow events starting earliest (1425 UTC), with the marginal events occurring slightly later (1543 UTC), and the fast events the latest (1600 UTC). Fast events show a swift change in wind direction which could require the extra hour of daytime heating in order to occur. Slow events exhibit a more gradual change in wind direction which may not need as much daytime heating to initiate as the fast events. The marginal events contain weaker sea breezes that exhibit both fast and slow transitions and therefore it is natural for the mean time of onset to fall in between the two. Also, since the mean is shifted more towards the fast event mean, perhaps the marginal events are slightly more influenced by fast sea breeze characteristics.

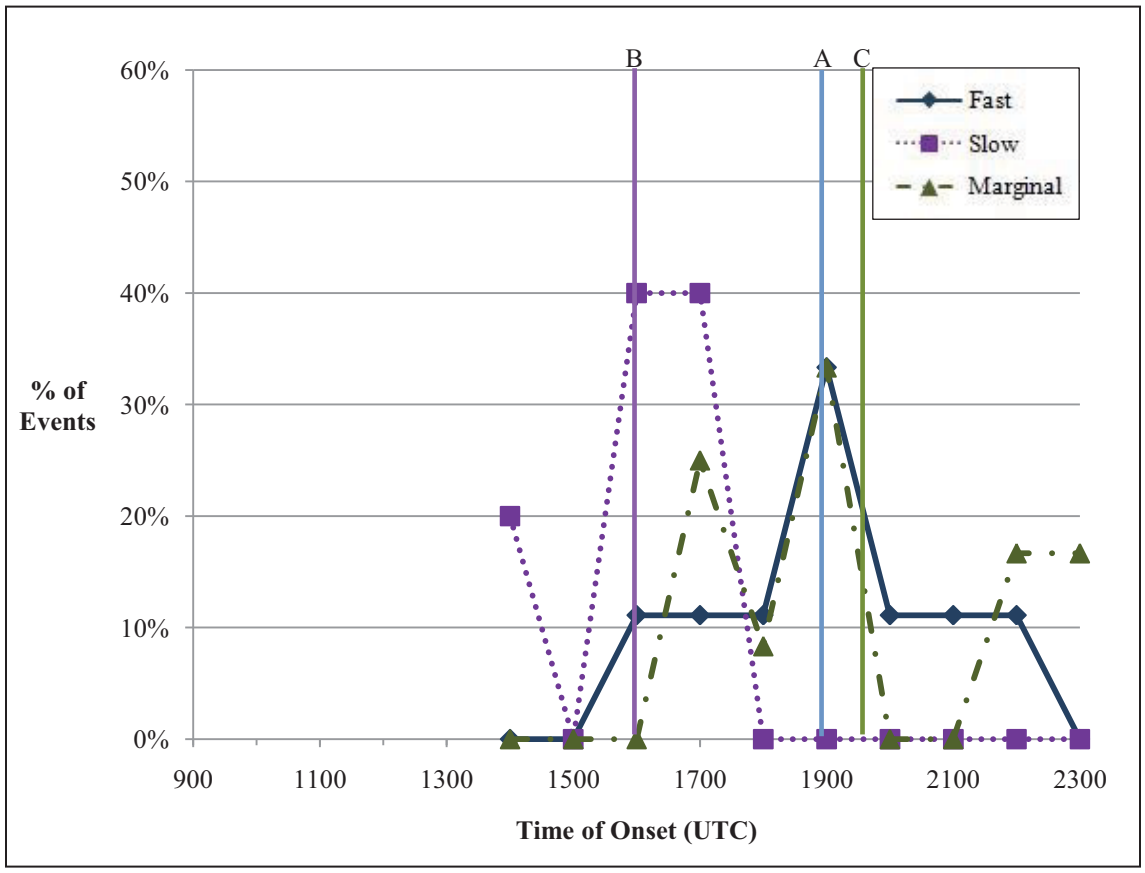

Figure 3.4: Time of onset distributions for the winter overlaid based on percentage of events. Line A is fast event mean, line B is slow event mean, and line C is marginal event mean.

These distributions can be broken down further by plotting them seasonally. The distribution for winter shows the times of onset shifted to later hours of the day (Fig. 3.4). This is expected since it would take longer for sufficient daytime heating to occur in winter. There were 9 fast sea breeze events, 5 slow sea breeze events, and 12 marginal sea breeze events in this distribution making the statistical significance of the winter data questionable. Notice that the order of the onset means has changed from the overall plot in Figure 3.3. The marginal events have the latest mean at 1935 UTC which is 35 minutes later than that of the fast events at 1900 UTC. This suggests that in winter, marginal

events tend to behave more like a fast sea breeze than a slow sea breeze. The mean for the slow events is much earlier, at 1600 UTC.

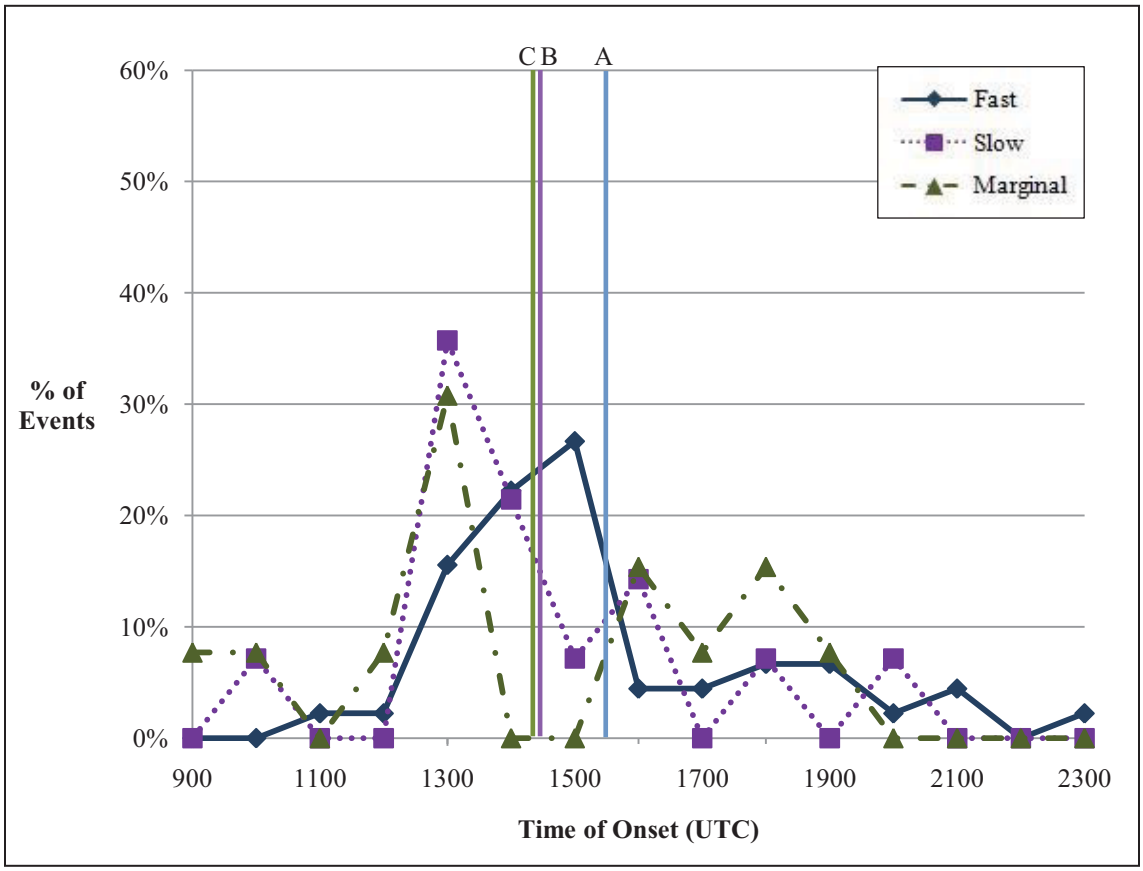

Figure 3.5: Time of onset distributions for the spring overlaid based on percentage of events. Mean lines same as in Fig. 3.4.

The spring distribution is shown in Figure 3.5. There again is a change in the order of the mean time of onset for each event. The marginal events seem to be influenced more by the slow events during spring. The marginal and slow events also share the same maximum for the time of onset at 1400 UTC. The time of onset for all events has become much earlier than it was in winter. The mean time of onset for the fast events is 1528 UTC with a sample size of 45 events. With 15 events, the mean of the slow sea breeze events is 1426 UTC. Lastly, the marginal events had a mean time of

onset of 1423 UTC with 13 events, which is the earliest mean onset of this event type. The duel maxima noted in the overall plot (Fig. 3.3) can be seen evidently in the spring distribution.

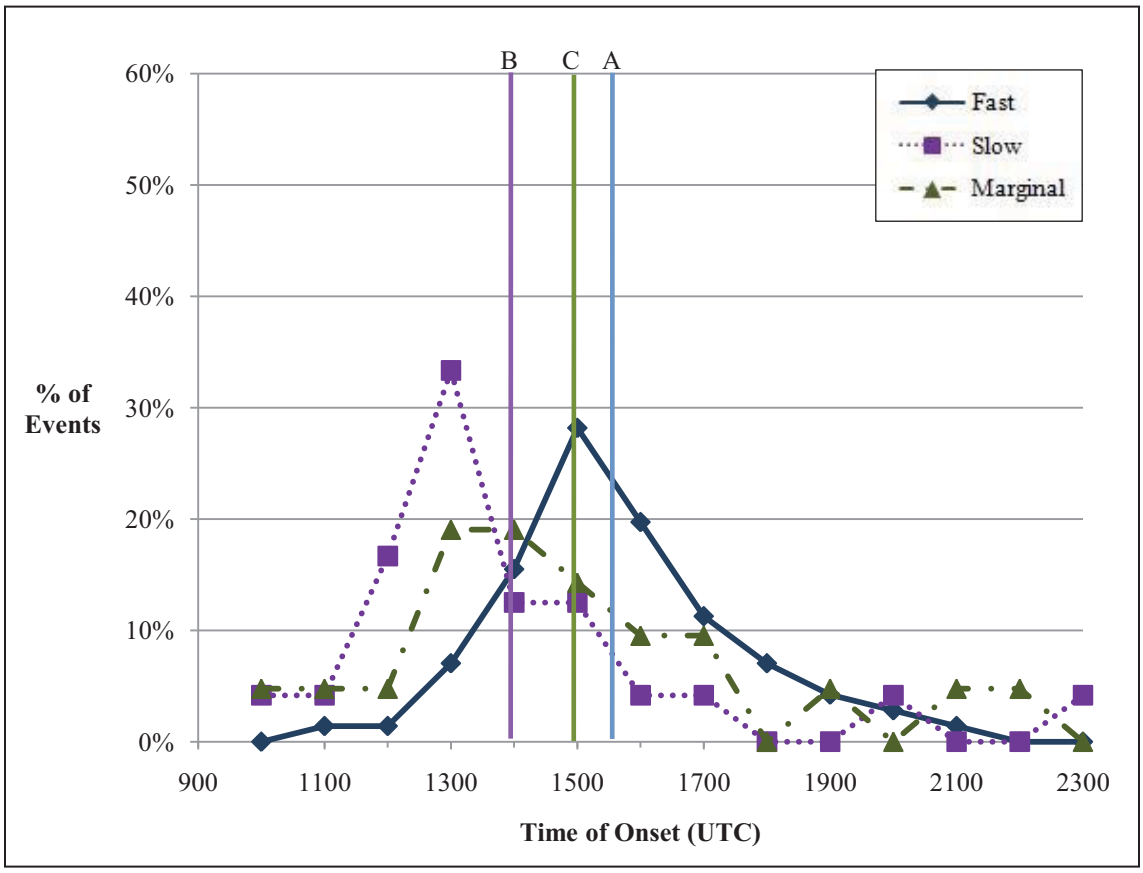

Figure 3.6: Time of onset distributions for the summer overlaid based on percentage of events. Mean lines same as in Fig. 3.4.

The distribution for summer (Fig. 3.6) has the mean times of onset in the same order as the overall distribution. Again, the mean time of onset for the marginal events is back between the fast and slow events. The summer months show a maximum in sea breeze events, which has a heavy influence on the overall plot. There were 71 fast sea breezes, 23 slow sea breezes, and 21 marginal sea breezes in summer for this study. The

mean time of onset for the fast events was at 1538 UTC which is the earliest mean time of onset for fast events overall. The same is true for the slow events which had a mean time of onset at 1400 UTC. The mean time of onset for the marginal sea breezes was at 1457 UTC. These early times of onset are clearly attributed to the abundant daytime heating available in the summer. The slow and marginal distributions seem to be right-skewed while the fast distribution is less skewed and almost a normal bell-curve. Although the mean onset of the marginal events falls slightly closer to that of the fast sea breezes, the distribution seems more similar to the distribution of the slow sea breezes.

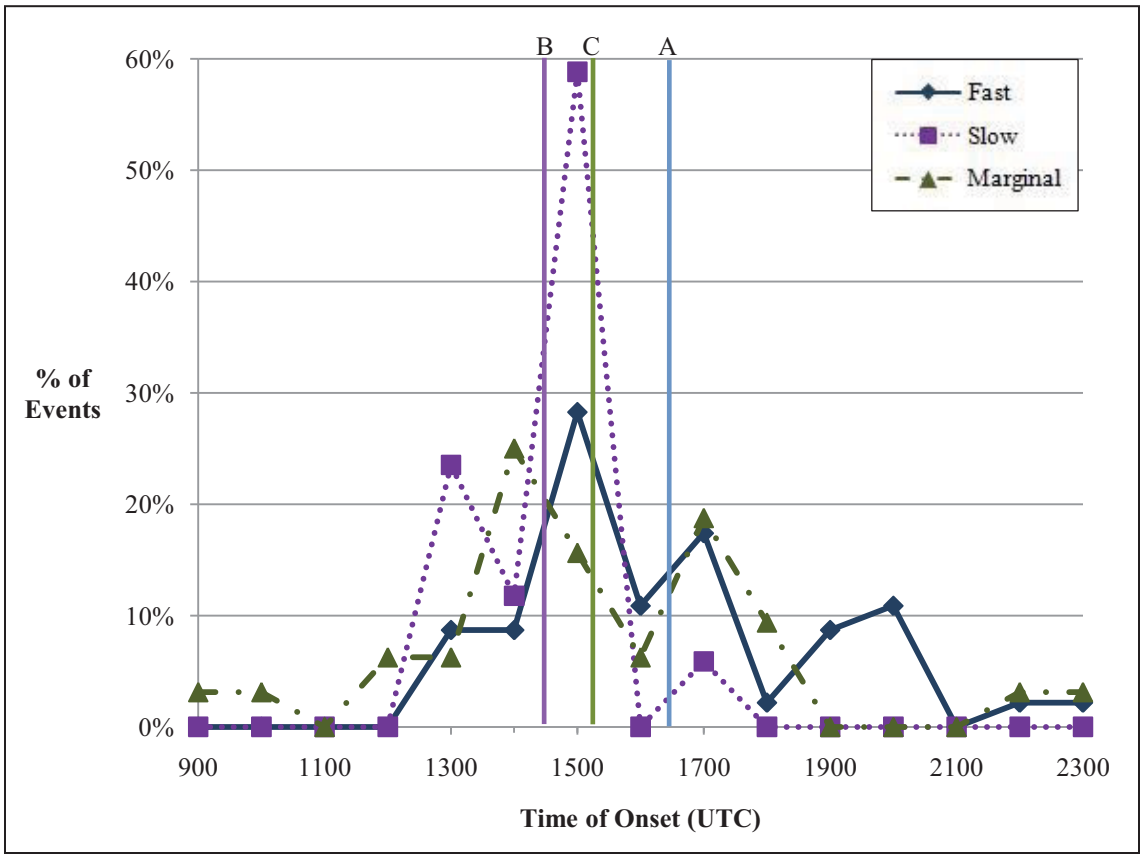

Figure 3.7: Time of onset distributions for the fall overlaid based on percentage of events. Mean lines same as in Fig. 3.4.

In the fall, the distributions for each event type show similar features (Fig. 3.7). There are three main peaks for the fast and slow events. The marginal events have two major peaks although there is a hint of another maximum at 1200 UTC. Both the fast and marginal events show an additional crest during the evening hours. The order of the mean time of onset is again like the overall plot with slow events being the earliest at 1432 UTC, followed by marginal events at 1517 UTC, and the fast events coming in the latest at 1629 UTC. There are 46 fast events, 17 slow events, and 32 marginal events for the data set in fall. There is a strong maximum at 1500 UTC for slow sea breezes with nearly 60% of all events occurring at this time. The range of the time of onset for slow events is also small (1300 UTC to 1700 UTC). The mean time of onset for the marginal sea breezes fall slightly closer to the slow events, however, the marginal events distribution seems to follow the fast event distribution.

The time of onset shows expected variation by season. The latest times of onset occur in winter when it takes longer for adequate daytime heating to develop. The overall results showed that the fast events occur the latest and the slow events occur the earliest with the marginal events falling in between. The seasonal distribution showed that this was true for summer and fall. In winter, marginal events tended to occur slightly later than the fast events while in spring marginal events occurred slightly earlier than the slow events. Since these two seasons have the lowest number of marginal events, it's arguable that with a larger sample size the marginal events may fall in between the fast and slow events like the overall plot shows.

b. Event Duration

The time of onset and the end time of each event type (fast, slow, and marginal) were recorded in the initial acquisition of the data set. The possible event durations for each type were then plotted alongside the mean with an error bar of three standard deviations (Fig. 3.8). All of the observed event durations fall within the three standard deviations for each event type. Notice that the standard deviation values for the fast and slow events are almost the same; 3.17 hrs and 3.09 hrs respectively. The marginal events have a significantly larger standard deviation at 5.11 hrs. Marginal events were defined as events that lasted one hour or less, had no clear start or finish, or had periods of "calm" or "light and variable" winds during the event. Marginal events were not further categorized by the transition into the sea breeze like the fast and slow sea breeze events and therefore contain both types of transitions. The diversity of events categorized as marginal events may have lead to this variance in the standard deviation.

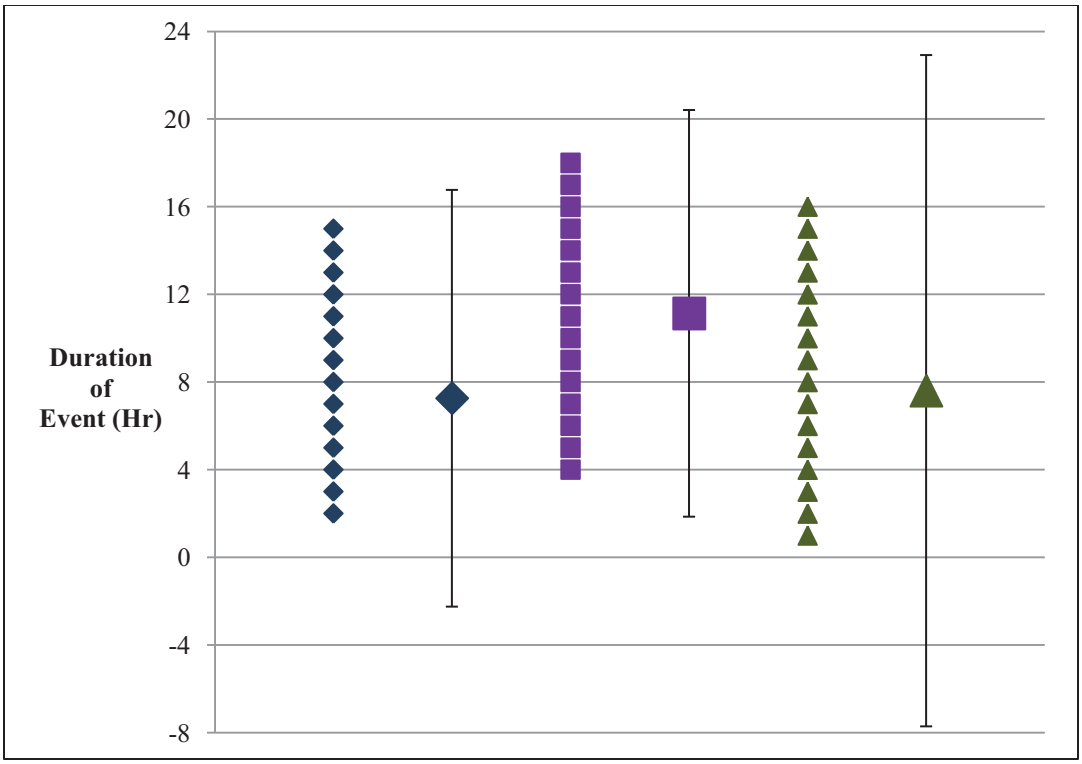

Figure 3.8: Plot of event durations by event type alongside the mean with error bars of three standard deviations. The fast events are the blue diamond, the slow events are the purple square, and the marginal events are the green triangles.

The overall distribution of event durations is shown in Figure 3.9. Most of the fast events have duration 10 hrs or less as shown in Figure 3.9a. The mean fast event duration is 7.26 hrs. Distribution of the slow event durations (Fig. 3.9b) appears to be more normal than that of the fast event durations. The majority of the events have a duration between 9 and 14 hrs and the mean duration is 11.13 hrs. With marginal event durations there seem to be no discernible pattern present in the distribution (Fig. 3.9c). The most notable feature in this distribution is that there is a strong peak for an event duration of 1 hr which is to be expected as it is one part of the definition of the event type. The mean duration for marginal events is 7.6 hrs. Figure 3.10 shows the three event types overlaid on one plot.

The long duration of the slow sea breezes is an aspect of the definition of the event. This type of sea breeze shows a gradual transition into a sea breeze and the duration starts once it passes into the sea breeze direction (10° to 190°). The strongest sea breeze winds generally are between the directions of 100° and 130° for the sea breeze at KBOS. Slow sea breezes eventually settle at these directions after the longer transition has occurred. Fast sea breeze events do not contain a long transition period which results in a shorter duration. The marginal events contain a strong outlier, by definition, with numerous one hour events skewing the mean towards a shorter duration.

To break down the distributions further, the event durations were plotted by season as well. Figure 3.11 shows the distribution for winter (December, January, and February) plotted as an overlay for the three event types. Notice that the order of the means remains the same as in the overall plot (Fig. 3.10). The mean duration of the fast events is the shortest at 4.90 hrs and that of the marginal events is the next shortest at 5.08 hrs. Slow events have the longest mean duration at 10 hrs. Also, the pattern from the overall distribution (Fig 3.10) is apparent in the winter plot for both the fast and marginal events. The marginal event duration shows the expected peak at 1 hr. The distribution of the slow events is not quite the same which is likely related to sample size issues as there were only 5 slow sea breeze events in the winter. There were also 9 fast sea breeze events and 12 marginal sea breeze events in this distribution. As stated earlier in the time of onset section, the statistical significance of the winter data is questionable.

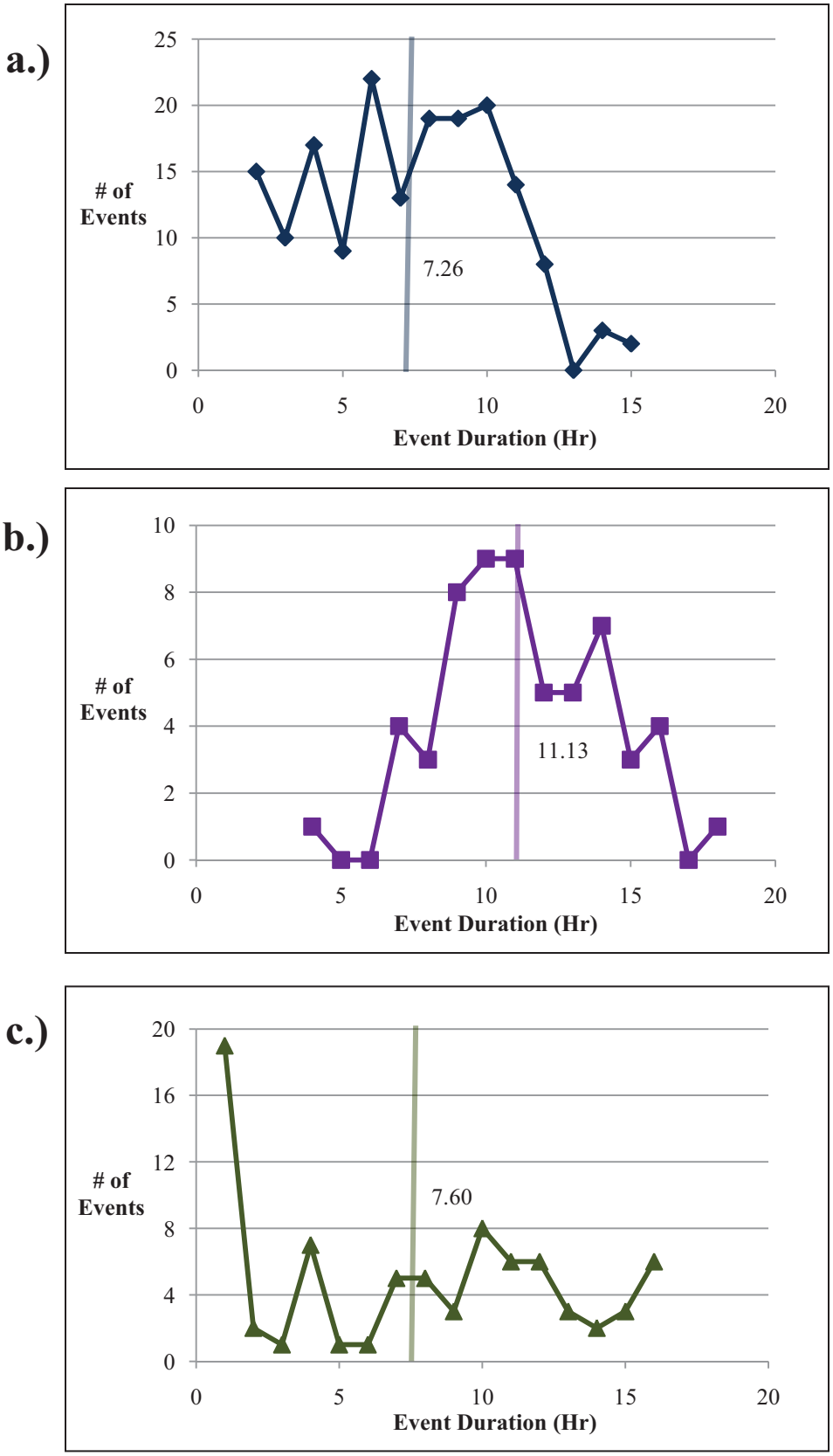

Figure 3.9: Event duration distributions by event type. a.) fast, b.) slow, and c.) marginal. Vertical line indicates mean.

The spring (March, April, and May) distribution for the three event types is shown as an overlaid plot in Figure 3.12. Again, the expected duration peak of 1 hr for the marginal events is present. There are multiple secondary peaks for the marginal events making the spring distribution similar to the overall distribution for marginal events (Fig. 3.10). The main peak of the fast event durations is 9 hrs and the spring distribution looks different from the overall distribution (Fig. 3.10). The spring distribution of the slow event durations has comparable peaks to the overall distribution of the slow event durations. The slow event durations peak at 9 and 10 hrs. The mean durations show a slightly different order in the spring distribution compared to the overall distribution. Marginal events now have the shortest mean duration at 7.46 hrs. Fast events have the next shortest mean duration at 8.04 hrs indicating that fast events become longer in spring. Slow events still have the longest mean duration at 10.93 hrs which is about an hour longer than the winter duration and just under the overall mean duration. There were 45 fast sea breeze events, 15 slow sea breeze events, and 13 marginal sea breeze events in this distribution.

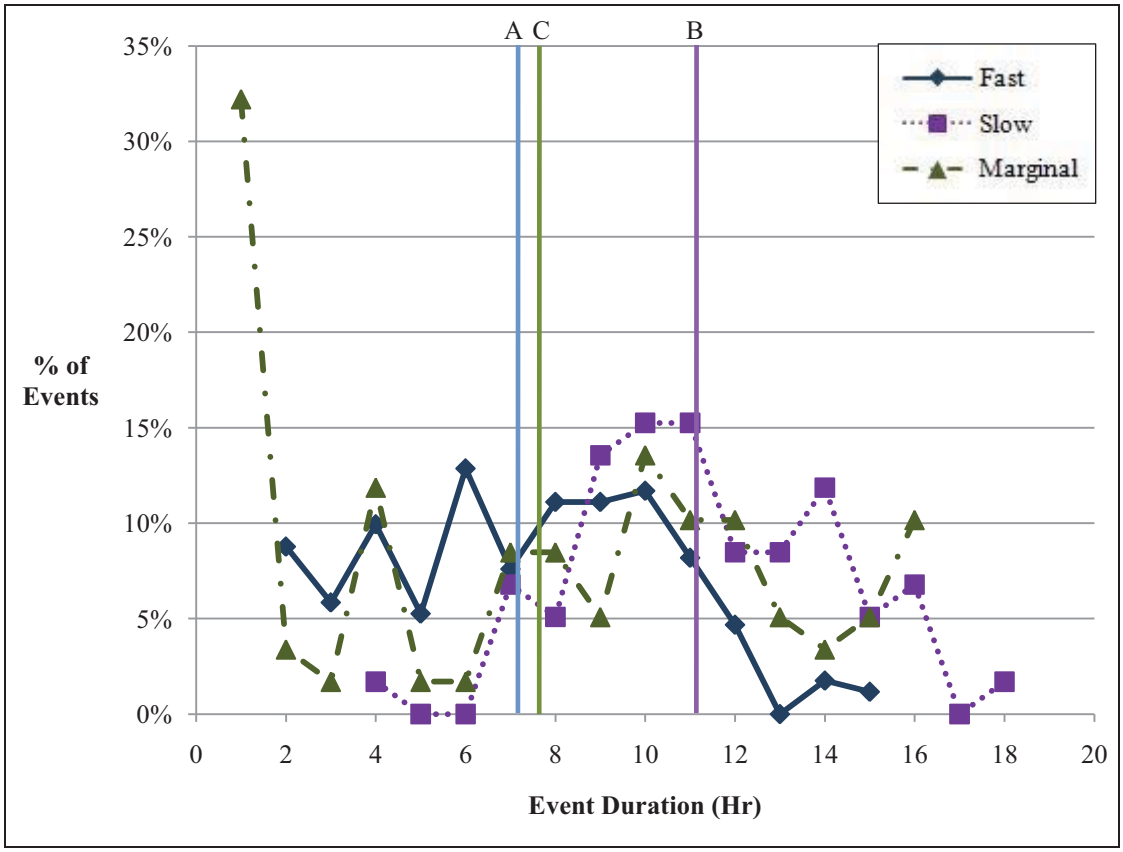

Figure 3.10: Event duration distributions overlaid based on percentage of events. Line A is fast event mean, line B is slow event mean, and line C is marginal event mean.

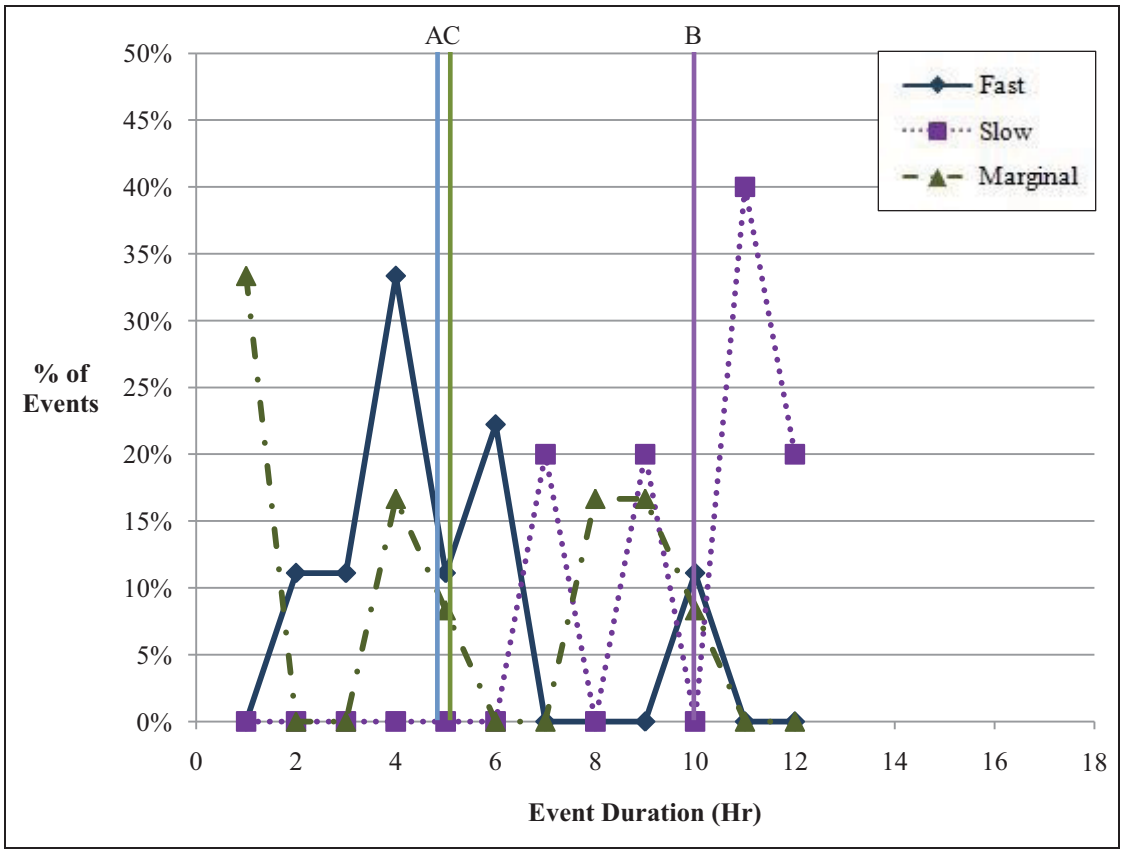

Figure 3.11: Event duration distributions for the winter overlaid based on percentage of events. Line A is fast event mean, line B is slow event mean, and line C is marginal event mean.

The distribution of the three event types for summer (June, July, and August) is depicted as an overlay in Figure 3.13. The 1 hr peak duration for the marginal events is not prominent in summer. There were 21 marginal events during the summer months. This minimum in 1 hr events supports the idea that sea breezes are stronger during summer with greater daytime heating available. There were 71 fast sea breezes and 23 slow sea breezes for this season. Arrangement of the mean durations is the same as with the overall plot (Fig. 3.10) with fast events being the shortest at 7.37 hrs, followed by marginal events at 8.38 hrs, and slow events being the longest at 11.50 hrs.

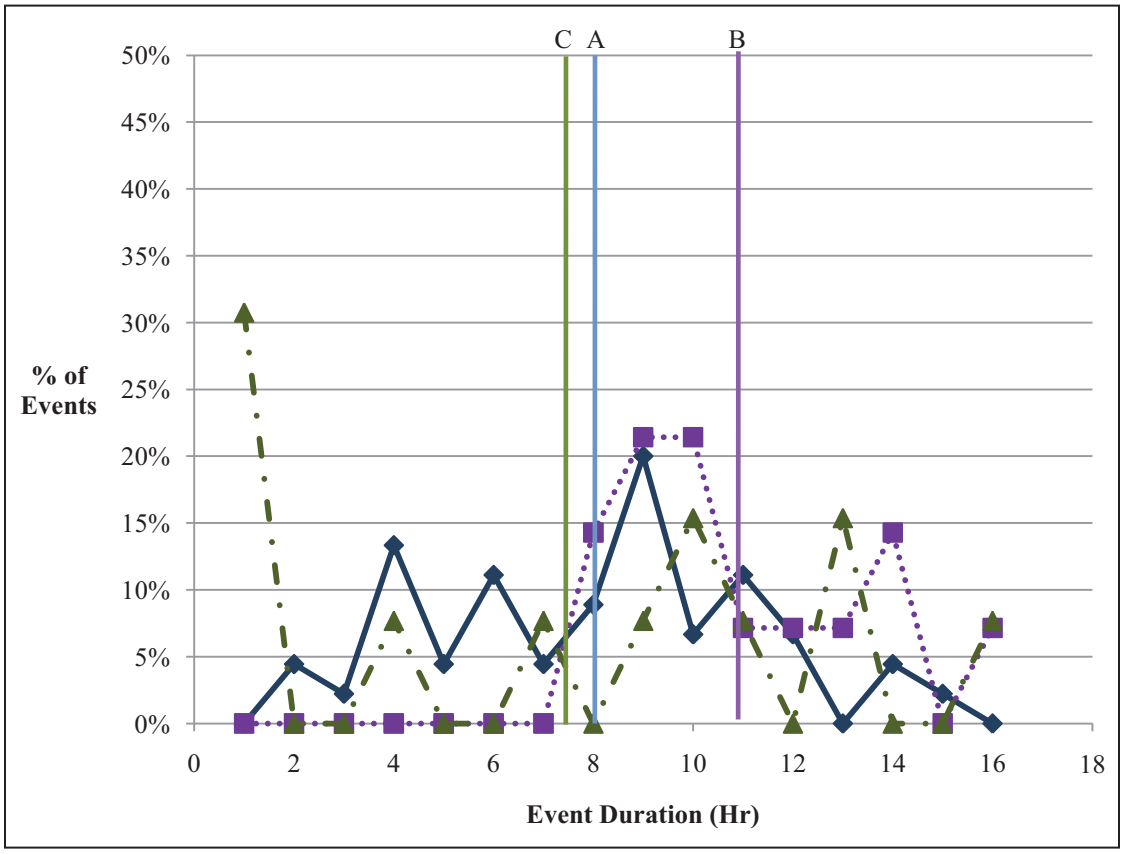

Figure 3.12: Event duration distributions for the spring overlaid based on percentage of events. Line A is fast event mean, line B is slow event mean, and line C is marginal event mean.

The fall distribution (Fig. 3.14) carries similar characteristics to the overall distribution (Fig. 3.10) for both fast and marginal events. The earlier peaks of 4 and 6 hrs for fast events are more prominent in the fall distribution that the later peaks of 8, 9, and 10 hrs compared to the overall distribution. Again, the 1 hr duration peak is present for the marginal events. Mean durations follow the same order as the overall with fast at 6.78 hrs, marginal at 8.09 hrs, and slow at 11.12 hrs.

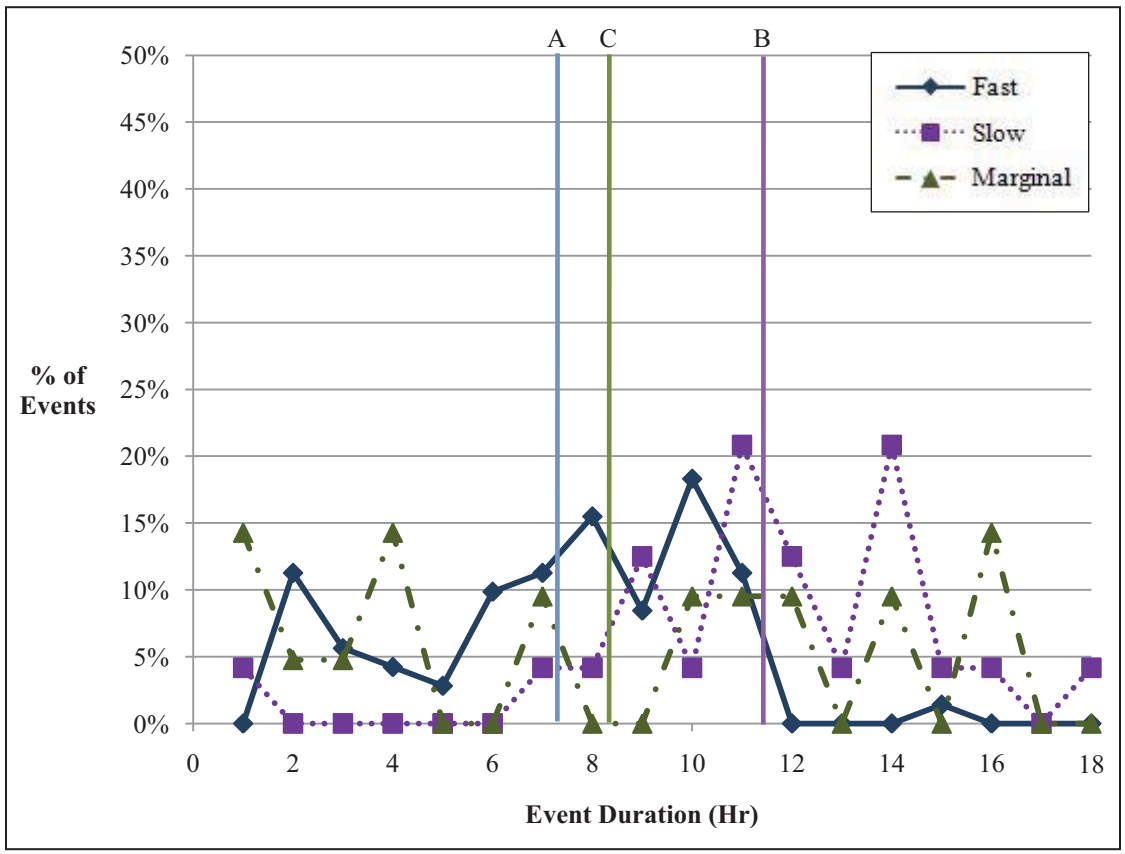

Figure 3.13: Event duration distributions for the summer overlaid based on percentage of events. Line A is fast event mean, line B is slow event mean, and line C is marginal event mean.

The duration varies between event types and shows some variance between seasons. The shortest event mean durations for all event types occurred during winter. The longest mean duration for the fast events occurred in spring while that of the slow and marginal events occurred during summer. These minima and maxima are logical as there is less daytime heating available in winter compared to spring and summer. It is interesting that the maximum mean duration for fast events occurred in spring while the maximum for slow and marginal events occur in summer. More research is needed to determine a cause of this.

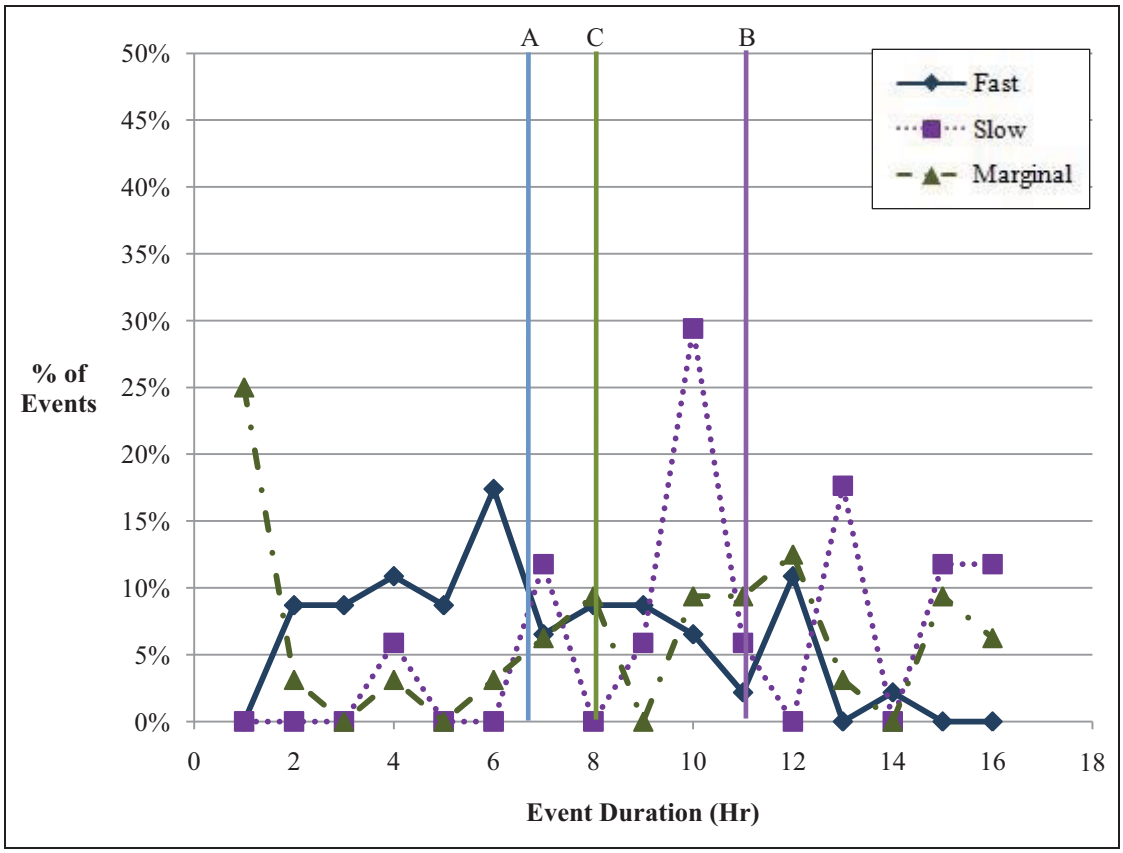

Figure 3.14: Event duration distributions for the fall overlaid based on percentage of events. Line A is fast event mean, line B is slow event mean, and line C is marginal event mean.

CHAPTER 4

4. Synoptic Classes & Inland Penetration

a. Synoptic Classes

To compare the variation in synoptic class for classes one through three for each event type, a conceptual schematic was created. The schematic (Fig. 4.1) shows the location of the composite high pressure center and measures the pressure gradient along a line perpendicular to the isobars over the study area. The perpendicular line varies in length with the different event types and synoptic classes. The line is drawn from the centermost isobar to the outermost isobar of the pressure system. Composites were generated from a list of dates and times for each event as described above.

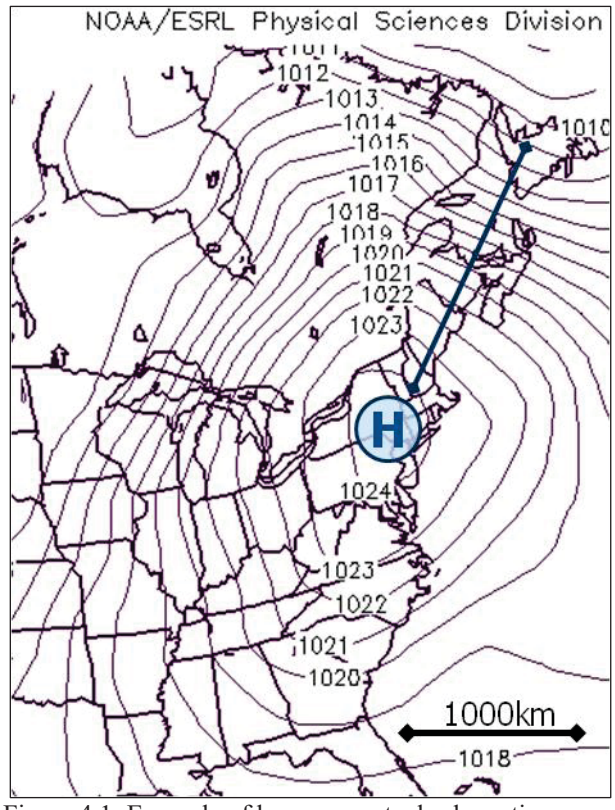

Figure 4.1: Example of how conceptual schematics were created. Fast transition sea breeze synoptic class 1.

For synoptic class 1, the composite high centers for fast, slow, and marginal events are almost colocated over eastern New York State with the slow event's high being slightly further north (Fig. 4.2). The center of the composite high pressure system with the non-sea breeze events is located further south over West Virginia and Maryland, creating a stronger gradient over the study area, and increasing the strength of the synoptically-driven offshore wind resisting the landward movement of the sea breeze. The mean gradient for the non-sea breeze events is also higher at 1.22 hPa/100km, which supports this reasoning (Table 4.1).

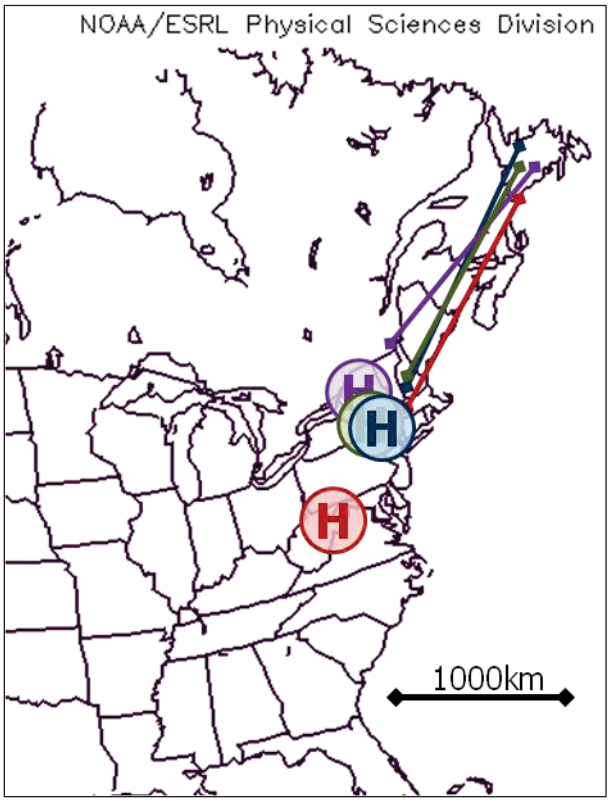

Figure 4.2: Conceptual schematic for synoptic class 1. Blue is fast event, purple is slow event, green is marginal event, and red is non-event.

Table 4.1: Gradients calculated along gradient lines in Figure 4.2.

Event Type	*Gradient (hPa/100km)*	*No. of Events*
Fast SB	0.83	42
Slow SB	0.89	14
Marginal	0.86	26
Non-Event	1.22	86

For synoptic class 2, the composite high pressure centers are somewhat more spread out; however, the non-sea breeze events' composite high center is the still farthest south (Fig. 4.3). The pressure gradient for the non-sea breeze event is 1.36 hPa/100km (Table 4.2), again making the gradient strongest for these events.

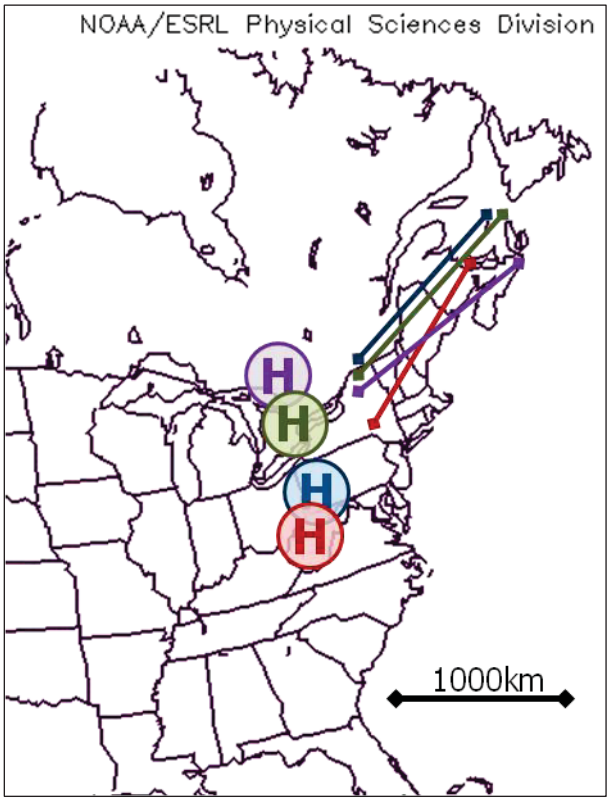

Figure 4.3: Conceptual schematic for synoptic class 2. Labeling is the same as Figure 4.2.

Table 4.2: Gradients calculated along gradient lines in Figure 4.3.

Event Type	*Gradient (hPa/100km)*	*No. of Events*
Fast SB	0.70	36
Slow SB	0.74	11
Marginal	0.71	8
Non-Event	1.36	177

For synoptic class 3, results were not as clear. Although non-sea breeze events still have the strongest composite pressure gradient at 1.39 hPa/100km (Table 4.3), the composite high center is not the farthest south (Fig. 4.4). There are *two* high centers for the marginal events, one of which represents the most southerly high center. These irregularities may be attributed to the small sample size. For synoptic class 3, there were only 4 fast sea breeze events, 2 slow sea breeze events, and 6 marginal events. Compared to the 132 non-sea breeze events, a larger sample size for the sea breeze events is needed to get a more statistically-meaningful composite analysis of the sea breeze with synoptic class 3.

A pattern can be found in the seasonal variation of each event type within these three synoptic classes (Fig. 4.5). Figure 4.5a (class 1) shows a peak in sea breeze events occurring in late spring and early summer. It also shows that synoptic class 1 non-sea breeze events happen least during the late spring and early summer. In Figure 4.5b (class 2), the peak of sea breeze events occurs closer to midsummer than with synoptic class 1. Again, the minimum for non-sea breeze events occurs at the same time as the sea breeze event peak. Finally, in Figure 4.5c (class 3), the peak appears similar to class 2 only there is much less variation between seasons.

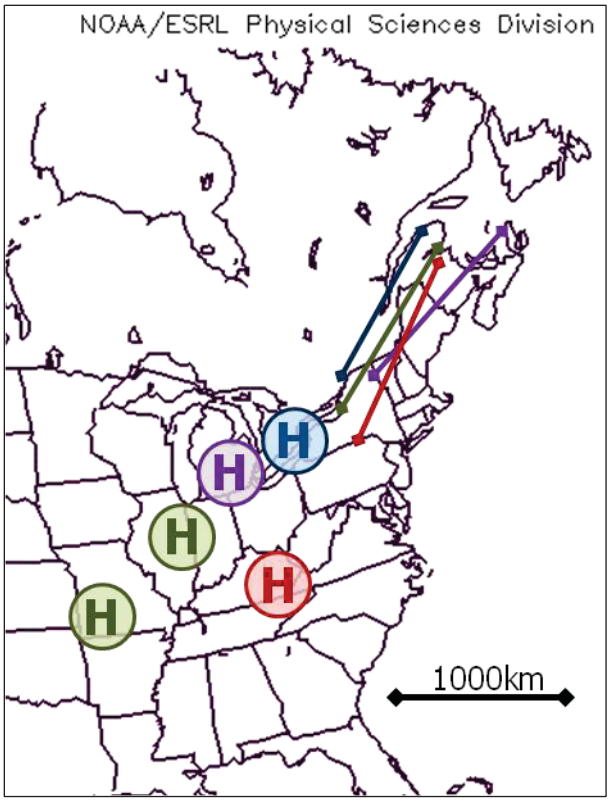

Figure 4.4: Conceptual schematic for synoptic class 3. Labeling is the same as Figure 4.2.

Table 4.3: Gradients calculated along gradient lines in Figure 4.4.

Event Type	*Gradient (hPa/100km)*	*n=No. of Events*
Fast SB	0.95	4
Slow SB	0.79	2
Marginal	0.64	6
Non-Event	1.39	132

Classes 1 through 3 behave as if they are along a single spectrum of class, with one and three at opposite extremes, and two in the middle. The same general trend for individual event types is evident in each class. Moreover, in moving along the continuum, the number of non-sea breeze events becomes greater; 15.4% for class 1, 38.2% for class

2, and 81.8% for class 3. The sample size of sea breeze events (fast, slow, and marginal) is small for synoptic class 3 which takes away from the statistical significance of the distribution. A larger data set is necessary to improve the worth of this distribution.

The composite analyses of synoptic class 4 for each event type (Fig. 4.6) show a noticeable increase in pressure gradient between fast sea breeze events and non-sea breeze events. There is also a clear rotation of the orientation of the isobars. For a fast sea breeze event the flow at the top of the boundary layer is shore parallel, making it easier for the sea breeze front to move inland. For the non-sea breeze event, the isobars are oriented shore-perpendicular, causing a stronger wind component at the top of the planetary boundary layer opposing the landward movement of the sea breeze.

The location of the low pressure system in Canada varies between fast and slow sea breeze events. For a fast sea breeze event, the low is centered farther north into Hudson Bay. This causes the pressure gradient over the study area to be much weaker. For a slow sea breeze event the low is centered farther south over James Bay, causing a slightly stronger pressure gradient over the study area.

a.)

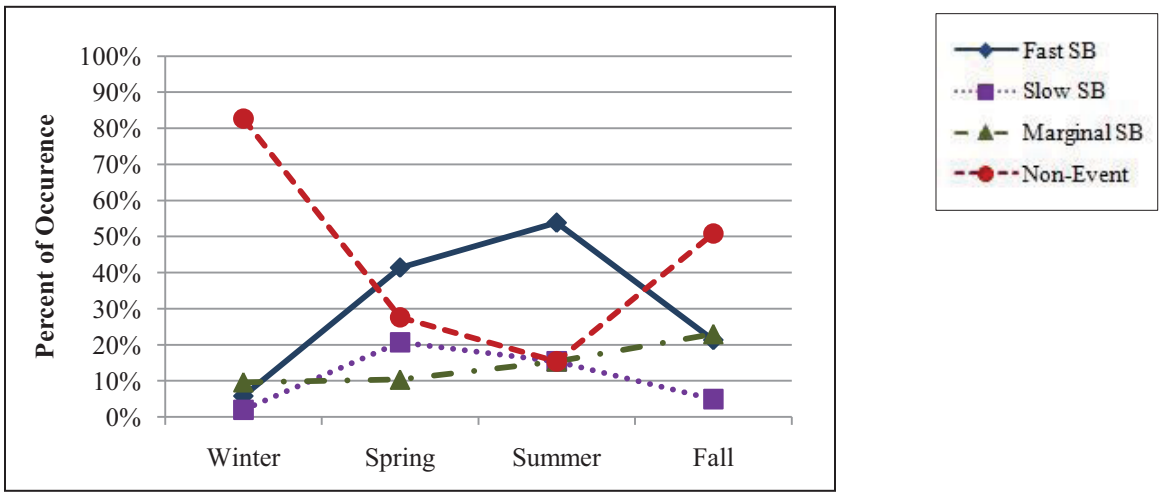

b.)

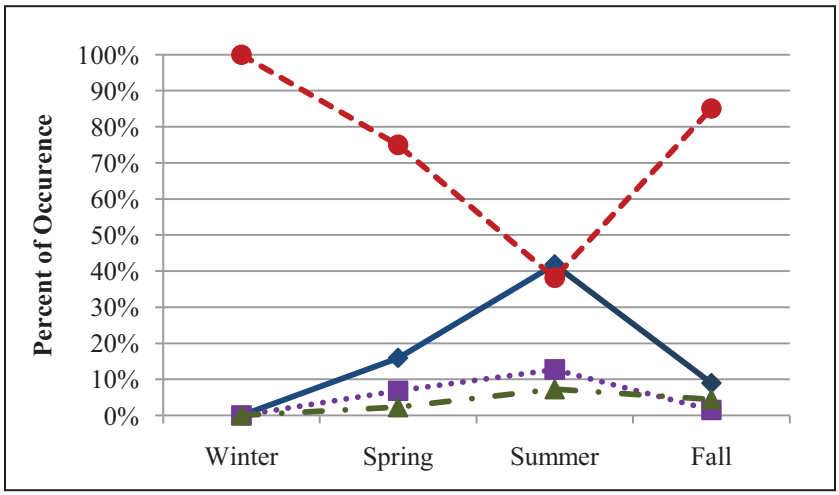

c.)

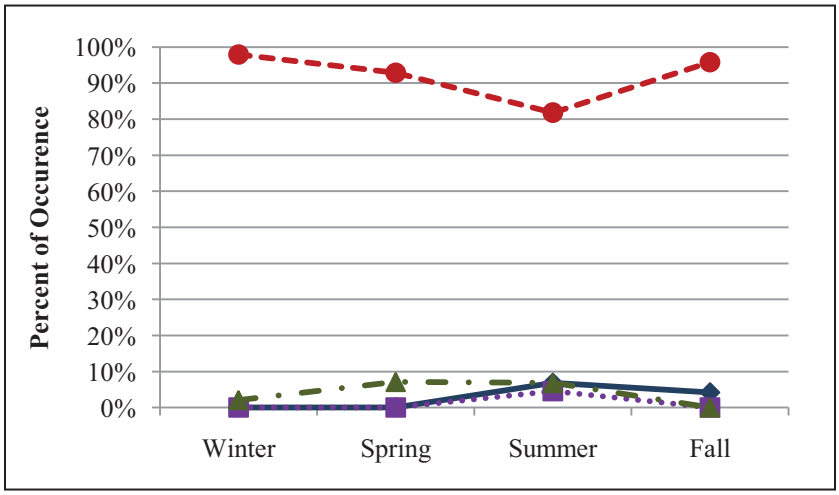

Figure 4.5: Seasonal variation of event type occurrence for a.) synoptic class 1, b.) synoptic class 2, and c.) synoptic class 3.

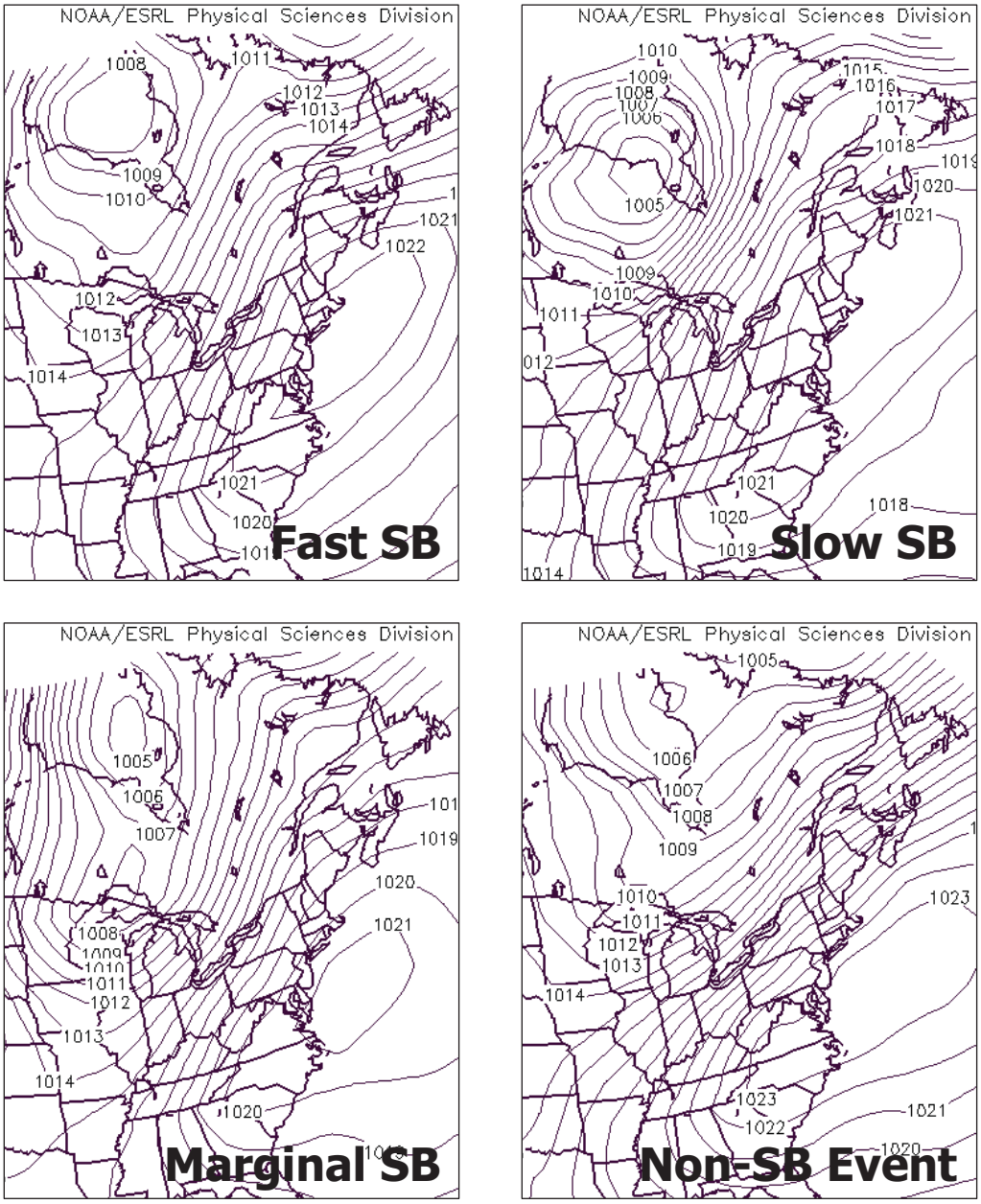

Figure 4.6: Composite analyses of synoptic class 4 for each event type.

The seasonal variation of synoptic class 4 is shown in Figure 4.7. Notice that the fast events are inversely related to non-events, increasing when the non-events decrease and vice versa. The same can be seen with the slow and marginal events. Similar characteristics beyond synoptic class seem to exist between these pairs. There seems to

be an unknown determining factor governed by season that distinguishes whether a fast event will occur versus a non-event. The factor could be as simple as the available daytime heating from season to season, but further research is needed to establish the cause. There were a total of 53 fast events, 7 slow events, 23 marginal events, and 108 non-events.

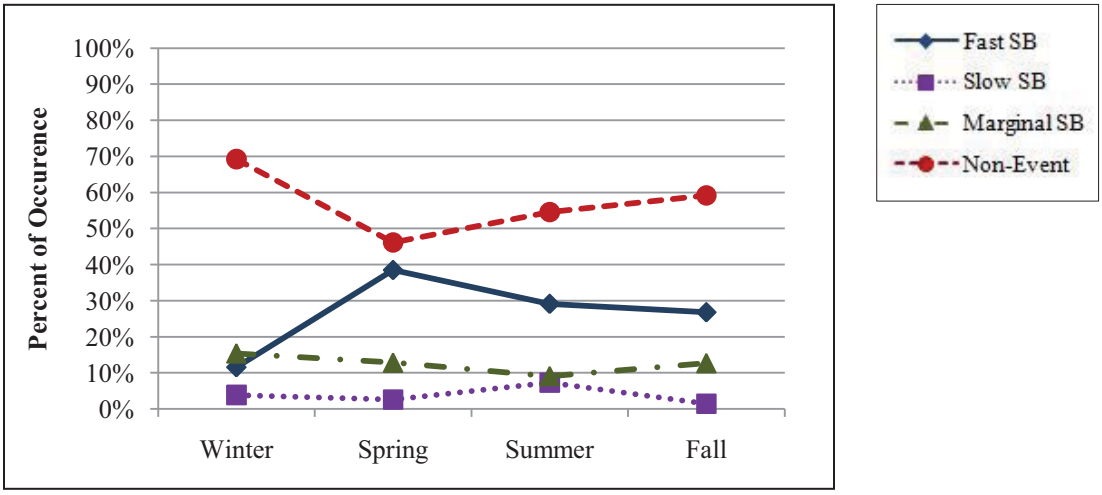

Figure 4.7: Seasonal variation of event type occurrence for synoptic class 4.

For synoptic class 5 (Fig. A-5), only non-sea breeze events occurred, confirming the findings of Miller and Keim (2003). There were a total of 22 non-events.

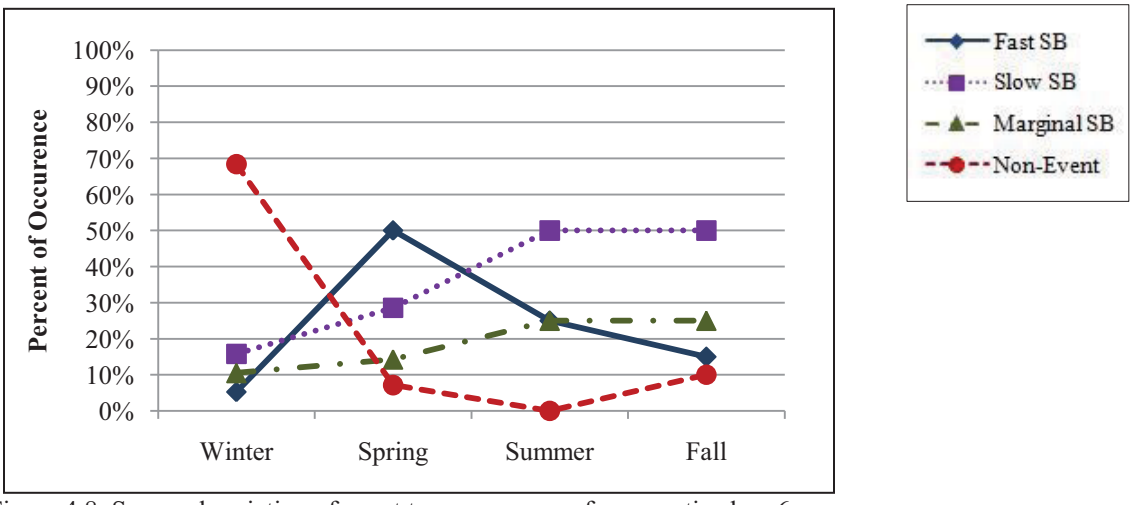

Figure 4.8: Seasonal variation of event type occurrence for synoptic class 6.

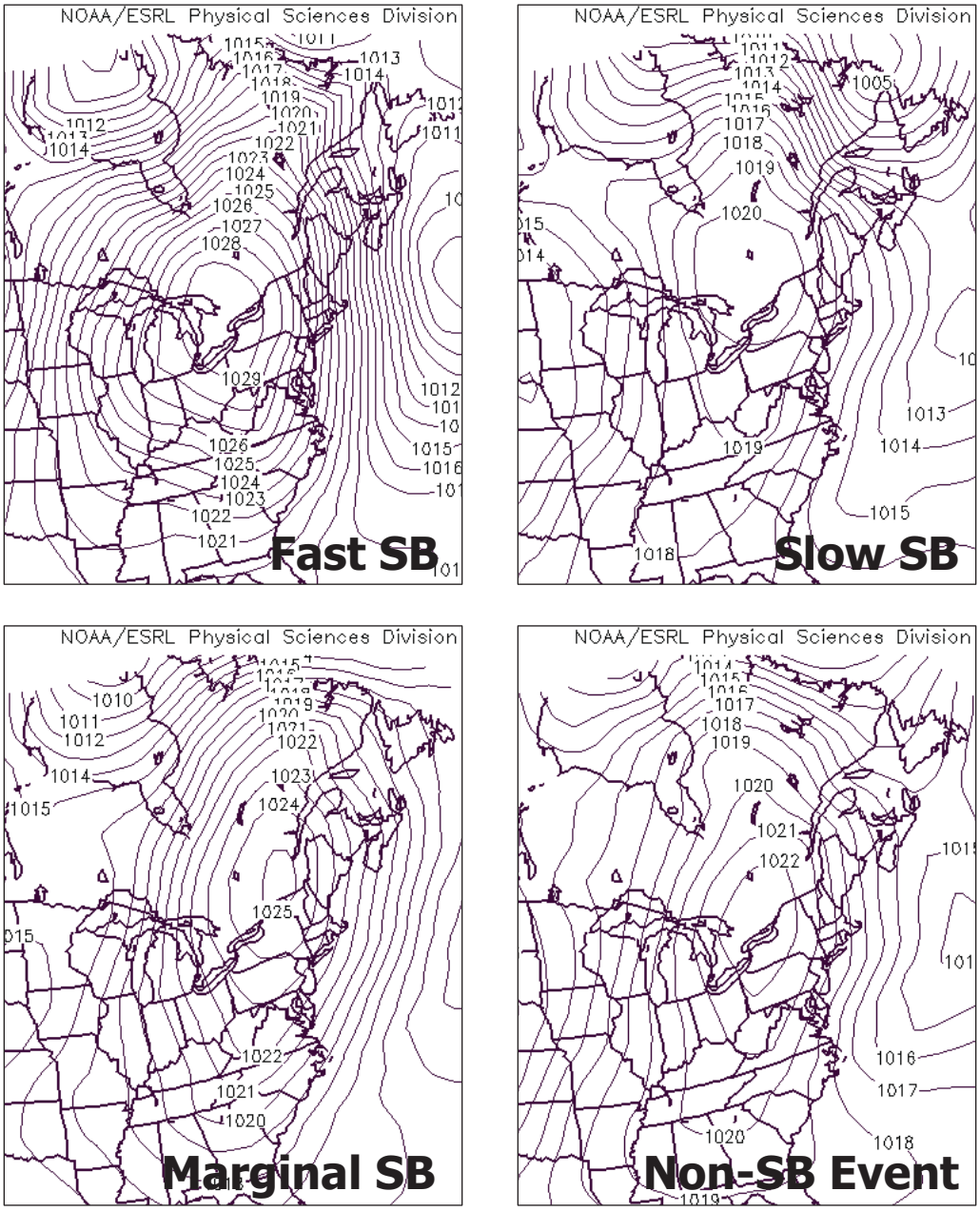

Figure 4.9: Composite analyses of synoptic class 6 for each event type.

For synoptic class 6 it is interesting to note that the seasonal variation of event type shows each event peaking in a different season (Fig.4.8). Non-sea breeze events peak in winter, fast sea breeze events peak in spring, and the slow and marginal events peak together in summer and fall. These peaks are likely related to the variations in

daytime heating available to initiate the sea breeze. There were 13 fast events, 21 slow events, 11 marginal events, and 16 non-events. The composite analyses for synoptic class 6 showed an increase in pressure gradient over the study area between fast sea breeze events and non-sea breeze events (Fig. 4.9). The center of the high is located farthest west in the non-sea breeze event which creates the stronger gradient over the study area.

b. Inland Penetration

Wind vector plots were generated to help visualize the extent and shape of the inland penetration of the sea breeze circulation. Gridded data generated using the Barnes analysis was plotted using MATLAB. The location of the sea breeze front was then subjectively analyzed based on wind shift to determine the shape and depth of penetration. The front was only analyzed based on the eastern coastline of Massachusetts and sea breezes from the south were ignored. Plots were made for the 5 major synoptic classes for fast sea breeze events (class 1 to 4, 6).

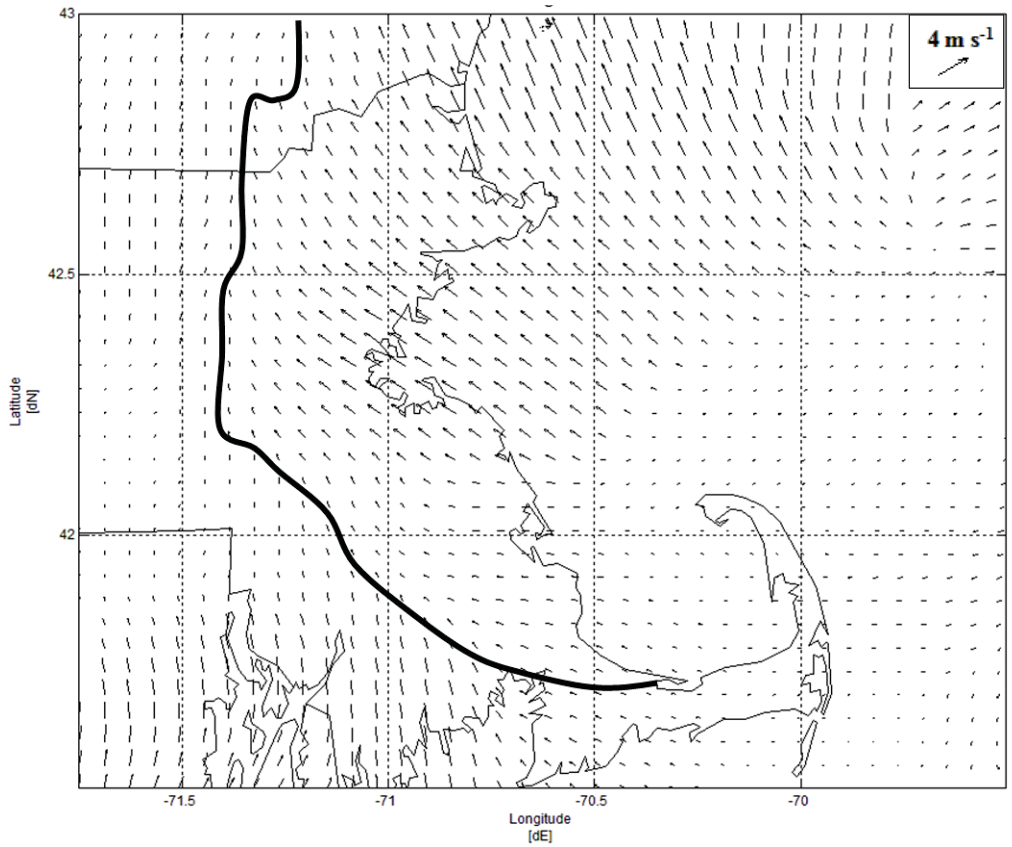

Figure 4.10: Plot of the mid-event average wind vectors for synoptic class 1. Solid black line represents the analyzed location of the sea breeze front.

Synoptic class 1, northwesterly anticyclonic flow, is shown in Figure 4.10. The wind vectors in this plot represent the average mid-event flow pattern for the 6 chosen dates described in chapter 2. Notice the depth of penetration relative to the coastline remains almost the same overall. The northern portion of the sea breeze seems to penetrate slightly further inland than the southern portion. This is clearly related to the strong southeasterly winds in the northern portion of the sea breeze flow compared to the much weaker east-southeasterly flow in the southern portion.

Figure 4.11 shows the wind vector plot of the mid-event average for synoptic class 2. The depth of inland penetration remains at a constant for the Massachusetts coastline. There is very little inland progression in New Hampshire with this synoptic

class. Synoptic class 2 has a neutral (neither anticyclonic nor cyclonic) northwesterly flow over the study area. The sea breeze from the Rhode Island Sound and Buzzard's Bay seems to be stronger with synoptic class 2 and can be seen further into Massachusetts than with synoptic class 1 (Fig. 4.10).

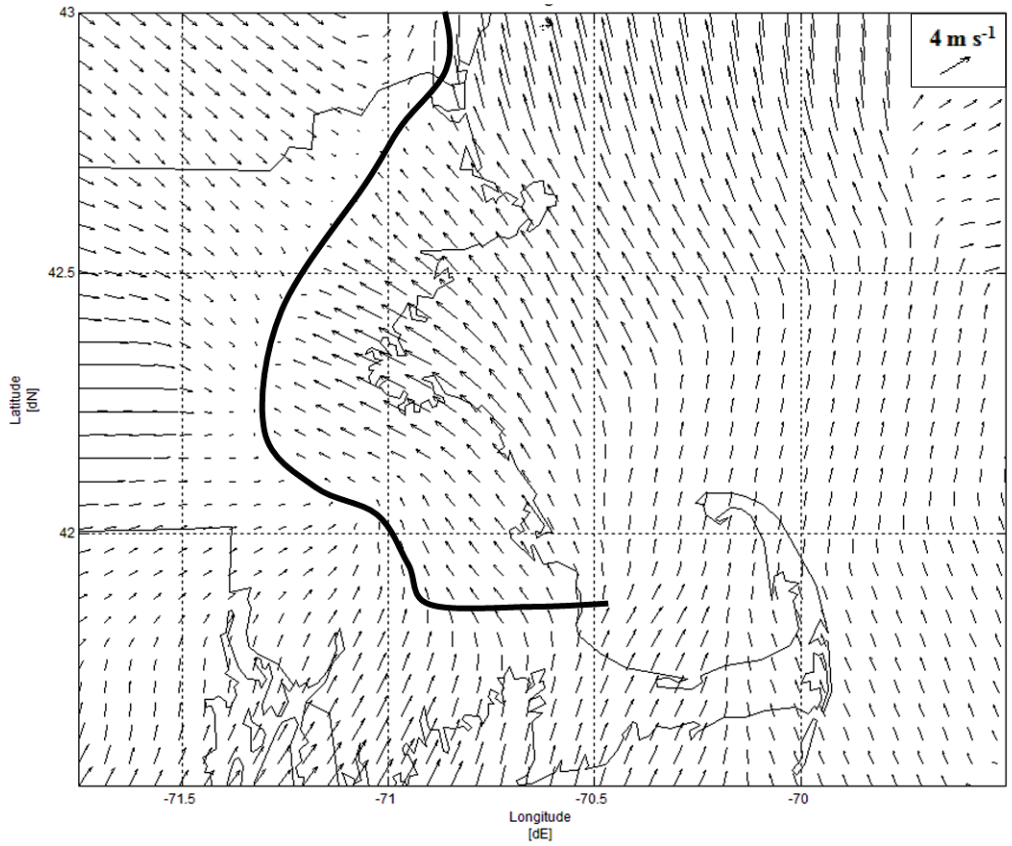

Figure 4.11: Plot of the mid-event average wind vectors for synoptic class 2. Same as Fig. 4.12.

The plot for cyclonic northwesterly flow, synoptic class 3, is shown in Fig. 4.12. This plot is only the average of 4 events unlike classes 1 and 2 which were 6 events. There were only 4 fast events in synoptic class 3 in the study overall. The inland progression of the sea breeze seems to be more limited with synoptic class 3 which is to be expected as the cyclonic winds would be stronger than the winds with classes 1 and 2.

The sea breeze also seems to push farther into New Hampshire compared to synoptic class 2 which is unexpected.

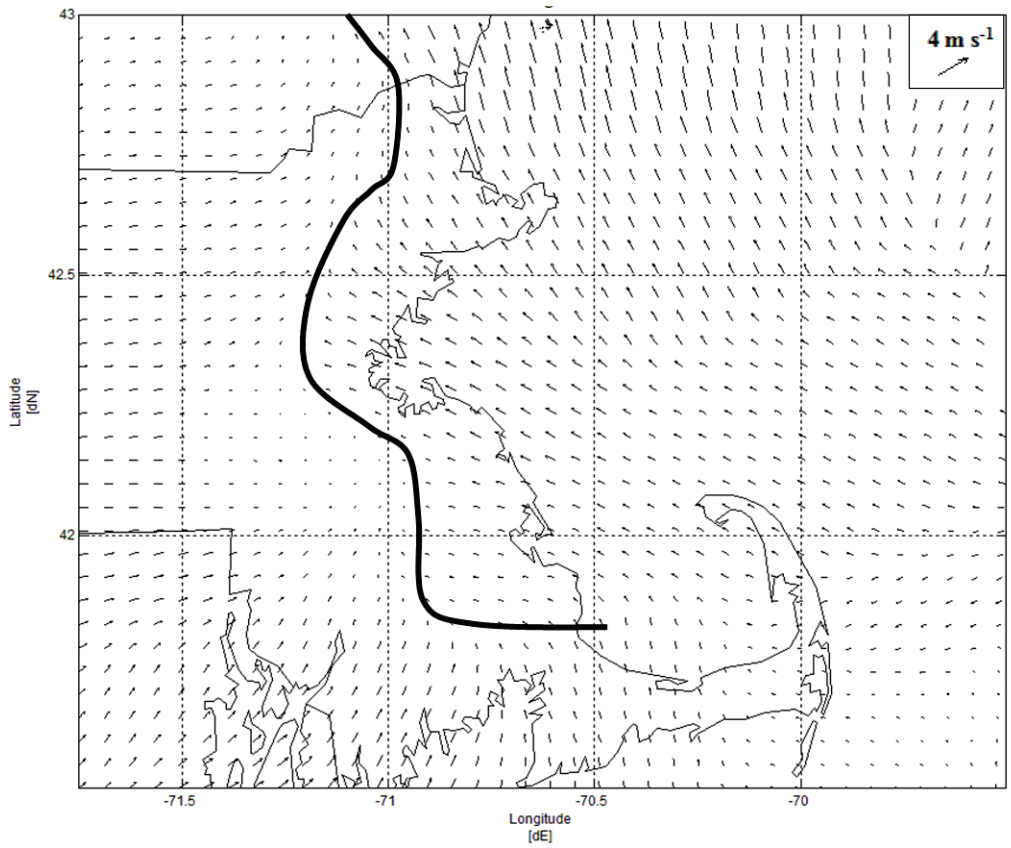

Figure 4.12: Plot of the mid-event average wind vectors for synoptic class 3.

The mid-event average wind vector plot for synoptic class 4, southwesterly flow, is shown in Figure 4.13. Inland propagation of the sea breeze is extremely limited south of Boston due to the strong effect of the southwesterly flow. The flow also somewhat limits inland penetration north of Boston as the sea breeze front is not as far inland as with synoptic class 1. The effect of the southwesterly flow is much more distinct than with the other flow regimes. I hypothesize that the southwesterly synoptic flow regime is

enhancing the sea breeze flow from the Rhode Island and Long Island Sounds thus vastly reducing the inland penetration of the Massachusetts Bay sea breeze flow.

Figure 4.14 shows the mid-event average wind vector plot for synoptic class 6. This class is characterized by shore-parallel, northeasterly surface wind flow. There were only 5 events used in this plot as mentioned in chapter 2.

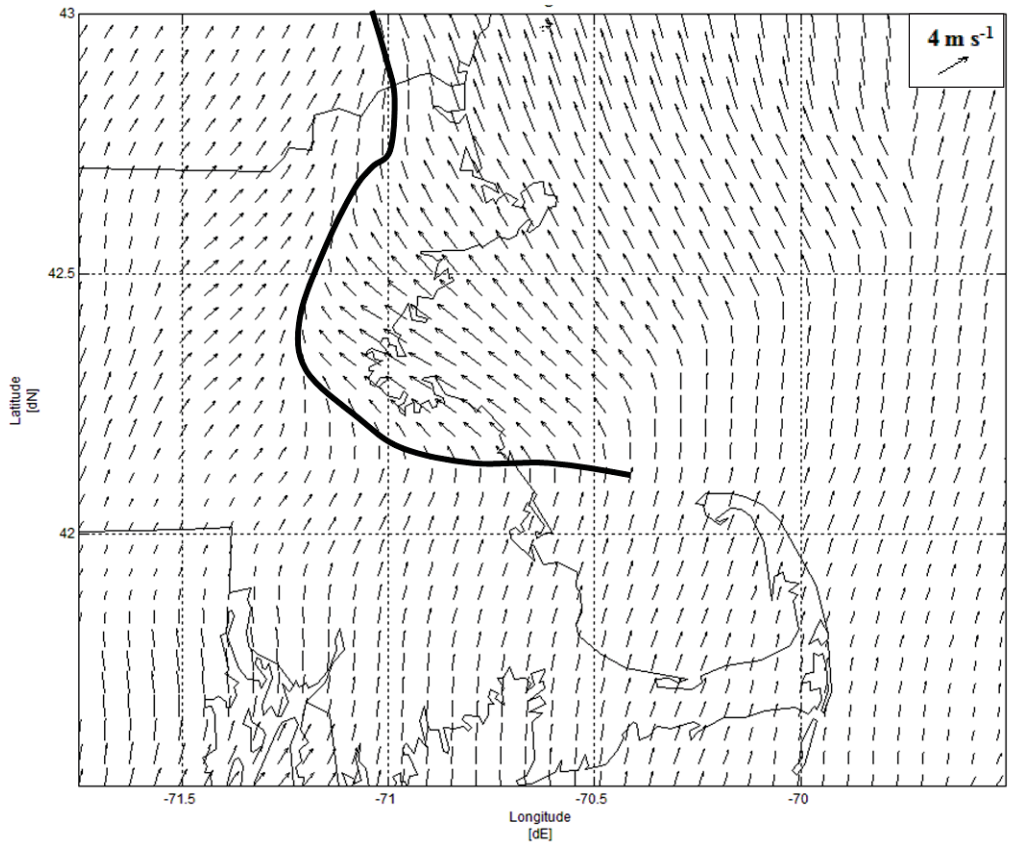

Figure 4.13: Plot of the mid-event average wind vectors for synoptic class 4.

Note that the greatest inland penetration occurs north of Boston. The sea breeze flow south of Boston also seems to progress further south compared to synoptic classes 2, 3, and 4. A slight enhancement of the sea breeze circulation by the synoptic scale flow may be the cause of this difference.

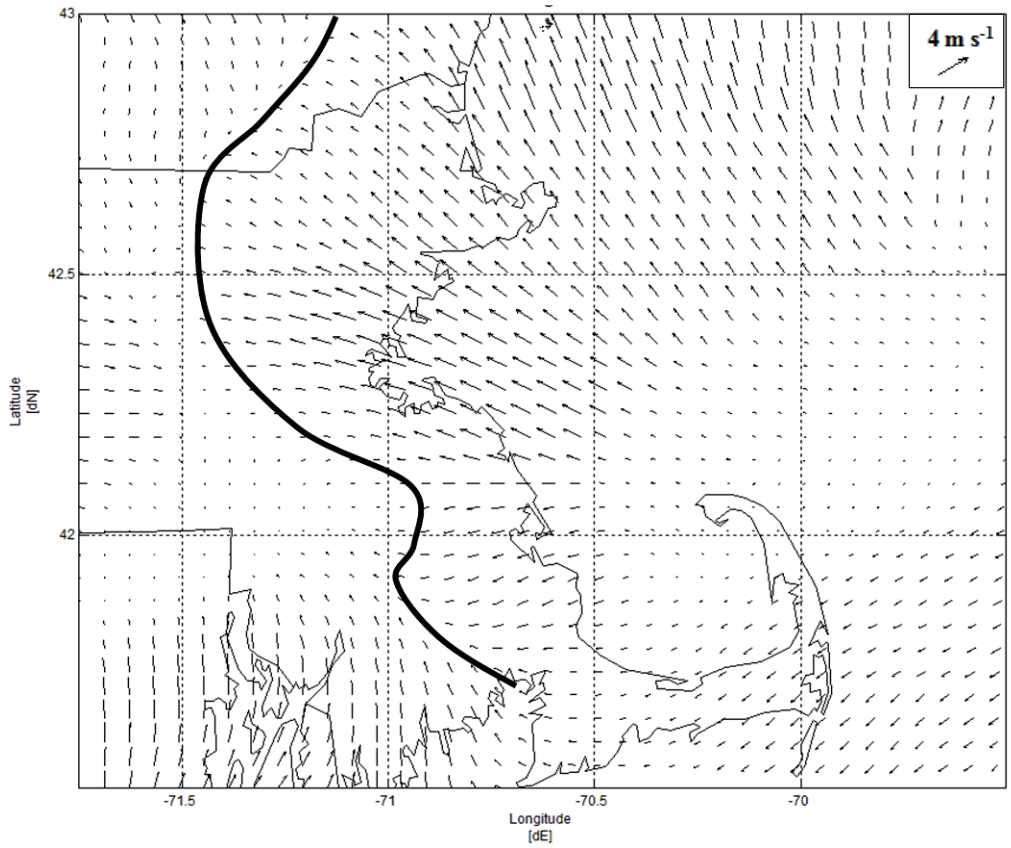

Figure 4.14: Plot of the mid-event average wind vectors for synoptic class 6.

A combined plot showing the location of each of the mid-event average sea breeze fronts is shown in Figure 4.15. This plot shows the decreasing inland penetration of the sea breeze circulation as the flow progresses from anticyclonic to neutral to cyclonic with classes 1 through 3. Synoptic class 4 seems to have the overall shallowest depth of propagation compared to all other classes. There are only subtle difference between the sea breeze fronts for classes 1 and 6. This indicates that northeasterly flow (class 6) and anticyclonic northwesterly flow (class 1) have nearly the same effect of the inland penetration of the sea breeze circulation.

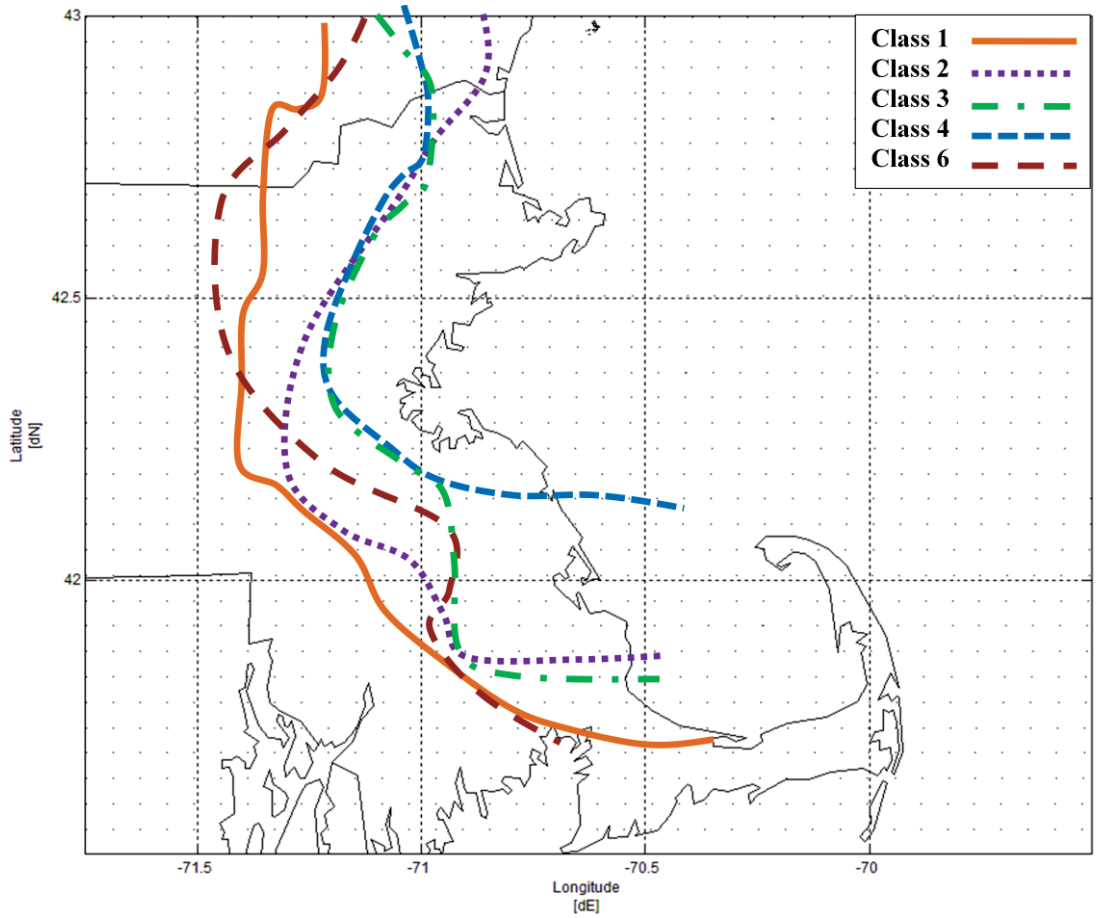

Figure 4.15: Combined plot of the mid-event average wind vectors for synoptic class 1 to 4 and 6. The lines represent the sea breeze front by synoptic class (See legend in upper-right corner).

More research is needed to explain these results. To reduce subjectivity, all of the fast events could be incorporated into the mid-event averages. This idea would prove to be computationally intensive but the resulting plots may have cleaner wind shifts. Also, including and comparing other event types beyond the fast sea breeze events may also introduce some interesting results.

CHAPTER 5

5. Mesoscale Calculations

a. 2-D Calculations

Results of the mesoscale calculations are shown in Figure 5.1, which are similar to the mesoscale results shown by Miller and Keim (2003) for Portsmouth, New Hampshire (*See Appendix E*). A total of 654 events are included in the overall diagram. There were missing data for 76 events and bad data for 149 of the non-events.

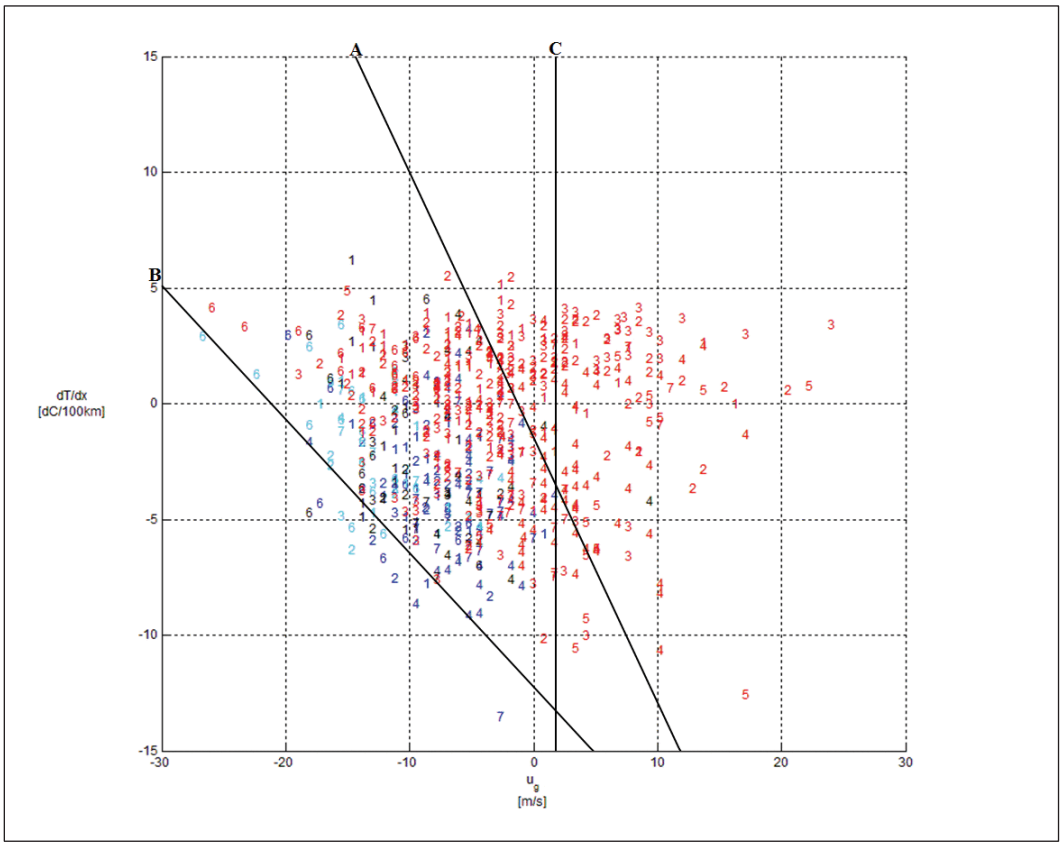

Figure 5.1: All sea breeze, marginal, and non-sea breeze events as a function of their associated cross-shore temperature gradients and geostrophic wind components. The numbers represent the synoptic class of the event. Fast sea breezes are blue (●), slow sea breezes are cyan (●), marginal sea breezes are black (●), and non-sea breezes are red (●).

The area enclosed by lines A, B, and C represents a transition area in which any type of event may occur. The lines represent critical limits between a sea breeze event (fast, slow, and marginal) and a non-sea breeze event. All events to the right of line A (Eq. 5.1) are non-sea breeze events. The area to the right of line C (Eq. 5.2) is also entirely non-sea breeze events, as the resisting u_G component is too strong for a sea breeze event to occur. All events to the left of line B (Eq. 5.3) are sea breeze events. It is evident that proportionally, more non-events fall to the right of the transition area compared to the number of sea breeze events that fall to the left of the transition area. Since the transition area is so large and includes more sea breeze events than non-events, the diagram was further broken down by synoptic class. No plots were created for synoptic class five as it only occurred with non-events, and for class 7 which was the miscellaneous class which contains a mixture of different synoptic patterns.

Line A: $y = -0.67x - 11.99$ (5.1)

Line B: $y = -1.12x - 1.82$ (5.2)

Line C: $x = 1.5$ (5.3)

Figure 5.2 shows only synoptic class 1 events using the same diagram style as described above. The transition area has been noticeably reduced and lines A and B (Eq. 5.4 and 5.5, respectively) are almost parallel. The position of line C (Eq. 5.6) moved slightly to the left. This indicates that synoptic class 1 sea breeze events require slightly less resistance from the seaward u_G component to develop compared to the limit set by line C for all events (Fig. 5.1). The distribution of the events in regards to the transition area has improved somewhat from the overall plot. A higher percentage of the sea breeze events fall to the left of the transition area compared to the plot of all synoptic classes.

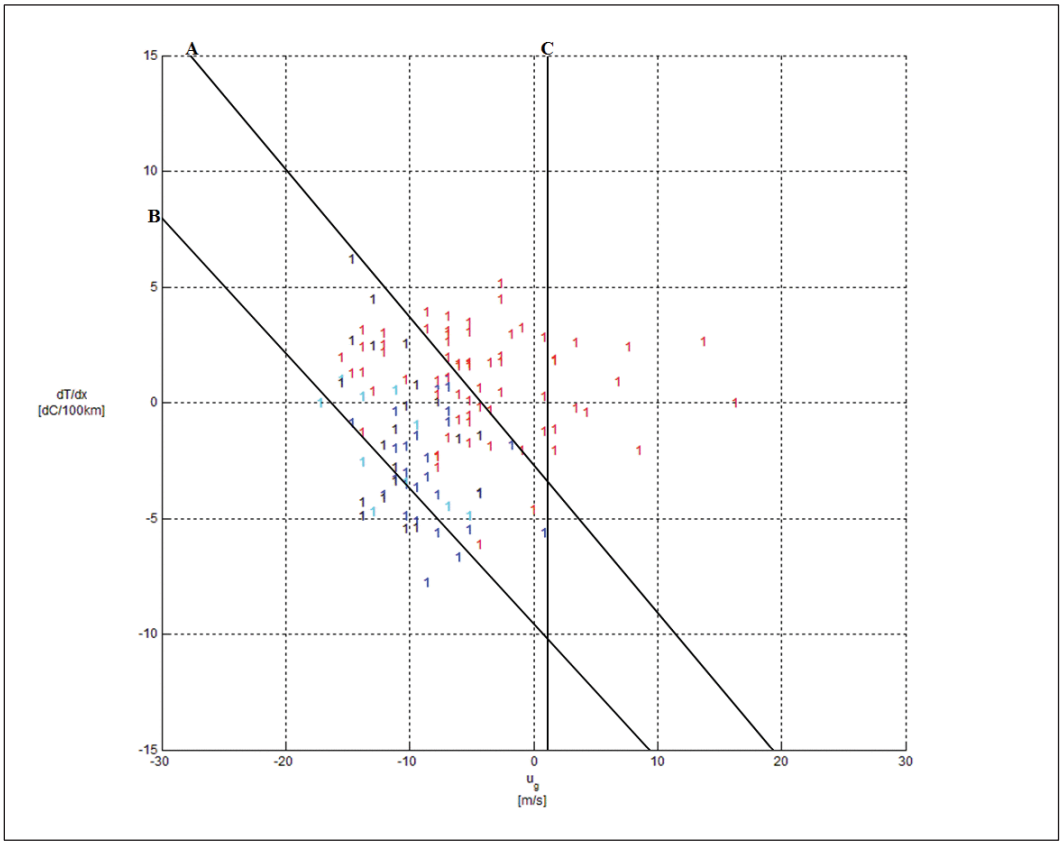

Figure 5.2: Same as Fig. 5.1 for synoptic class 1 only.

$$\text{Line A:} \qquad y = -0.62x - 3.05 \qquad (5.4)$$

$$\text{Line B:} \qquad y = -0.57x - 9.67 \qquad (5.5)$$

$$\text{Line C:} \qquad x = 1 \qquad (5.6)$$

The plot for synoptic class 2 is shown in Figure 5.3. The transition area shrinks compared to synoptic class 1 as lines A and B (Eq. 5.7 and 5.8, respectively) actually meet at the bottom of the diagram. Line C (Eq. 5.9) has become negative indicating that for a synoptic class 2 sea breeze to occur, a weak onshore u_G component is necessary. If any seaward u_G component exists under a synoptic class 2 flow regime, the sea breeze will not occur. The dispersion of events in this plot shows slightly more than half of the

sea breeze events falling to the left of the transition area which is an improvement from the overall plot (Fig. 5.1).

$$\text{Line A:} \qquad y = -1.12x - 6.64 \qquad (5.7)$$

$$\text{Line B:} \qquad y = -0.60x - 10.55 \qquad (5.8)$$

$$\text{Line C:} \qquad x = -2.25 \qquad (5.9)$$

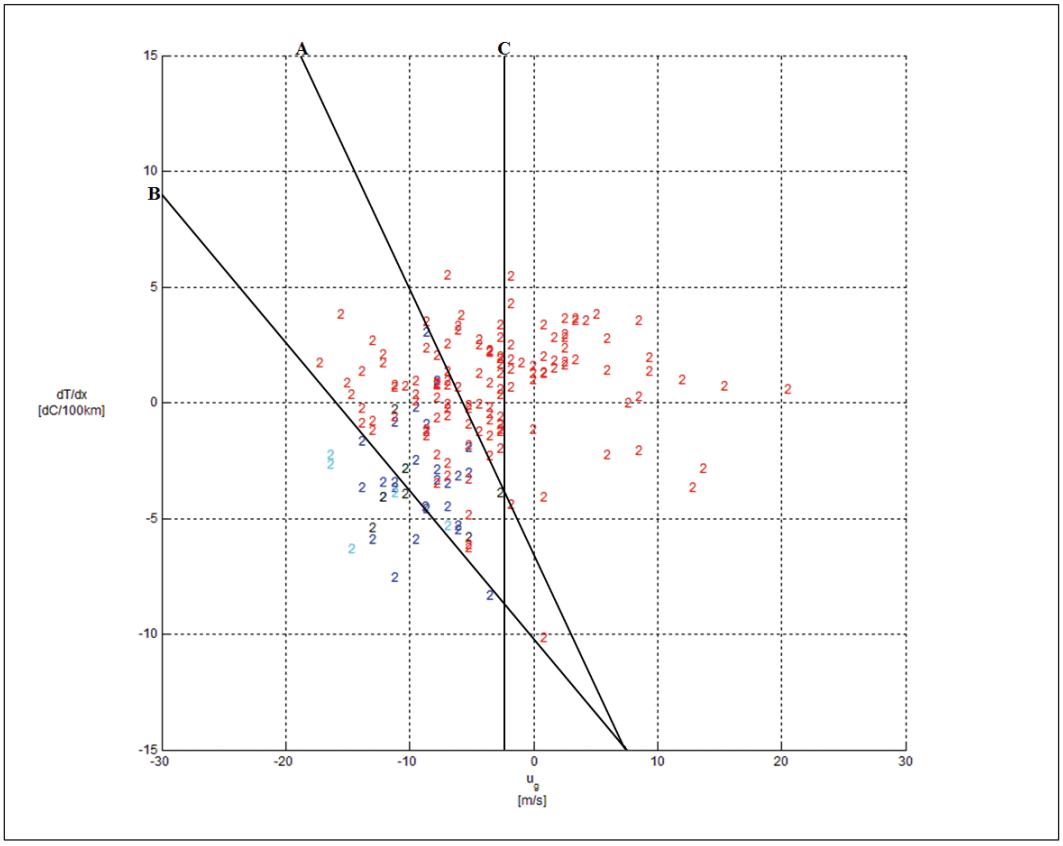

Figure 5.3: Same as Fig. 5.1 for synoptic class 2 only.

In Figure 5.4, the cross-shore components for synoptic class 3 are plotted. The transition area seems to have same width as synoptic class 2. Lines A and B (Eq. 5.10 and 5.11, respectively) meet in a point at the bottom of the plot like with synoptic class 2. Only one sea breeze event falls to the left of Line B which is believable as there were few sea breeze events with synoptic class 3. Of the overall 12 sea breeze events (4 fast, 2 slow, and 6 marginal), there were 3 events with missing data (2 fast and 1 marginal) that

were not plotted. This leaves only 9 events to be plotted versus the available 91 of 132 non-sea breeze events. Line C (Eq. 5.12) is -6.5 m s^{-1} indicating that a moderately strong onshore wind is necessary for a sea breeze to occur with synoptic class 3.

$$\text{Line A:} \qquad y = -1.67x - 17.08 \qquad (5.10)$$

$$\text{Line B:} \qquad y = -0.83x - 15.22 \qquad (5.11)$$

$$\text{Line C:} \qquad x = -6.5 \qquad (5.12)$$

If classes 1, 2 and 3 are examined as a single spectrum of synoptic class as was done in the synoptic scale analysis in Chapter 4, there is a noticeable progression from class 1 to class 3. Note the position of line C moves from 1.5 m s^{-1} with class 1 to -2.0 m s^{-1} with class 2 to -6.5 m s^{-1} with class 3. A stronger onshore mesoscale u_G component is necessary for class 3 sea breeze events to occur. Since class 3 is characterized by cyclonic northwesterly synoptic scale flow, a stronger onshore u_G component is needed to help the sea breeze overcome this opposing force.

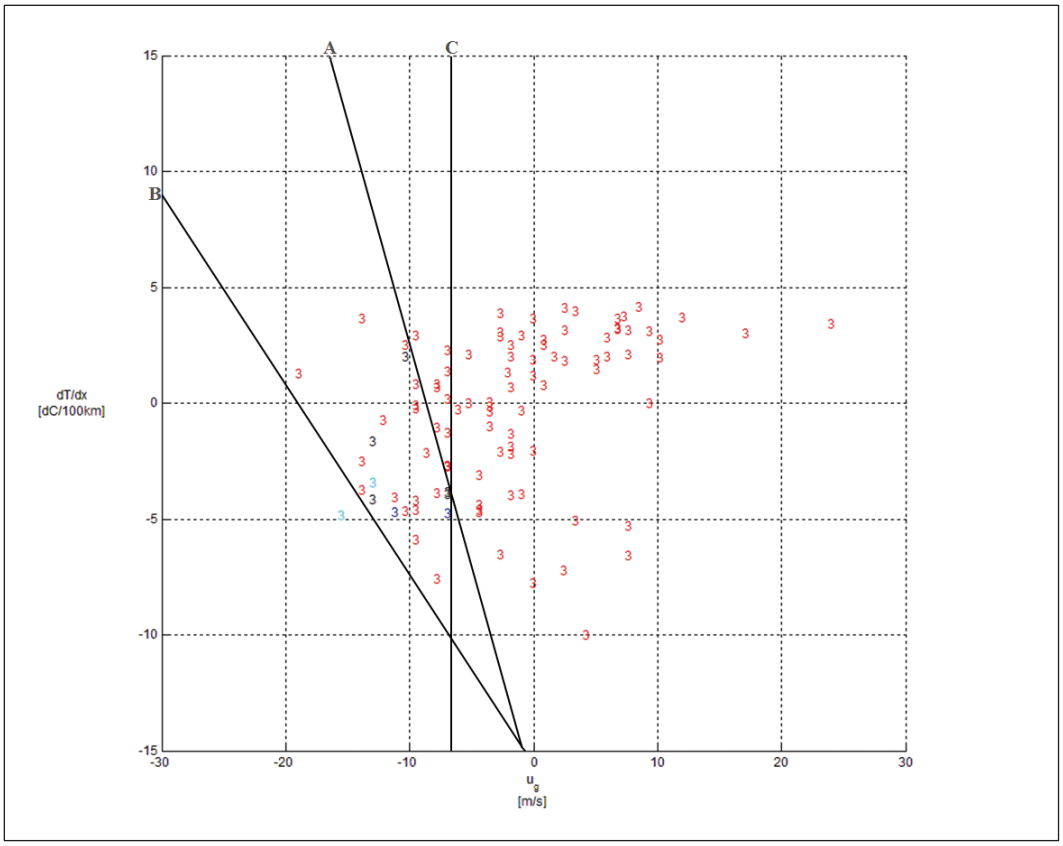

Figure 5.4: Same as Fig. 5.1 for synoptic class 3 only.

The plot of the cross-shore components for synoptic class 4 is depicted in Figure 5.5. Compared to classes 2 and 3, the shape of the transition area has reversed. Lines A and B (Eq. 5.13 and 5.14, respectively) nearly meet at the top of the plot. The transition area is also a little larger with synoptic class 4 compared to classes 1 through 3; though it is still smaller than the area in the overall plot (Fig. 5.1). About half of the sea breeze events fall to the left of the transition area, which is again an improvement compared to the plot of all synoptic classes. There also seems to be more non-events in the transition area than there are to the right of lines A and C (Eq. 5.15).

$$\text{Line A:} \qquad y = -0.63x + 0.05 \qquad (5.16)$$

$$\text{Line B:} \qquad y = -1.07x - 9.115 \qquad (5.14)$$

$$\text{Line C:} \qquad x = 1.5 \qquad (5.15)$$

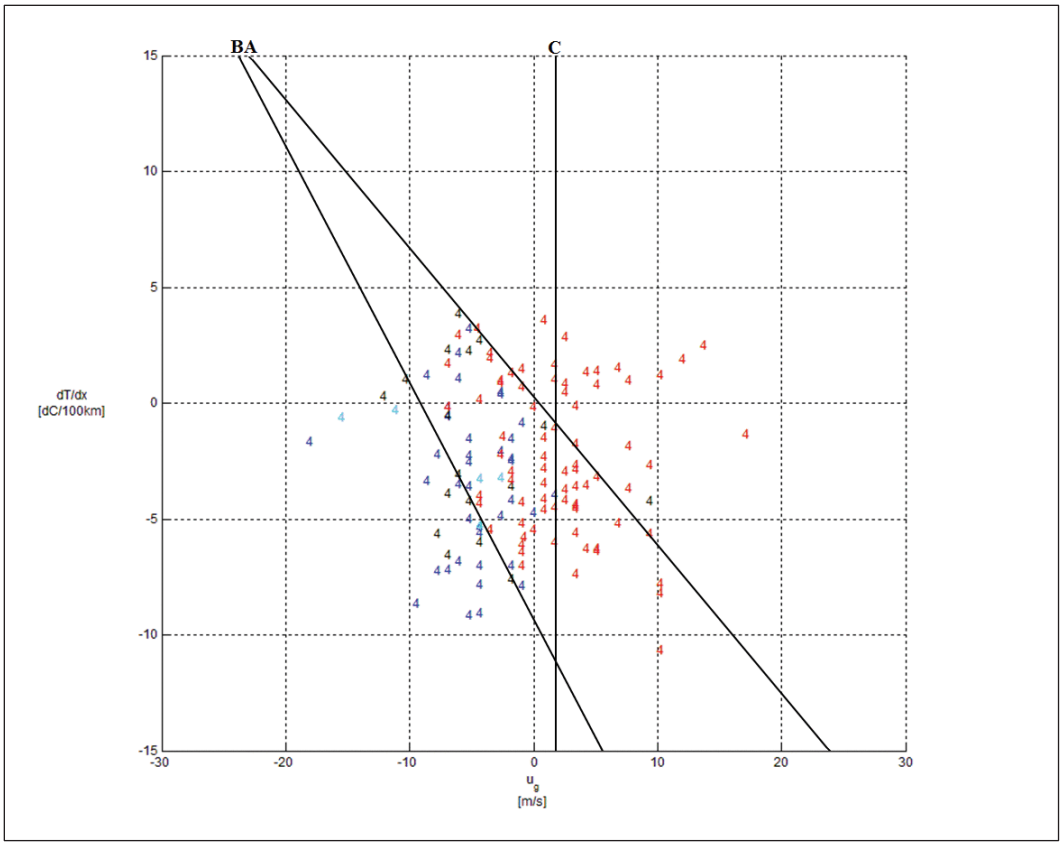

Figure 5.5: Same as Fig. 5.1 for synoptic class 4 only.

Figure 5.6 is the plot of the cross-shore components for synoptic class 6. As with synoptic classes 2 and 3, lines A and B (Eq. 5.16 and 5.17, respectively) meet at a point. The transition area is smallest with class 6; with most of the sea breeze events falling to the left of line B. Non-events make up about 25% of synoptic class 6 events. There was missing data for 1 of the non-event dates so only 15 non-events are plotted. This makes the positioning of line A questionable and makes line C (Eq. 5.18) a theoretical limit at which only non-events would occur. Line C is hypothetical since it is only derived from sea breeze event data and has no non-events to help verify its position. A larger data set could help position the critical limits of synoptic class 6 better.

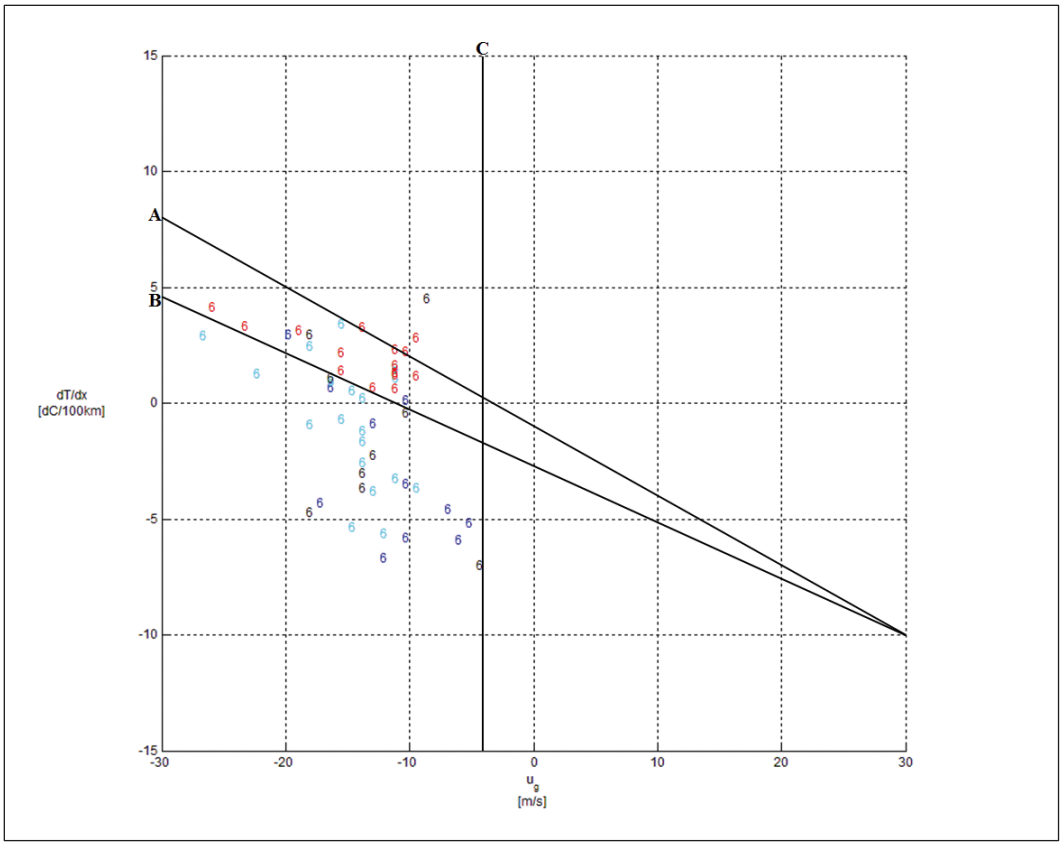

Figure 5.6: Same as Fig. 5.1 for synoptic class 6 only.

$$\text{Line A:} \qquad y = -0.30x - 1 \qquad (5.16)$$

$$\text{Line B:} \qquad y = -0.25x - 2.50 \qquad (5.17)$$

$$\text{Line C:} \qquad x = -4 \qquad (5.18)$$

Figures 5.7 shows line A for each synoptic class and for all events as an overlay. Figures 5.8 and 5.9 are the same as Figure 5.7 except for line B and line C, respectively. Notice the slope of line A becomes steeper between class 1 to class 2 and class 2 to class 3. Line A for classes 1 and 4 seem almost parallel. Line A from the plot of all events is almost parallel to that of synoptic class 2. Synoptic class 6 line A has the most gradual slope of all, although it may be slightly skewed due to a lack of non-events as mentioned before.

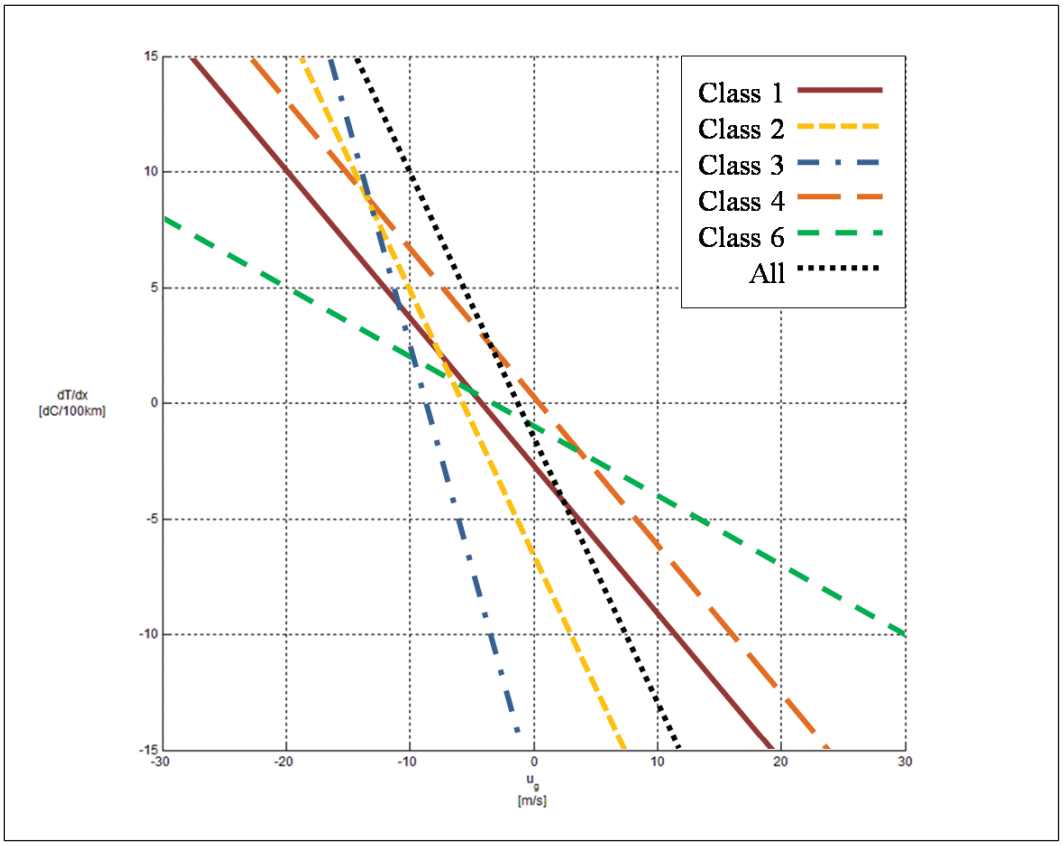

Figure 5.7: Overlay of line A for each synoptic class and for all events.

In Figure 5.8, line B for synoptic classes 1 and 2 are almost the same and they run somewhat parallel to line B for all events. Synoptic class 4 has the steepest slope for line B and synoptic class 6 has the most gradual slope like with line A. The increasing slope seen with line A for classes 1 to 3 (Fig. 5.7) is not present with line B (Fig. 5.8).

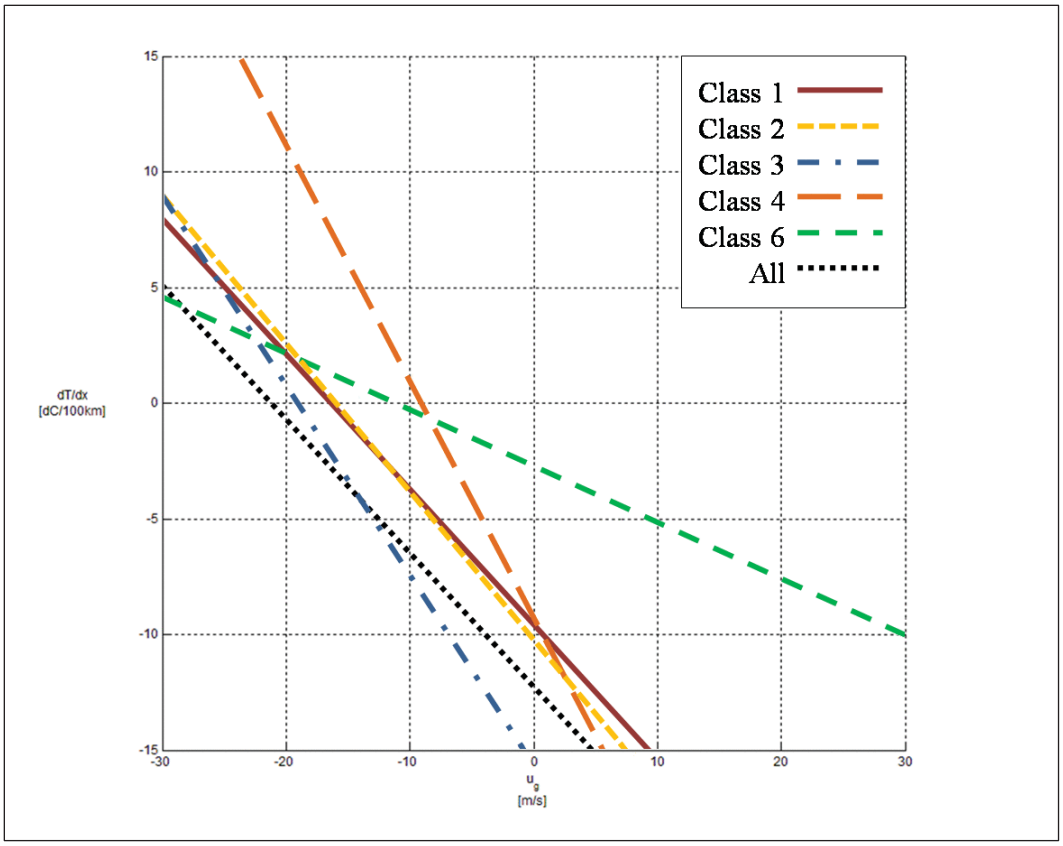

Figure 5.8: Same as Fig. 5.7 only for line B.

Line C gives a good idea how strong of an opposing wind the sea breeze can overcome with any given synoptic class or overall, in the case of the plot of all events. In Figure 5.9, line C for each class is plotted along with the line C from the overall plot (Fig. 5.1). The strongest offshore u_G wind component that events as a whole could overcome was approximately 2.0 m s^{-1}. This limit is set by synoptic class 4 as line C for class 4 is in the same place as line C for all events (Fig. 5.9). Synoptic class 1 is very close to this limit at about 1.5 m s^{-1}. Synoptic classes 2, 3, and 6 all require an onshore u_G wind component to develop.

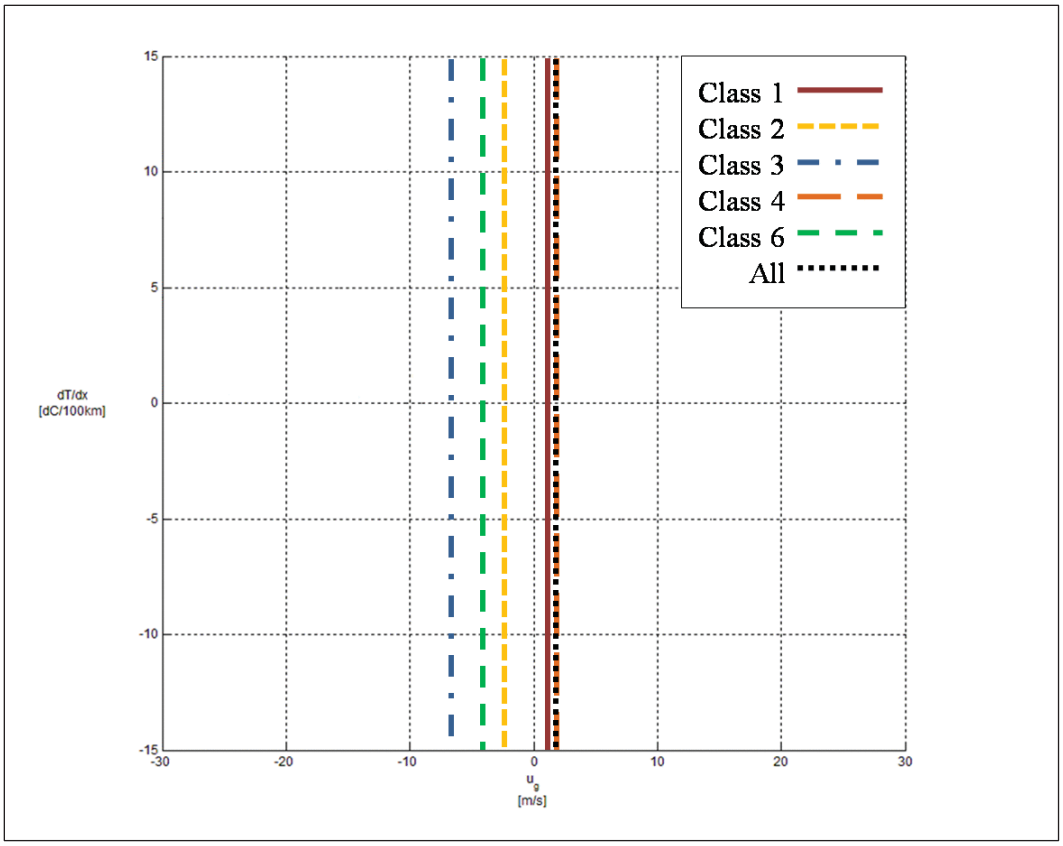

Figure 5.9: Same as Fig. 5.7 only for line C.

Figures 5.8 and 5.7 suggest a similarity in the way the sea breeze develops with synoptic classes 1 and 4. Lines B and C were almost the same for these two classes. For lines A and B, synoptic class 6 seemed to be the greatest outlier which is due to the lack of non-events. A larger data set may help to refine the critical limits for class 6. Synoptic class 3 seemed to need the largest onshore u_G wind component to develop which may be due to a lack of sea breeze events with this class. On the other hand, synoptic class 3 features the strongest northwesterly winds so a larger onshore u_G wind component is a plausible necessity for development.

b. 3-D Calculations

Sea breeze events (fast and slow only) were plotted against non-sea breeze events on a three-dimensional plot (Fig. 5.10). The variables used were the surface u_G wind component (m s^{-1}), the cross-shore temperature gradient (°C/100 km), and the 850 hPa u_G wind component (m s^{-1}). There are a total of 321 non-events on this plot and 127 sea breeze events.

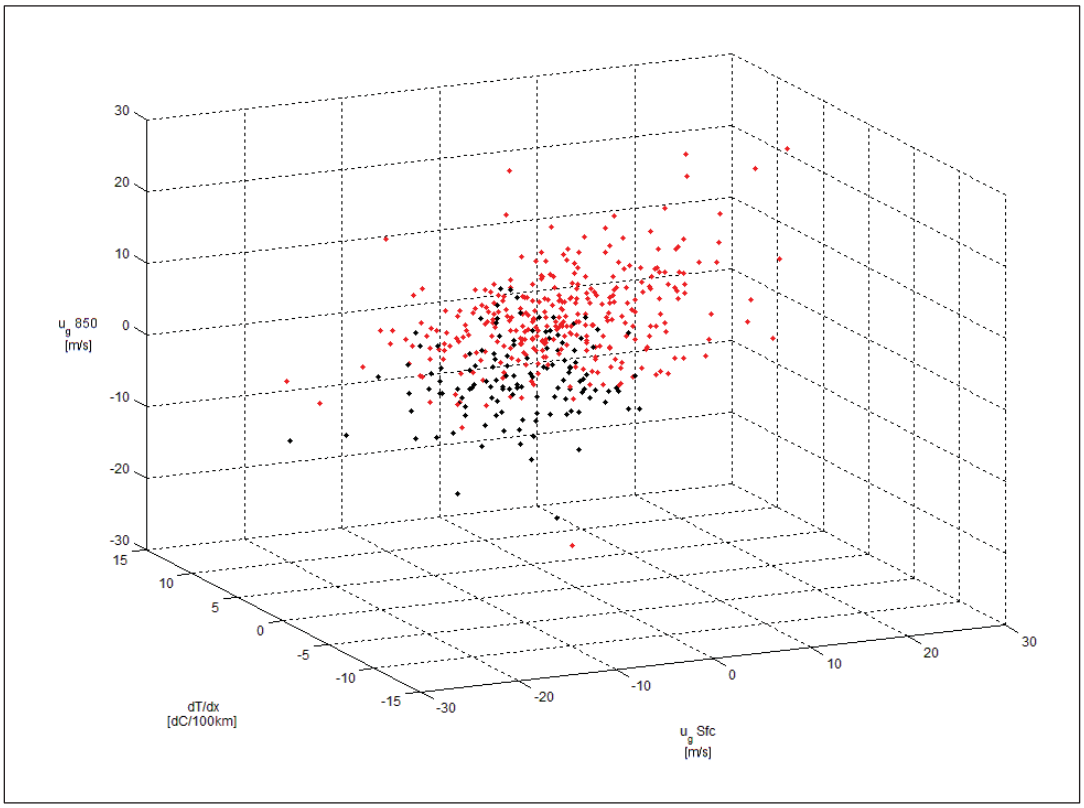

Figure 5.10: 3-D plot of surface uG wind component, cross-shore temperature gradient, and 850 hPa uG wind component. Black dots represent sea breeze events and red dots represent non-sea breeze events.

Some separation does exist between the sea breezes and the non-sea breezes, though there is a large transition area. One of the non-events, Sept. 26, 2006, has an 850 hPa u_G wind component of -25.1 m s^{-1} which is major outlier in comparison to all the other points. A low-level jet was present over Cape Cod at 0000 UTC on Sept. 27, 2006,

which is influencing the interpolated 850 hPa u_G wind component at 1500 UTC. The strongest opposing u_G wind component at 850 hPa that sea breeze events could overcome was 13.6 m s^{-1}, which can be seen in Figure 5.11.

Figure 5.11 shows a two-dimensional plot of the 850 hPa u_G wind component versus the cross-shore temperature gradient (at the surface). There is a large transition area containing both sea breeze and non-sea breeze events.

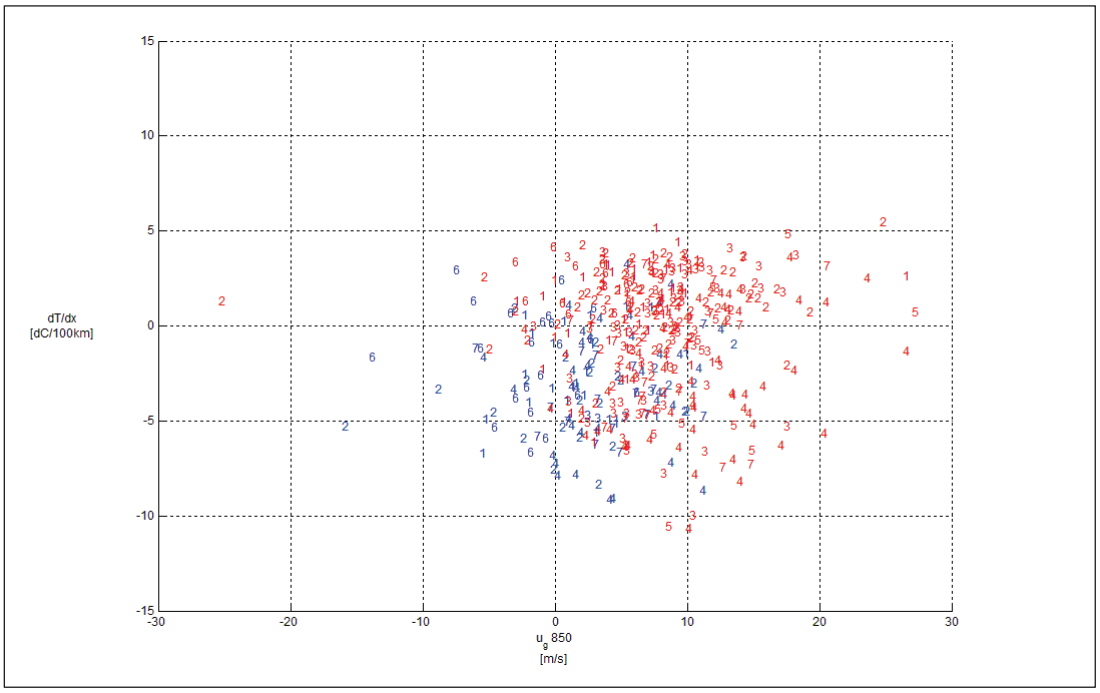

Figure 5.11: 2-D plot of the 850 hPa u_G wind component versus the surface cross-shore temperature gradient. The numbers represent the synoptic class of the event. The blue numbers are sea breeze events and the red numbers are non-sea breeze events.

Perhaps if the three-dimensional plot is broken down by synoptic class, as was done with the two-dimensional plot, a clearer separation between sea breeze and non-sea breeze events will emerge. It may also be useful to look at the u_G wind component at 925 hPa which would be deeper within the sea breeze. The sea breeze circulation only extends vertically to about 900 hPa and this depth can vary (Miller *et al.*, 2003). The

difference between 850 hPa and 925 hPa might mean being outside versus inside the circulation.

CHAPTER 6

6. Radar Analysis of Convection

Between 2002 and 2007, 24 dates were chosen that showed convection in a favorable region for the Massachusetts sea breeze. The favorable region was determined by examining the possible inland penetration of the sea breeze front in chapter 4. All event types were evaluated for existence of convection which included 110 fast events, 32 slow events, 48 marginal events, and 372 non-events; a total of 562 events. When conditions are favorable for a sea breeze to develop along the Massachusetts coastline, convection occurs about 4% of the time. The majority of the cases where convection passed near the Massachusetts coastline occurred on non-sea breeze event days. The non-event is defined based on observations at KBOS and therefore is only representative of that location; therefore, a sea breeze can still occur at other coastal locations despite the event type. Of the 24 days, there were only 5 fast events and no slow events. The remaining 19 events consisted of 4 marginal events and 15 non-sea breeze events.

The 24 dates were initially separated into two groups by whether or not the convection was affected by or caused by the sea breeze front. These two groups were further divided to create four total groups. The cases where convection was affected by the sea breeze were broken into two groups. One group contained cases where the sea breeze along the Massachusetts coastline was involved in the convective interaction (12 cases) and the other group was for cases where convection that was affected by a sea breeze along the Rhode Island or New Hampshire coastlines (2 cases). The cases not related to the sea breeze were classified into the other two groups, one for cases in which the sea breeze did not exist and convection still developed or was enhanced (7 cases), and one for cases where the sea breeze did not exist and no enhancement occurred (3 cases).

In the following subsections, two examples of each group (not including the non-Massachusetts cases) will be discussed.

a. Sea Breeze, Effect on Convection

On August 17, 2002, convective cells both develop along and interact with the sea breeze front (SBF). The SBF is visible in the radar imagery at 1925 UTC (Fig. 6.1), indicated by the "thin line" in reflectivity near the coast. By 2015 UTC, two convective cells can be seen at 41.75°N -70.75°E and 41.85°N -70.60°E (Fig. 6.2). The sea breeze is still visible in the reflectivity. The cells move northwest and at 2049 UTC, the first cell has moved to 42.85°N -70.7°E (into SBF) and has been enhanced (Fig. 6.3). By 2118 UTC this cell has weakened and begun to dissipate (Fig. 6.4). The wind vector plots for 1900 UTC and 2000 UTC are shown in Figures 6.5 and 6.6 respectively. Notice the position of the sea breeze front is the relatively the same as the "thin line" in the reflectivity.

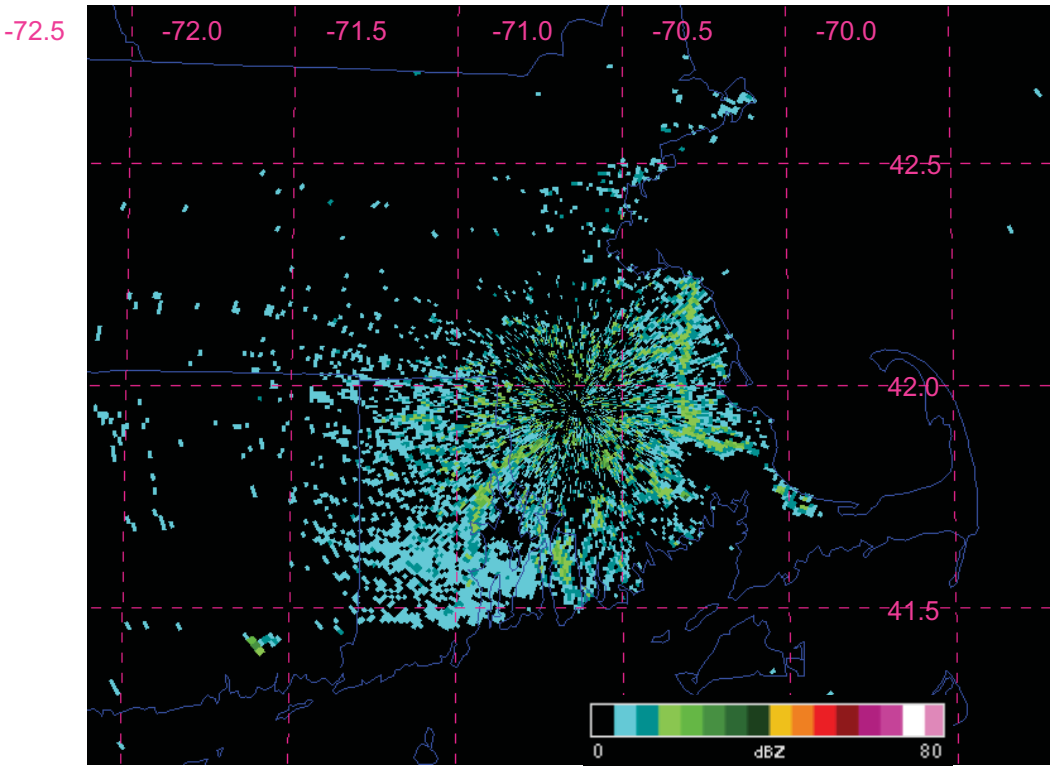

Figure 6.1: Base reflectivity at 1925 UTC from Taunton, MA (KBOX) radar on Aug. 17, 2002. Magenta dashed lines represent latitude and longitude (labeled in degrees N and E). The blue lines are state borders. Refer to legend at bottom-right for reflectivity values.

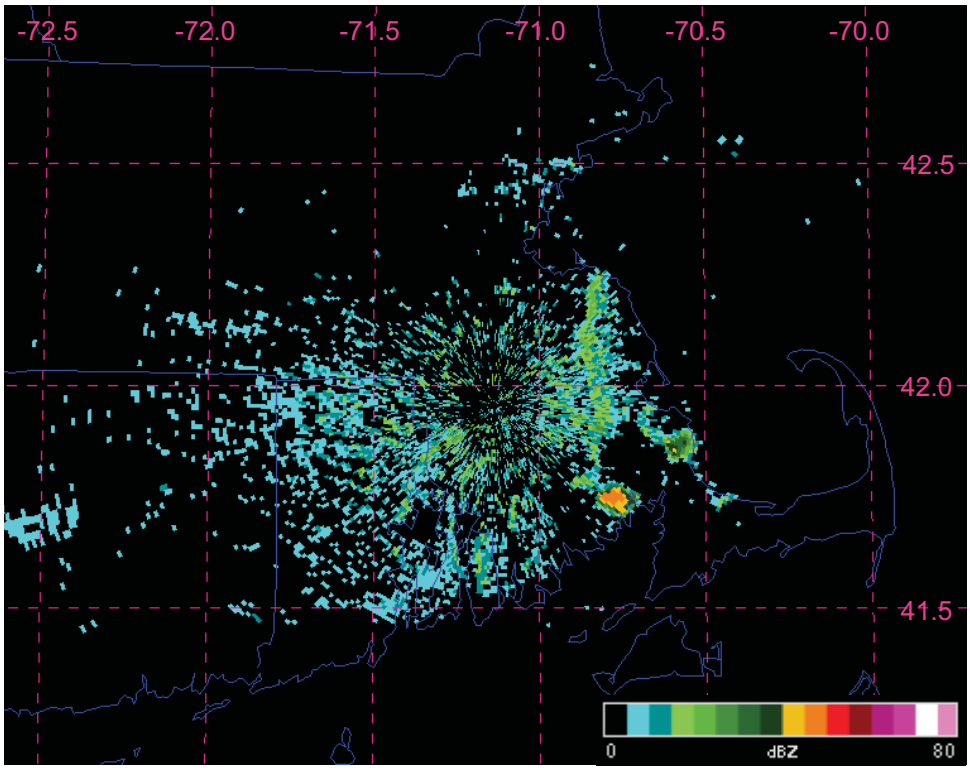

Figure 6.2: Same as Fig. 6.1 above except valid at 2015 UTC.

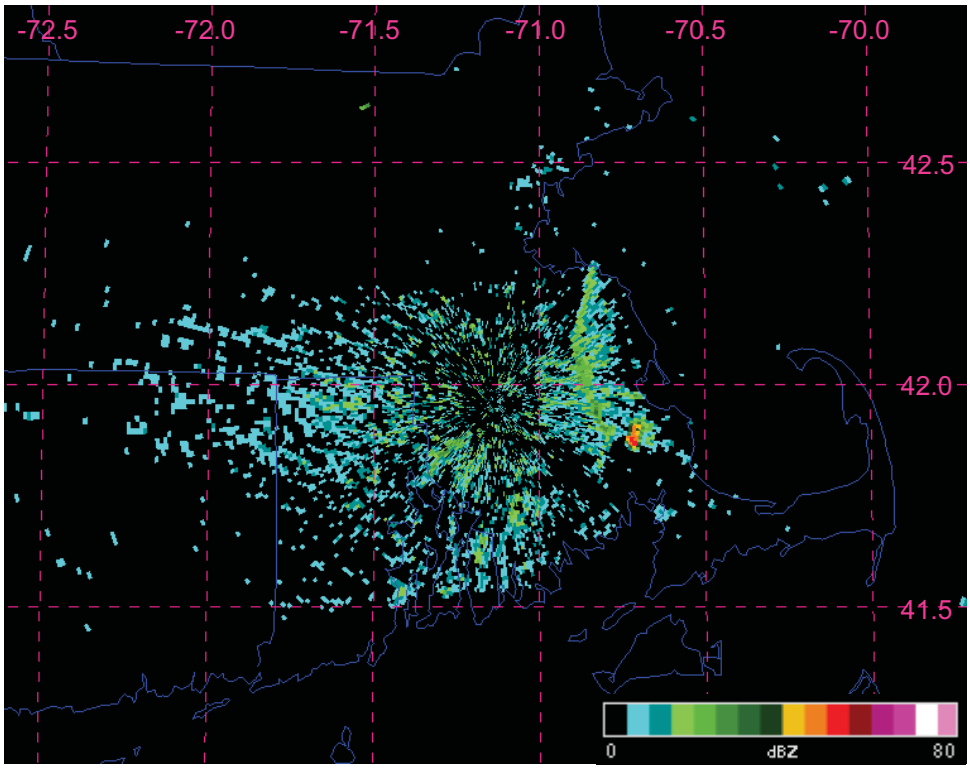

Figure 6.3: Same as Fig. 6.1 above except valid at 2049 UTC.

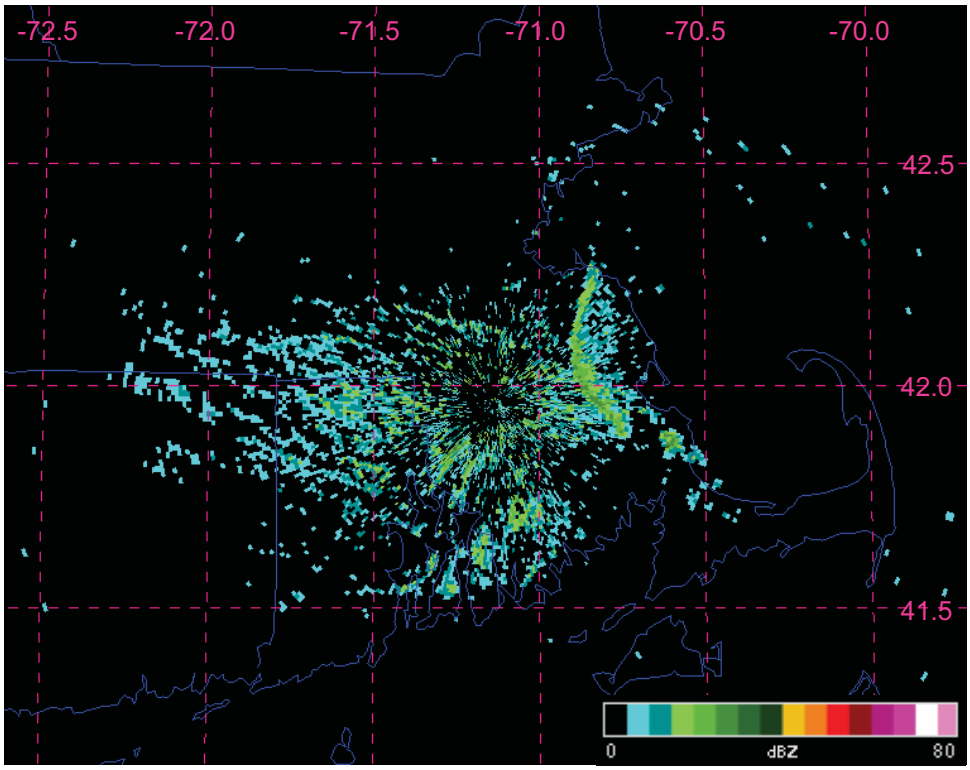

Figure 6.4: Same as Fig. 6.1 above except valid at 2118 UTC.

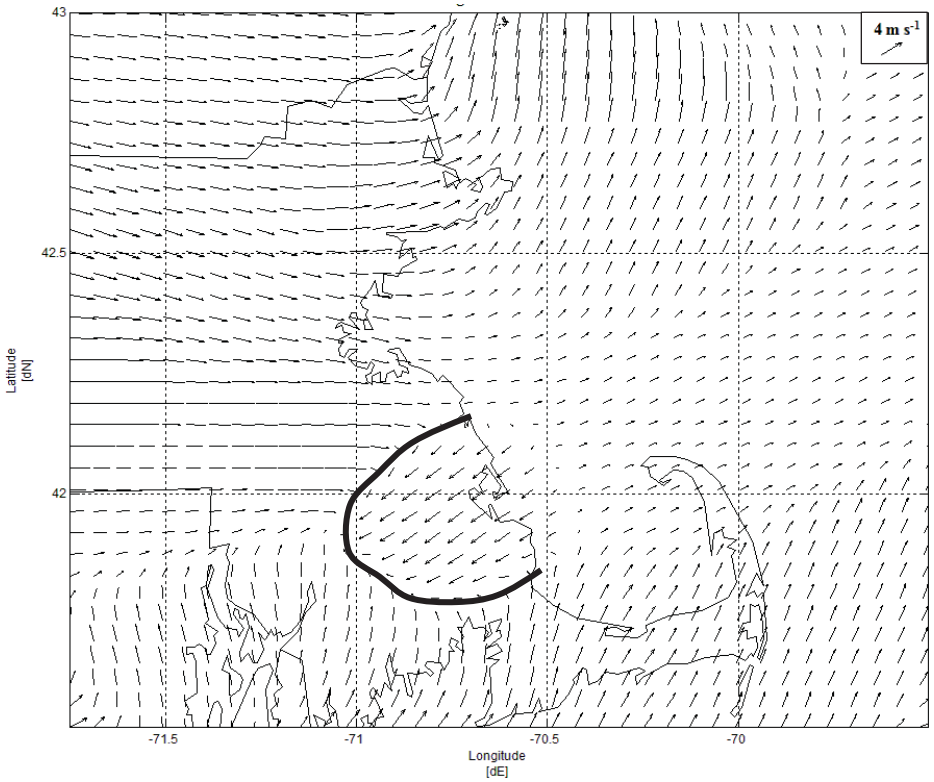

Figure 6.5: Wind vector plot for Aug. 17, 2002 at 1900 UTC. Solid black line indicates analyzed position of sea breeze front.

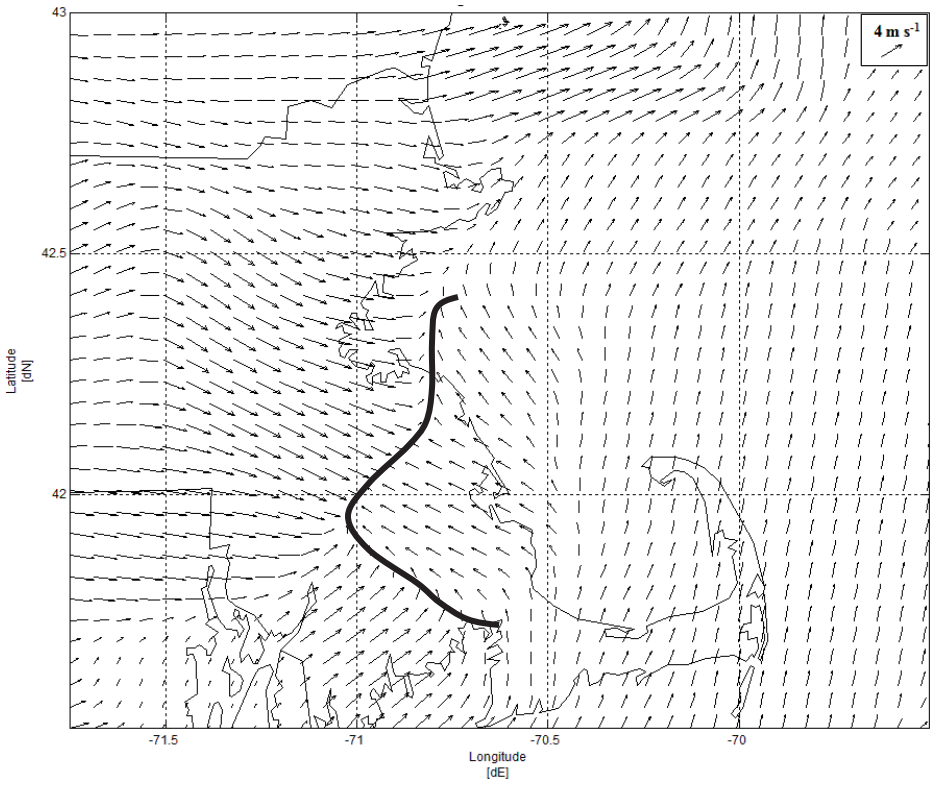

Figure 6.6: Same as Fig. 6.5 above except valid for 2000 UTC.

On August 29, 2004, a pre-existing cell interacts with the SBF and is enhanced. In Figure 6.7, the SBF is visible just northeast of the intersection of 42.50°N and -71.00°E. A cell has begun to develop at 42.40°N -71.25°E. The cell pushes northeast towards the SBF and at 1810 UTC shows no real enhancement (Fig. 6.8). At 1820 UTC, the cell has just encountered the SBF and has intensified to about 45 dBZ (Fig. 6.9). The cell reaches a maximum intensity of 50 dBZ at 1825 UTC (Fig. 6.10) and begins to weaken by 1845 UTC (Fig. 6.11). The wind vector plot for 1800 UTC (Fig. 6.12) shows the sea breeze front in the same location as the reflectivity “thin line”.

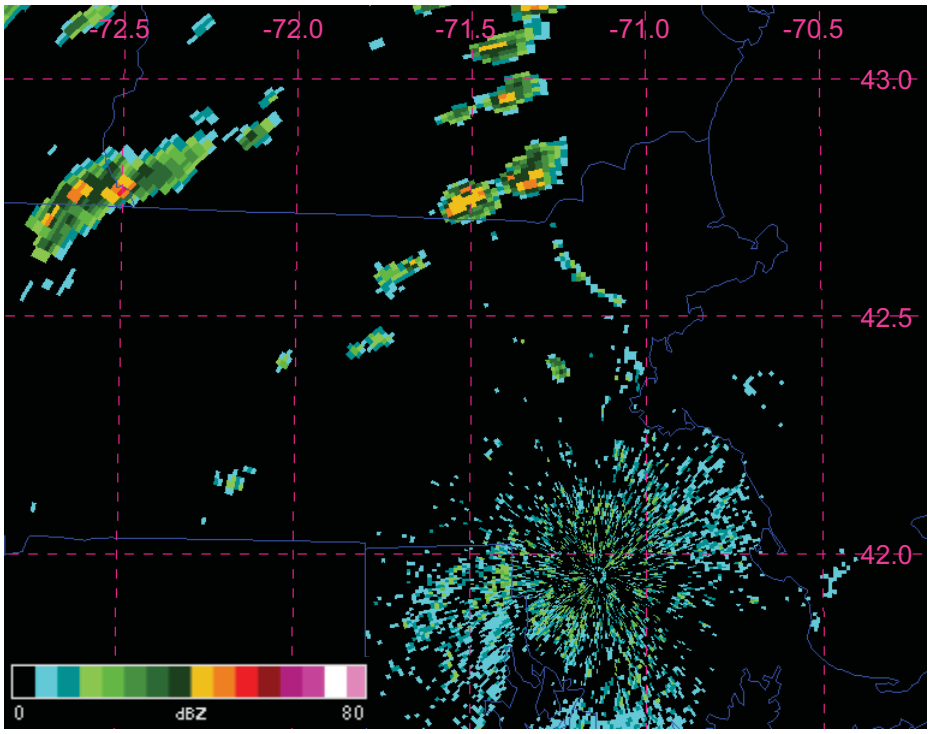

Figure 6.7: Base reflectivity at 1750 UTC from Taunton, MA (KBOX) radar on Aug. 29, 2004. Magenta dashed lines represent latitude and longitude (labeled in degrees N and E). The blue lines are state borders. Refer to legend at bottom-left for reflectivity values.

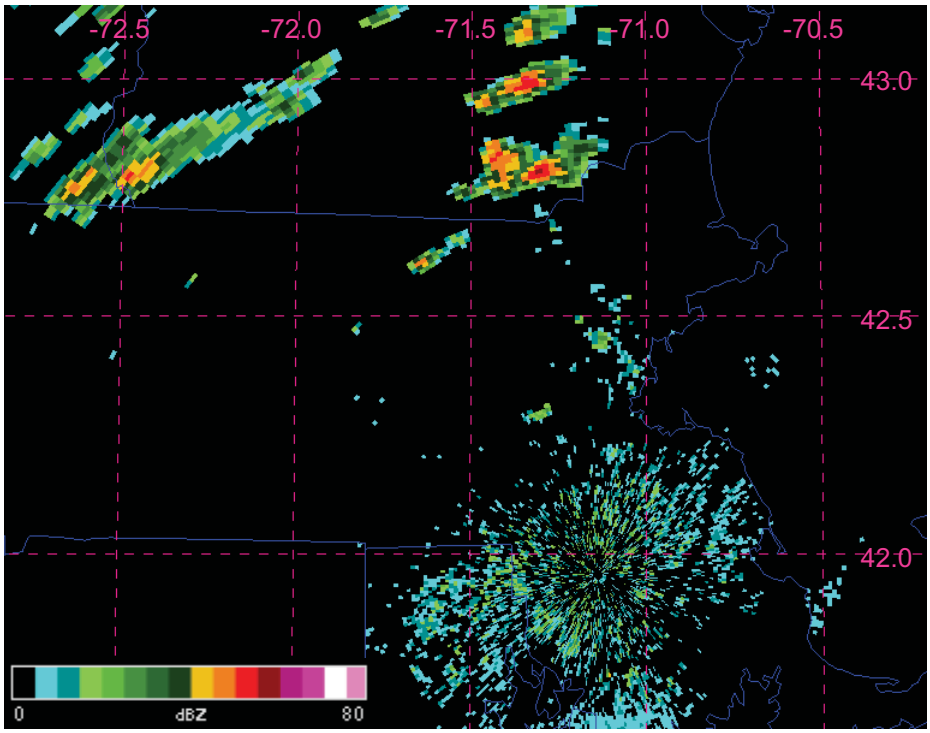

Figure 6.8: Same as Fig. 6.7 above except valid 1810 UTC.

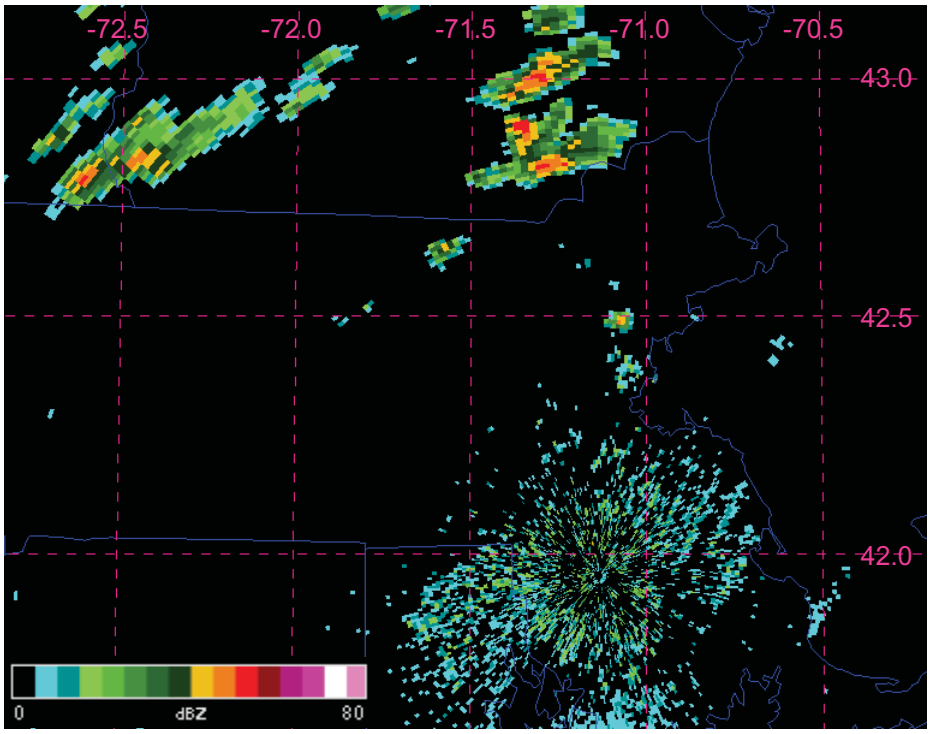

Figure 6.9: Same as Fig. 6.7 above except valid 1820 UTC.

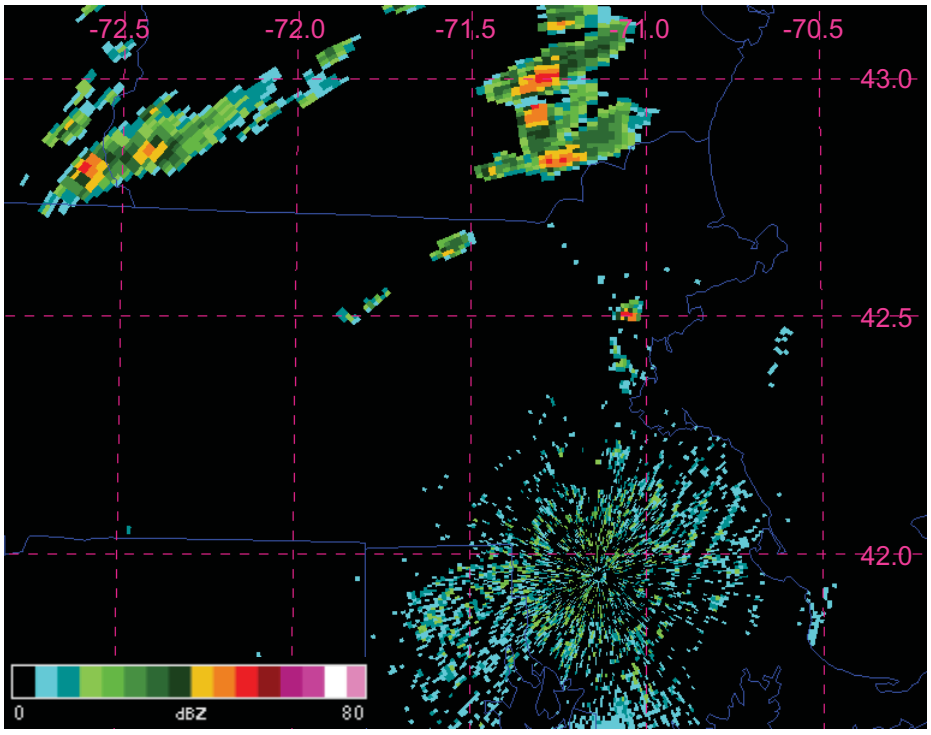

Figure 6.10: Same as Fig. 6.7 above except valid 1825 UTC.

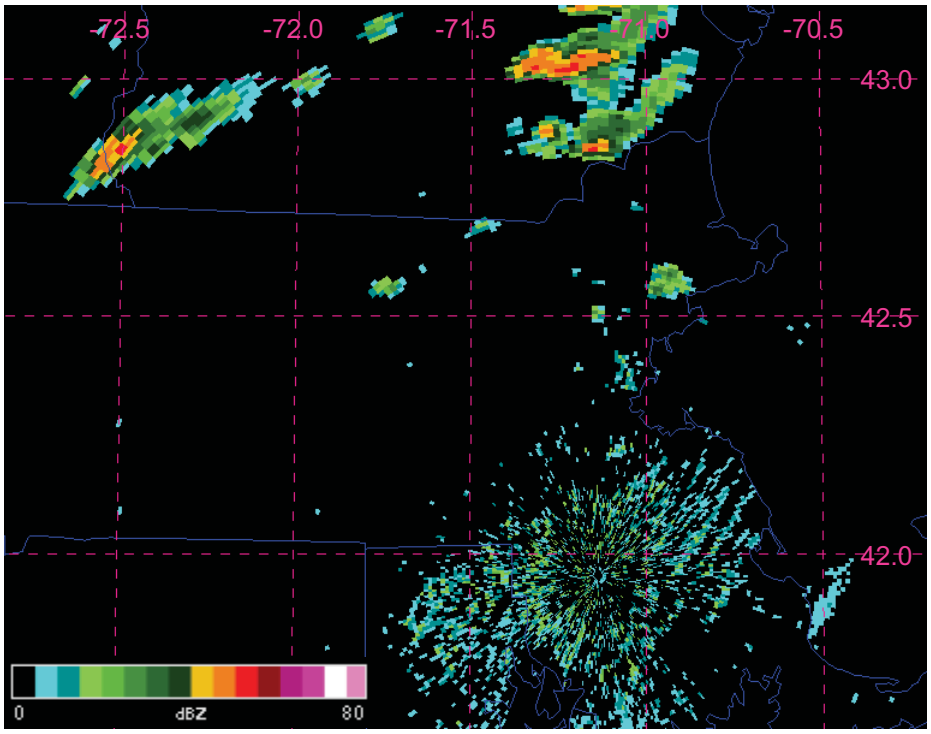

Figure 6.11: Same as Fig. 6.7 above except valid 1845 UTC.

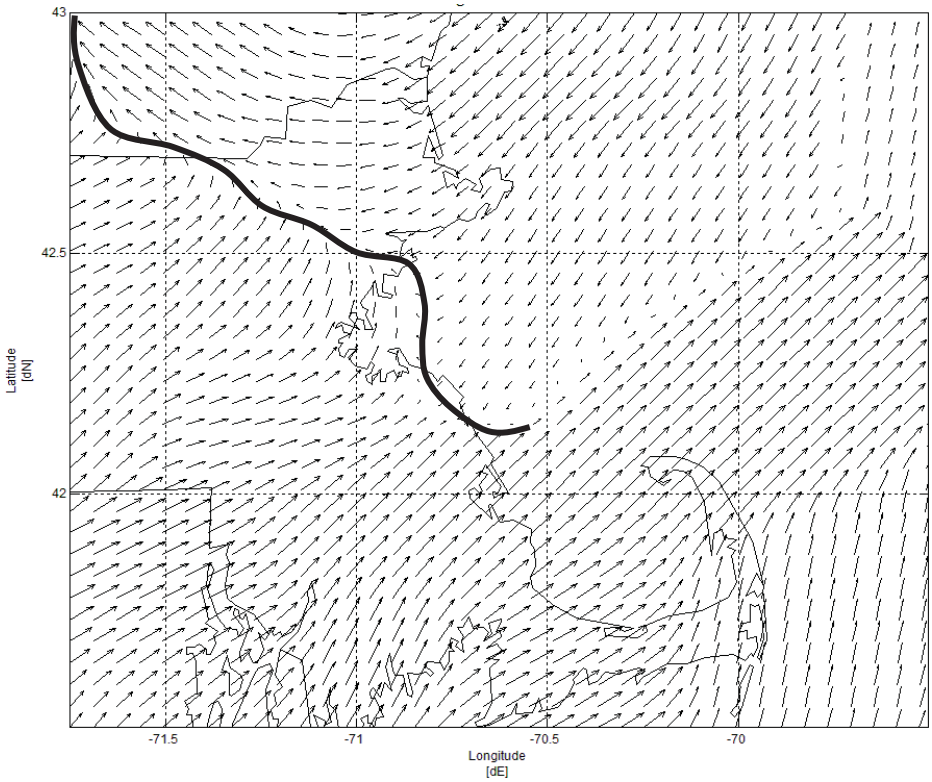

Figure 6.12: Wind vector plot for Aug. 29, 2004 at 1800 UTC. Solid black line indicates analyzed position of sea breeze front.

August 17, 2002 was a non-event and was categorized as a synoptic class 3 indicating a post-frontal cyclonic flow regime over Boston. The northwesterly flow is visible in the wind vector plots (Fig. 6.6 and 6.7). The event type was determined strictly from the KBOS METAR observations so although a sea breeze did not occur in Boston, it was still possible for one to develop somewhere along the coast.

August 29, 2004 was a fast event and was categorized as a synoptic class 4 indicating pre-frontal southwesterly surface flow which is visible in the wind vector plot (Fig. 6.12). The limited penetration of the sea breeze to the south of Boston matches the results of the inland penetration portion of this study in Chapter 4. The sea breeze is no longer in Boston at the time of the convection, but is still present inland, north of Boston.

b. No Sea Breeze, Convection Develops or is Enhanced

At 1900 UTC on July 10, 2006, a cell begins to develop at 41.90°N -71.30°E (Fig. 6.13). By 1912 UTC, the cell starts to strengthen and a tiny area of reflectivity equal to 40 dBZ develops (Fig. 6.14). The cell continues its progression northeast and intensifies slightly to 45 dBZ at 1918 UTC (Fig. 6.15). The cell reaches its maximum strength with a significant area of reflectivity around 45 dBZ at 1924 UTC (Fig. 6.16) and then weakens at 1941 UTC (Fig. 6.17). The wind vector plot for 1900 UTC shows this cell developed in an area of southwesterly winds with no visible convergence (Fig. 6.18).

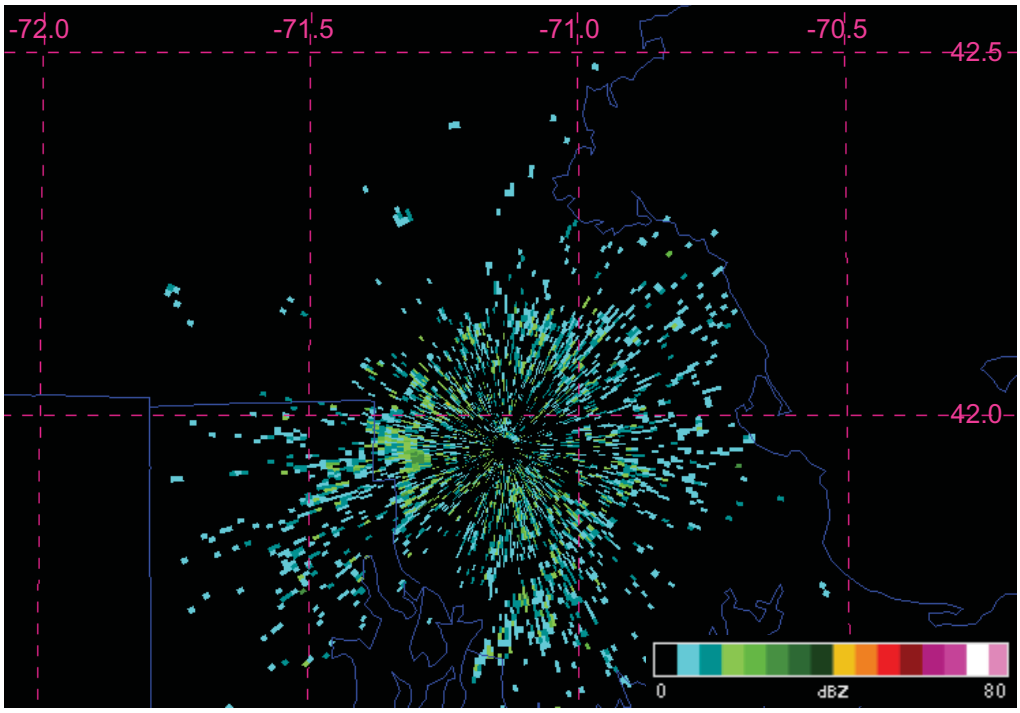

Figure 6.13: Base reflectivity at 1900 UTC from Taunton, MA (KBOX) radar on July 10, 2006. Magenta dashed lines represent latitude and longitude (labeled in degrees N and E). The blue lines are state borders. Refer to legend at bottom-right for reflectivity values.

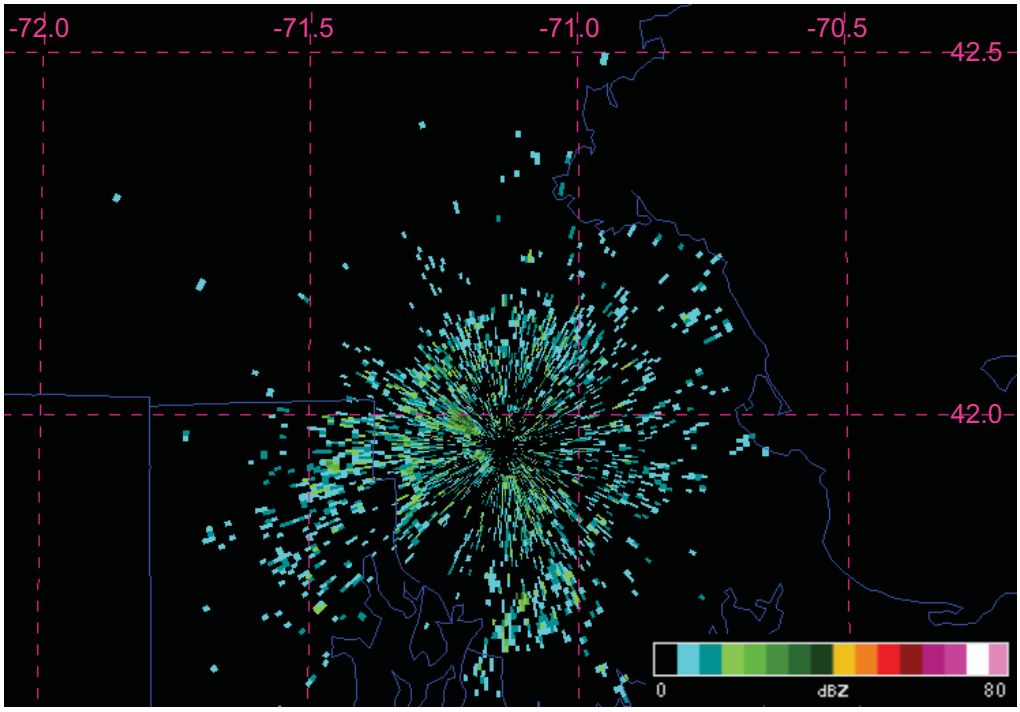

Figure 6.14: Same as Fig. 6.13 above except valid for 1912 UTC.

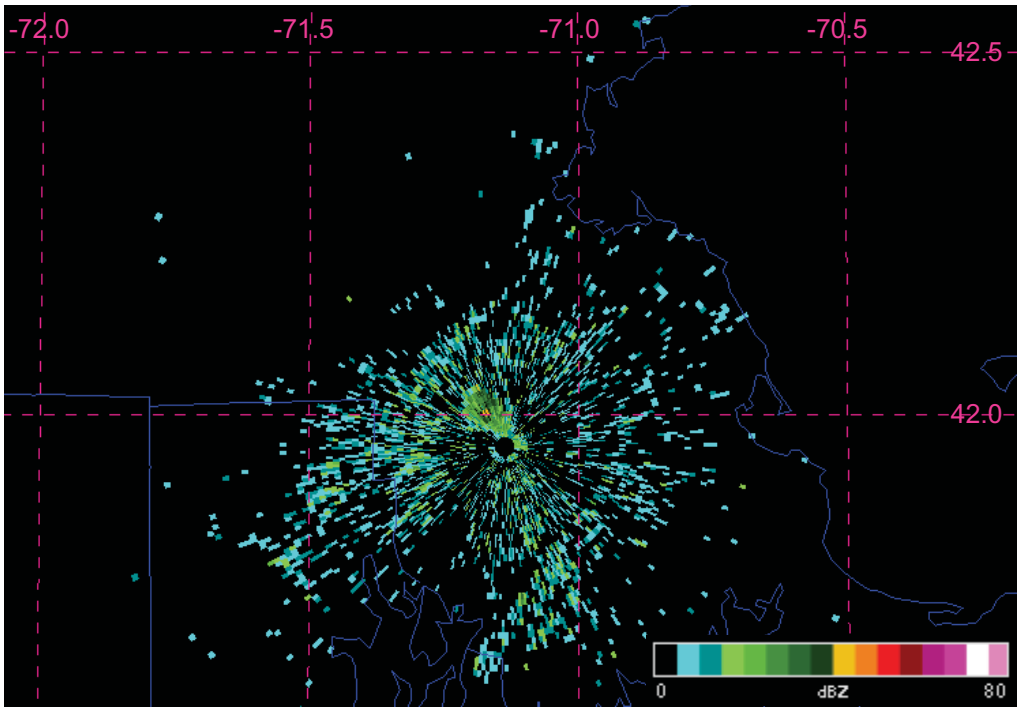

Figure 6.15: Same as Fig. 6.13 above except valid for 1918 UTC.

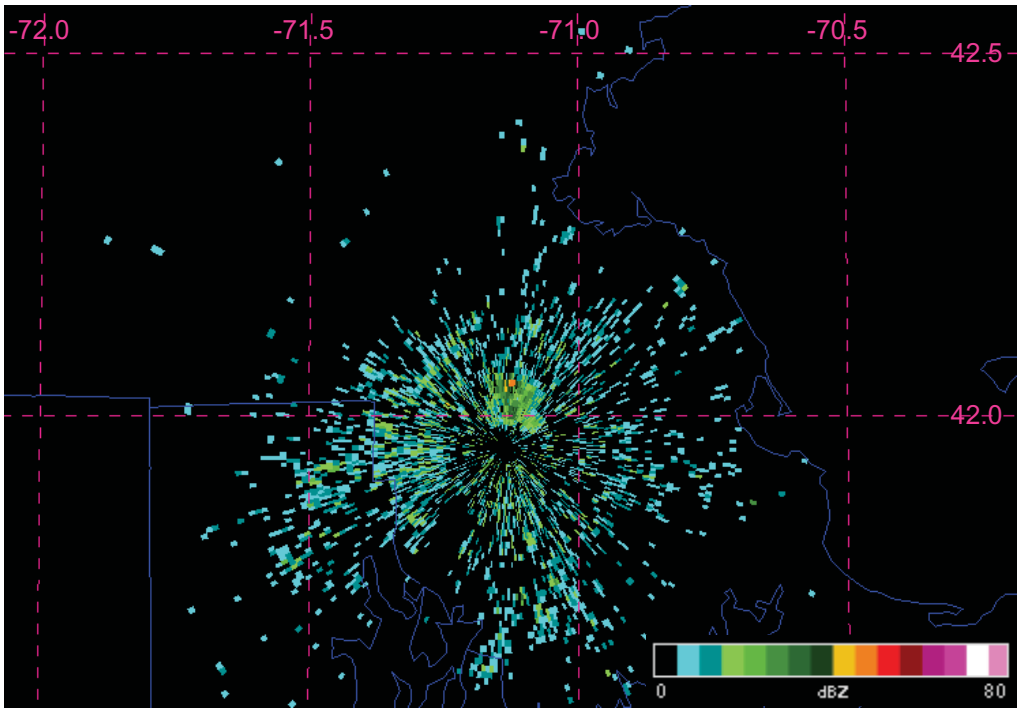

Figure 6.16: Same as Fig. 6.13 above except valid for 1924 UTC.

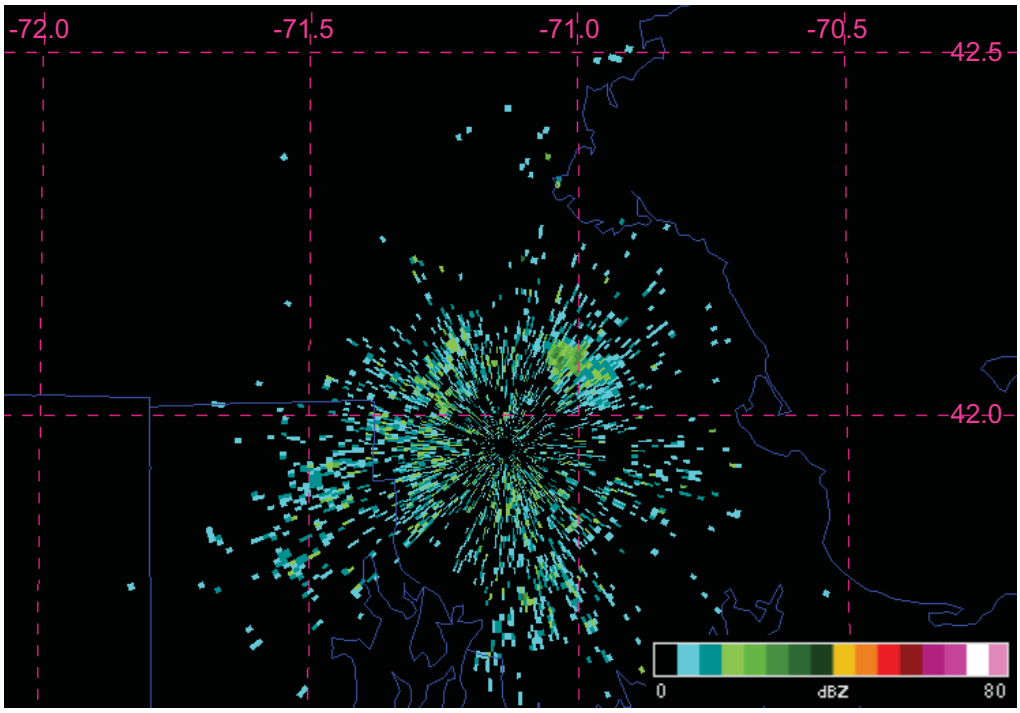

Figure 6.17: Same as Fig. 6.13 above except valid for 1941 UTC.

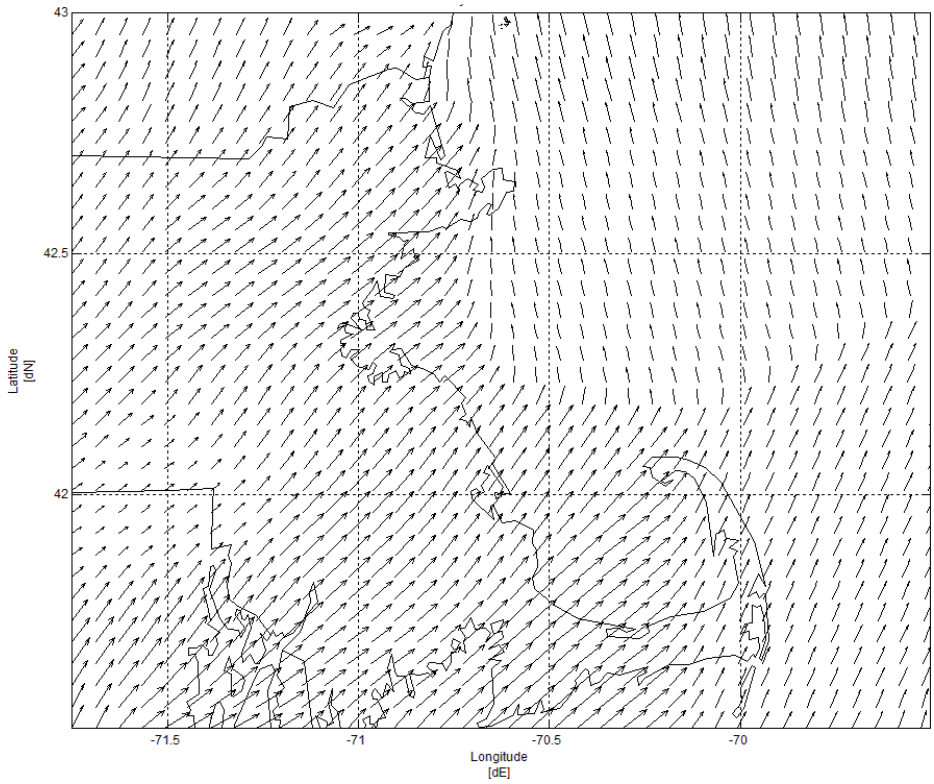

Figure 6.18: Wind vector plot for July 10, 2006 at 1900 UTC.

On September 9, 2006, a convective band of precipitation developed just west of Boston and intensified as it passed east of the city. The band begins development at 2306 UTC where three small cells can be seen at approximately 41.25°N -71.25°E (Fig. 6.19). The cells propagate east towards the coast (and Boston) becoming stronger and joining together (Fig. 6.20). Once the cells pass over Boston and out into the ocean (2334 UTC), they intensify to 45 dBZ (Fig. 6.21). The cells reach their maximum intensity (50 dBZ) and almost form a single cell at 2346 UTC (Fig. 6.22). At the 2357 UTC, the cells have begun to weaken (Fig. 6.23). The wind vector plots (Fig. 6.24 and 6.25) show some directional convergence as well as some weak speed convergence in this area which is causing the intensification of these cells. The large scale precipitation seen approaching the area in radar imagery is pre-frontal (Fig. 6.26).

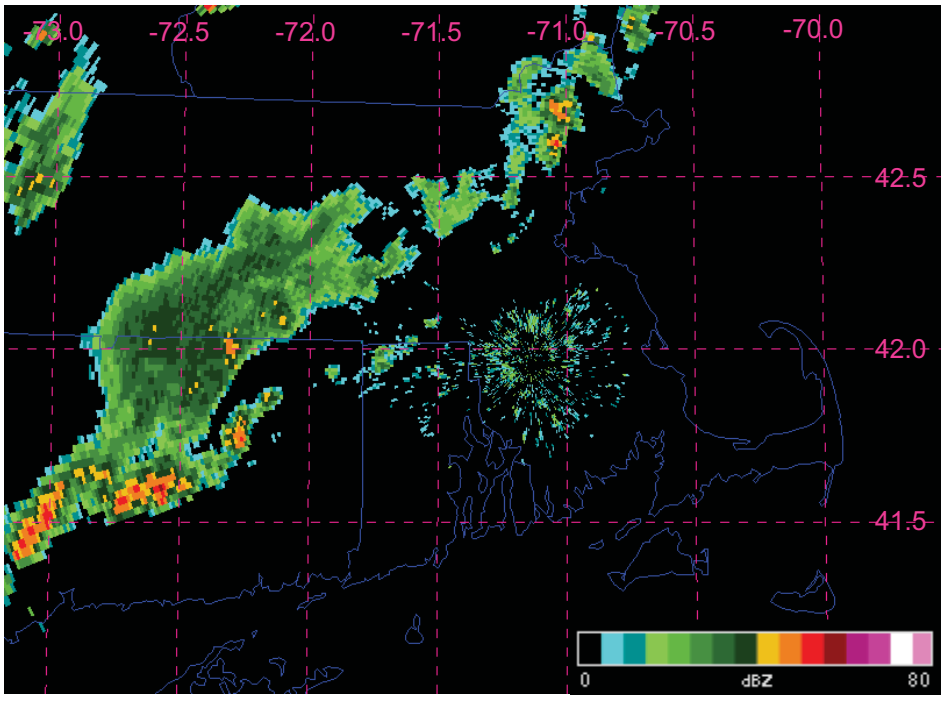

Figure 6.19: Base reflectivity at 2306 UTC from Taunton, MA (KBOX) radar on Sept. 9, 2006. Magenta dashed lines represent latitude and longitude (labeled in degrees N and E). The blue lines are state borders. Refer to legend at bottom-right for reflectivity values.

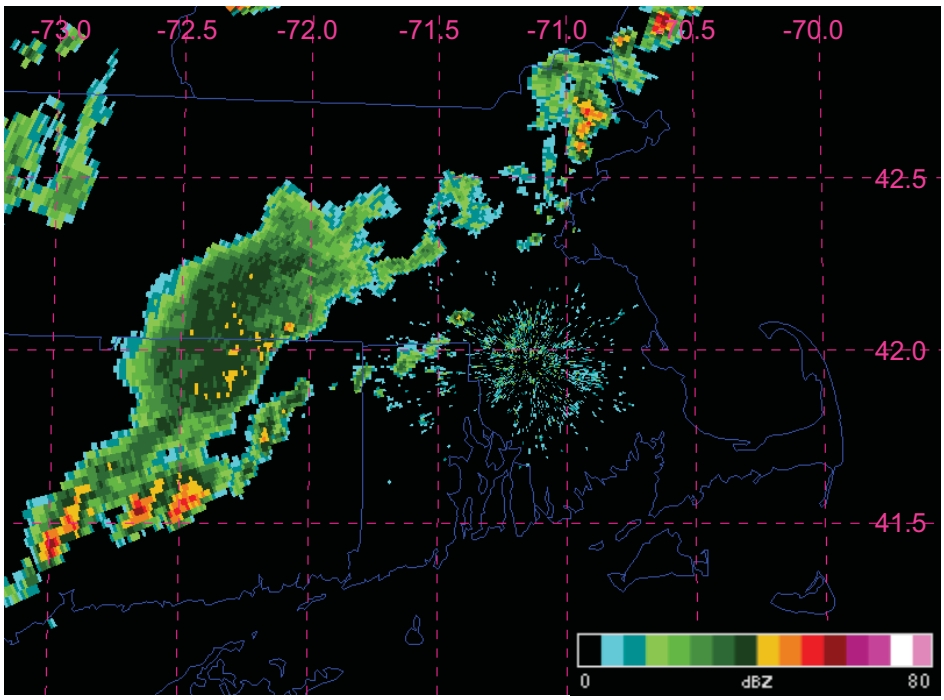

Figure 6.20: Same as Fig. 6.19 above except valid for 2317 UTC.

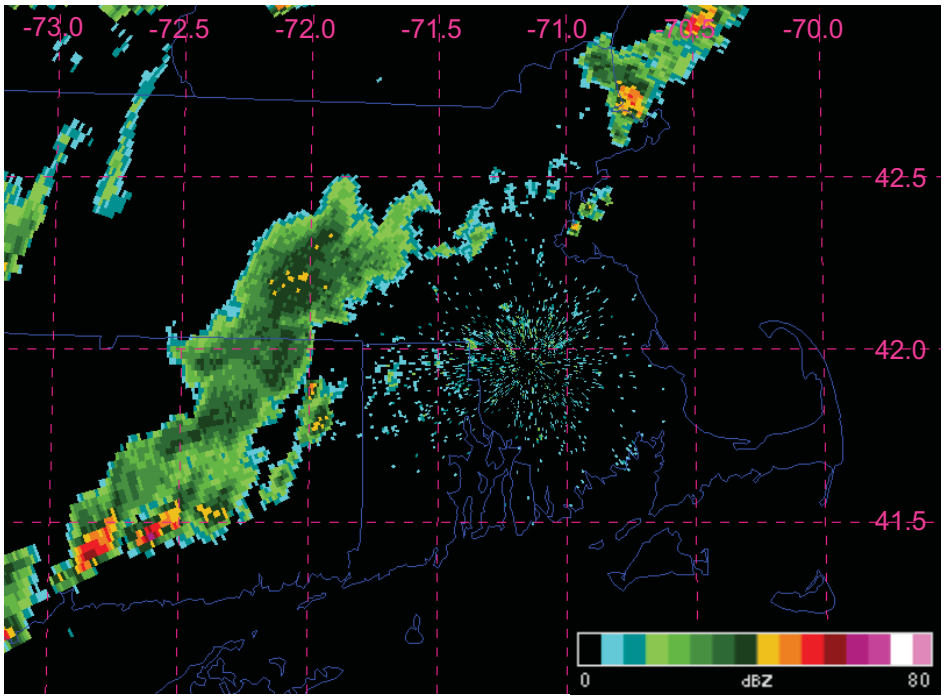

Figure 6.21: Same as Fig. 6.19 above except valid for 2334 UTC.

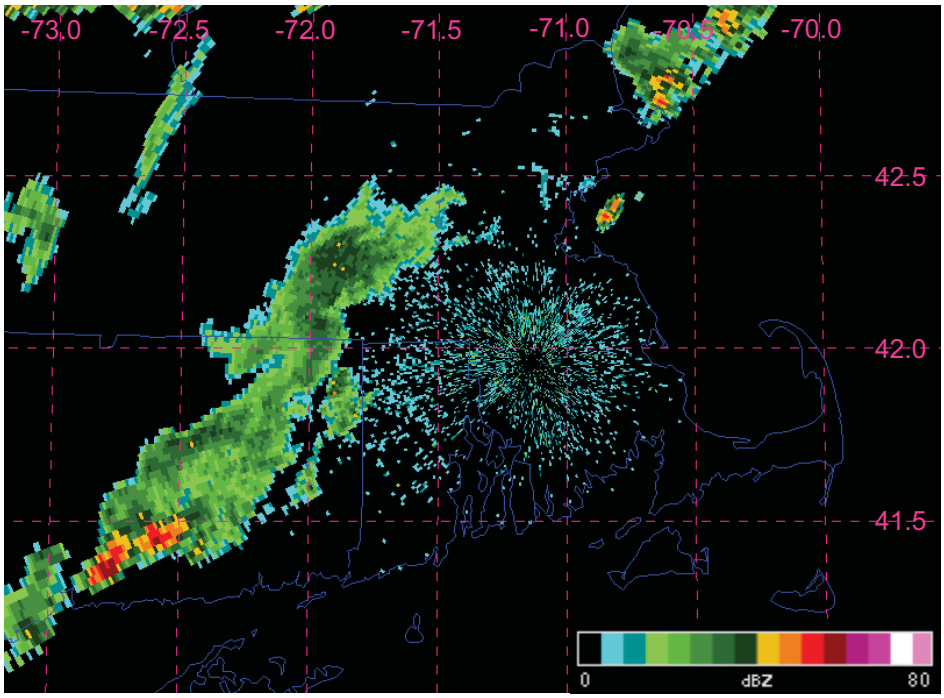

Figure 6.22: Same as Fig. 6.19 above except valid for 2346 UTC.

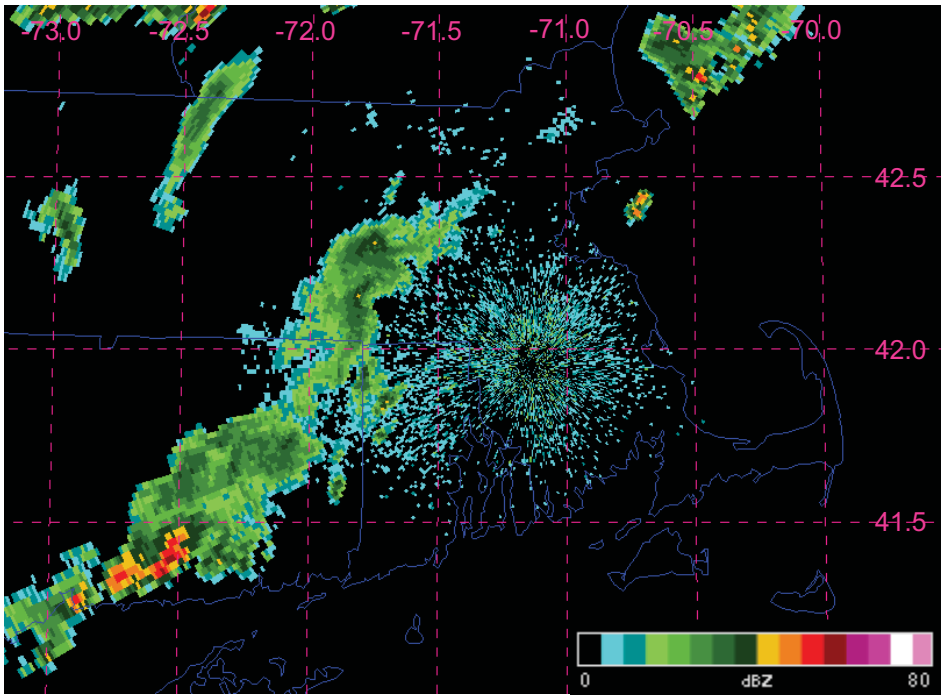

Figure 6.23: Same as Fig. 6.19 above except valid for 2357 UTC.

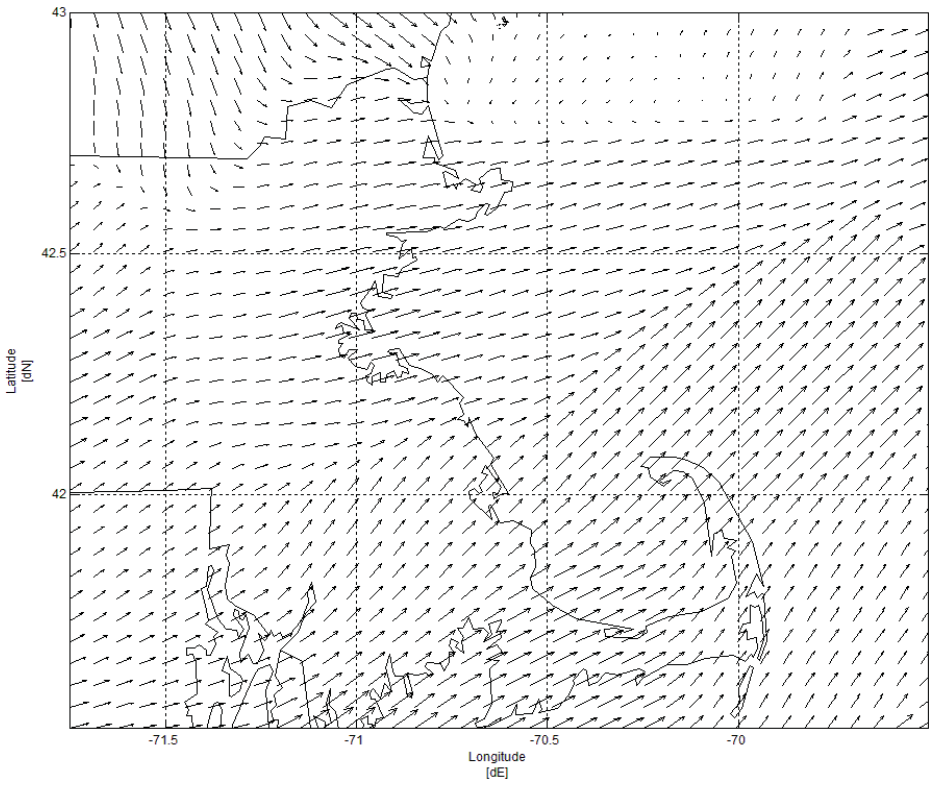

Figure 6.24: Wind vector plot for Sept. 9, 2006 at 2300 UTC.

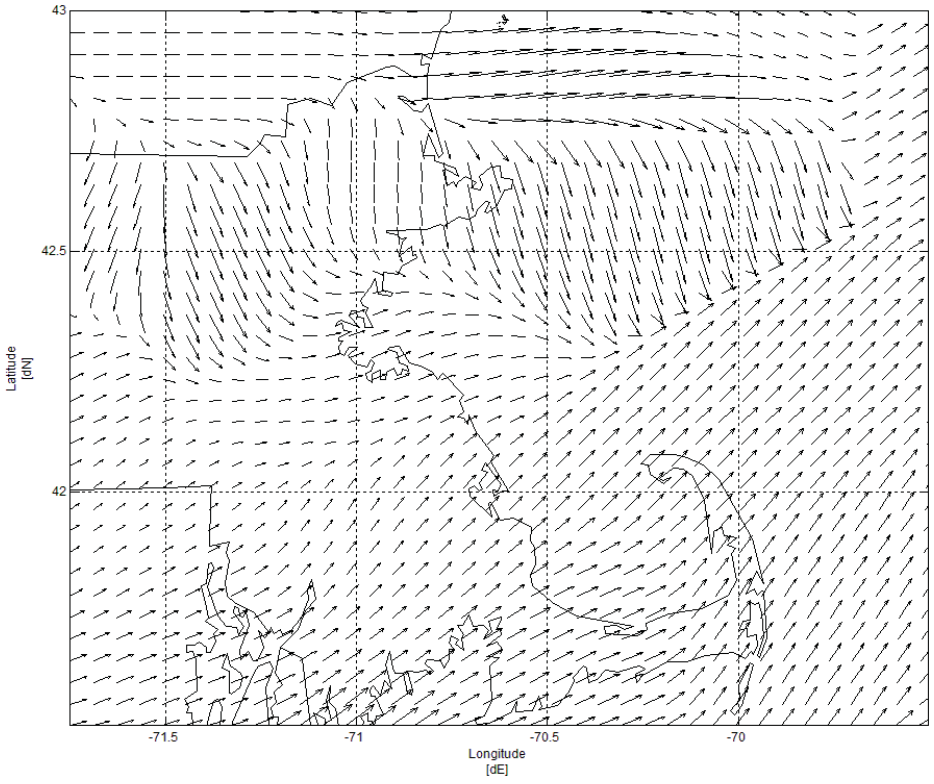

Figure 6.25: Wind vector plot for Sept. 10, 2006 at 0000 UTC.

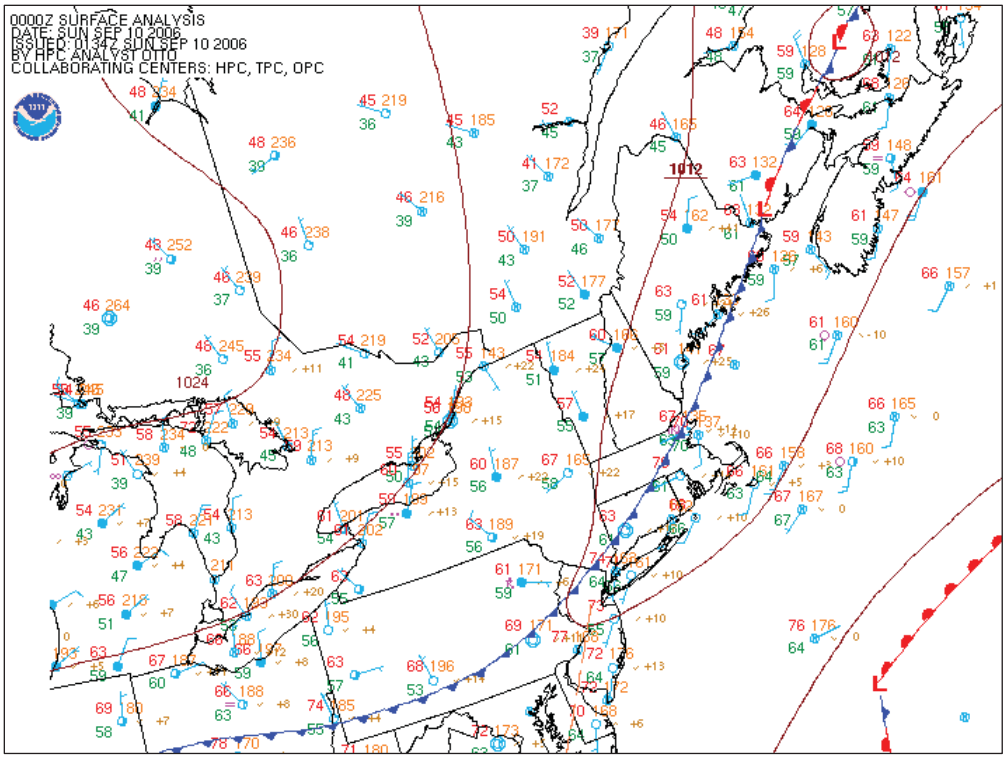

Figure 6.26: Surface analysis valid 0000 UTC Sept. 10, 2006. Obtained from NESDIS (2008).

Both events were non-sea breeze events and the sea breeze did not occur anywhere along the coast in these cases. July 10, 2006 was from synoptic class 4 and Sept. 9, 2006 was from synoptic class 7 (the miscellaneous class). The intensification of convection in September was due to convergence. Further research is needed to determine the cause of the convection in the July case.

c. No Sea Breeze, Convection Unchanged

On July 27, 2005, a line of pre-frontal precipitation passed through Massachusetts (and other New England states). At 2239 UTC, the line of storms has just begun to pass over the northern coast of Massachusetts (Fig. 6.27). The line contains many convective cells and is tracking northeast. By 2256 UTC, more of the storm has reached the coastline (Fig. 6.28). No intensification has occurred with these cells and at 2326 UTC more

convective storms have moved into the area (Fig. 6.29). By 2356 UTC, almost all of the convective precipitation has moved offshore and only stratiform precipitation remains (Fig. 6.30). Figures 6.31 and 6.32 show the absence of the SBF in the wind vectors.

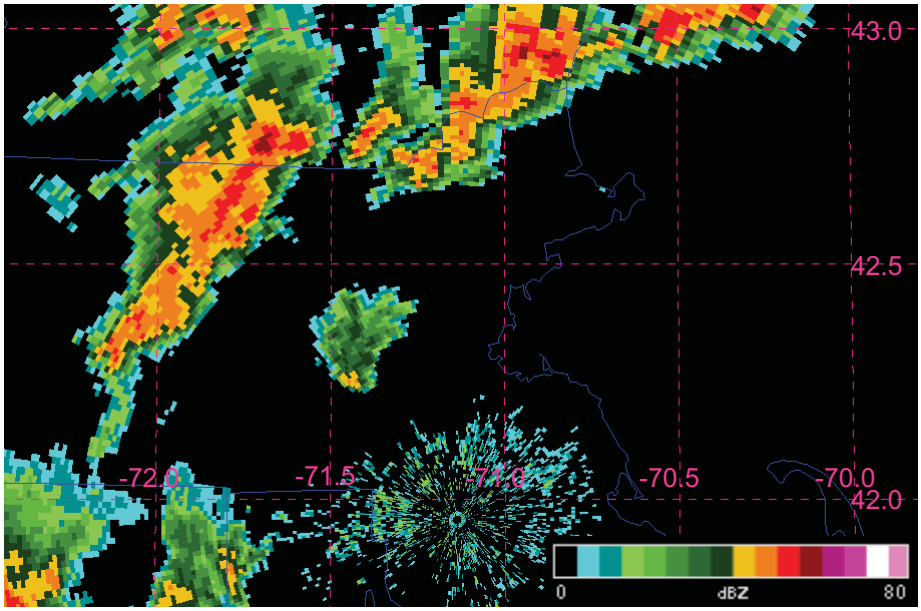

Figure 6.27: Base reflectivity at 2239 UTC from Taunton, MA (KBOX) radar on July 27, 2005. Magenta dashed lines represent latitude and longitude (labeled in degrees N and E). The blue lines are state borders. Refer to legend at bottom-right for reflectivity values.

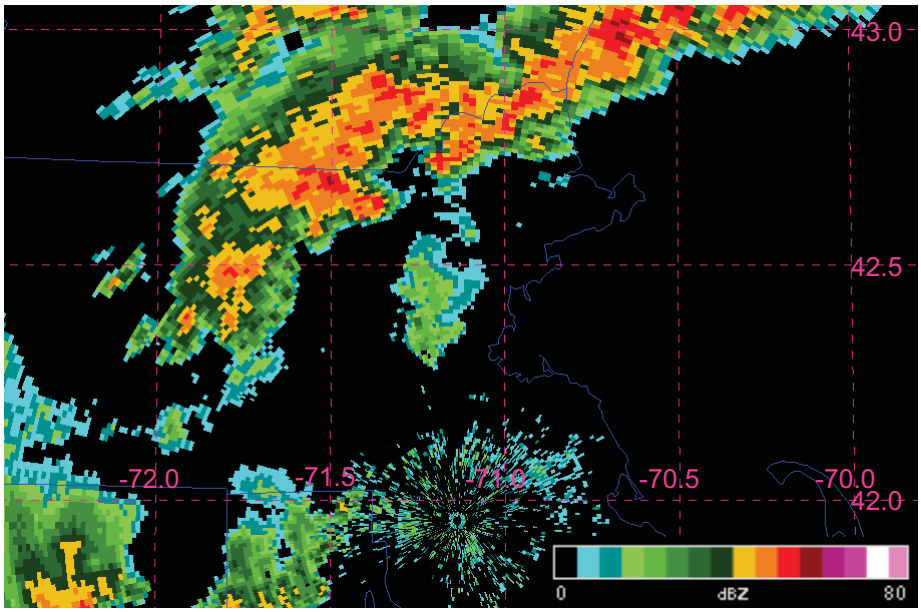

Figure 6.28: Same as Fig. 6.27 above except valid for 2256 UTC.

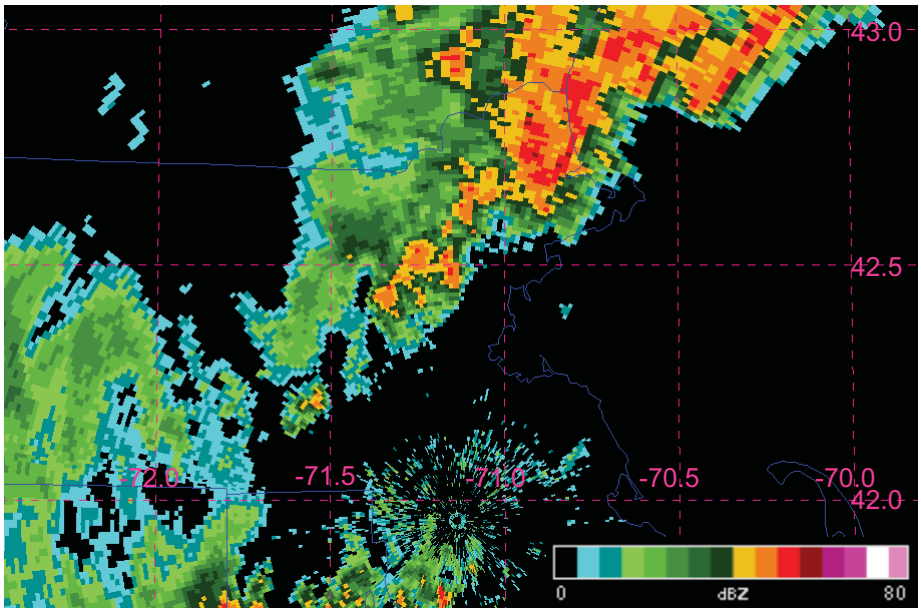

Figure 6.29: Same as Fig. 6.27 above except valid for 2326 UTC.

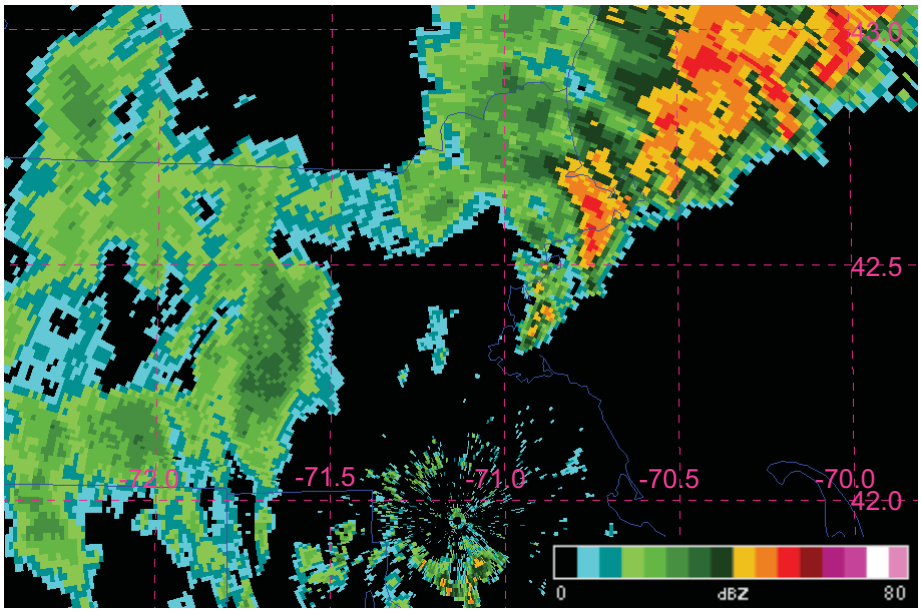

Figure 6.30: Same as Fig. 6.27 above except valid for 2356 UTC.

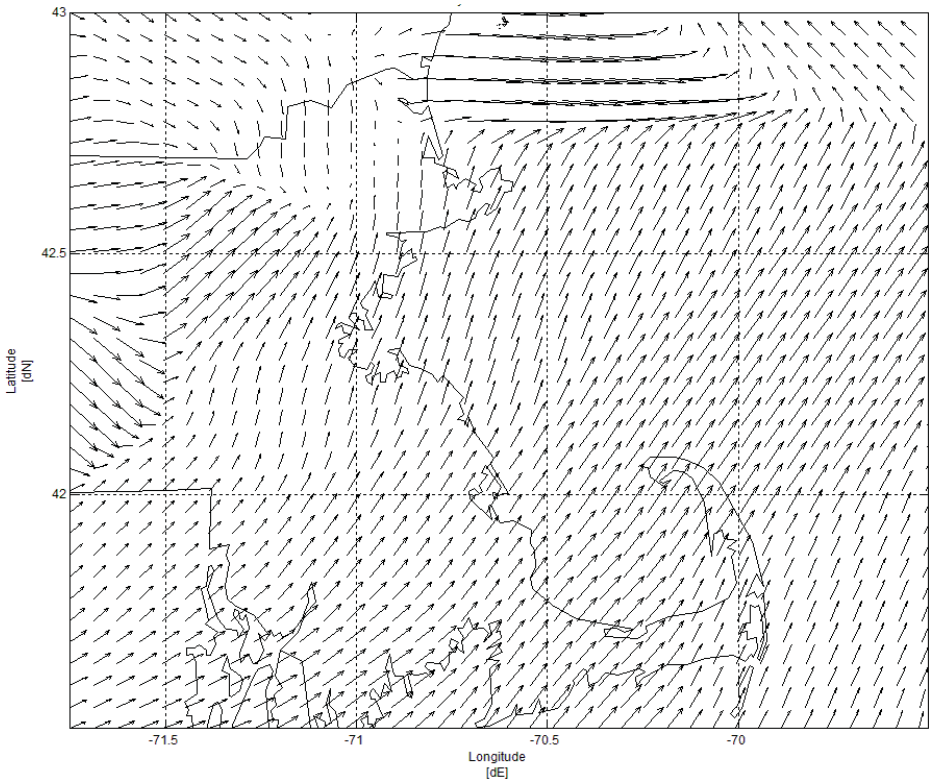

Figure 6.31: Wind vector plot for July 27, 2005 at 2300 UTC.

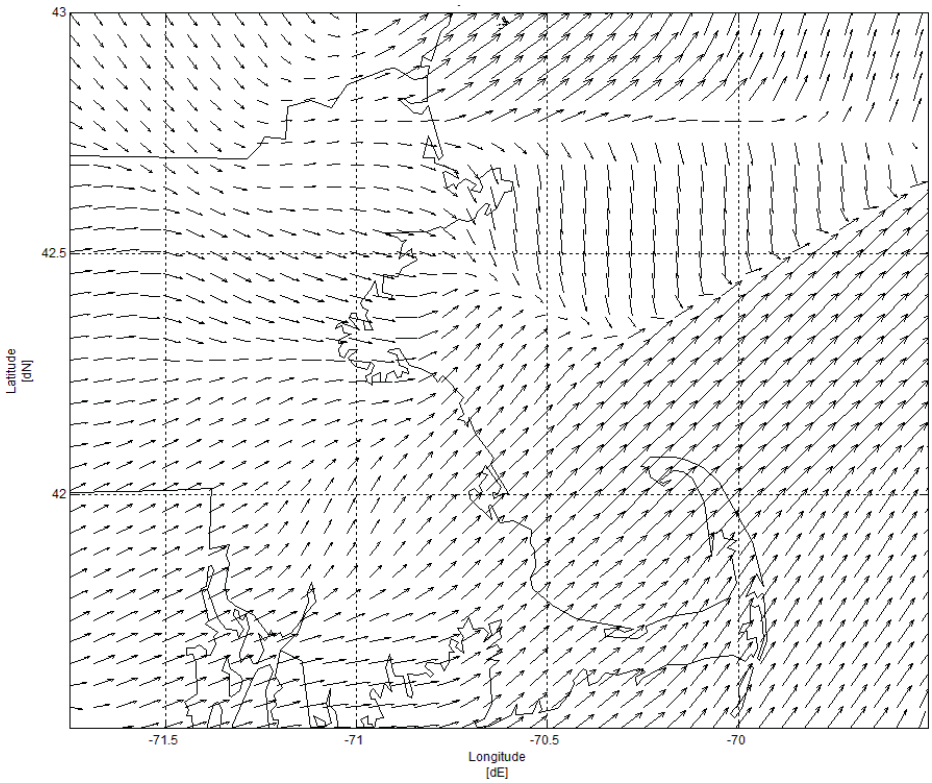

Figure 6.32: Wind vector plot for July 28, 2005 at 0000 UTC.

On August 2, 2006, a cluster of storms pushes its way through southern Massachusetts. At 2144 UTC, the storms can be seen along the southern border of Massachusetts (Fig. 6.33). These cells track southeasterly and by 2214 UTC, they have begun to enter northern Connecticut and Rhode Island (Fig. 6.34). The main cell cluster in Massachusetts passes directly over the radar (BOX) which distorts the reflectivity at 2231 UTC (Fig. 6.35). At 2243 UTC there is still no real intensification of convection (Fig. 6.36) and by 2334 UTC, the cells have begun to weaken (Fig. 6.37). The wind vector plots show no presence of a sea breeze at 2200 UTC or 2300 UTC (Fig. 6.38 and 6.39, respectively).

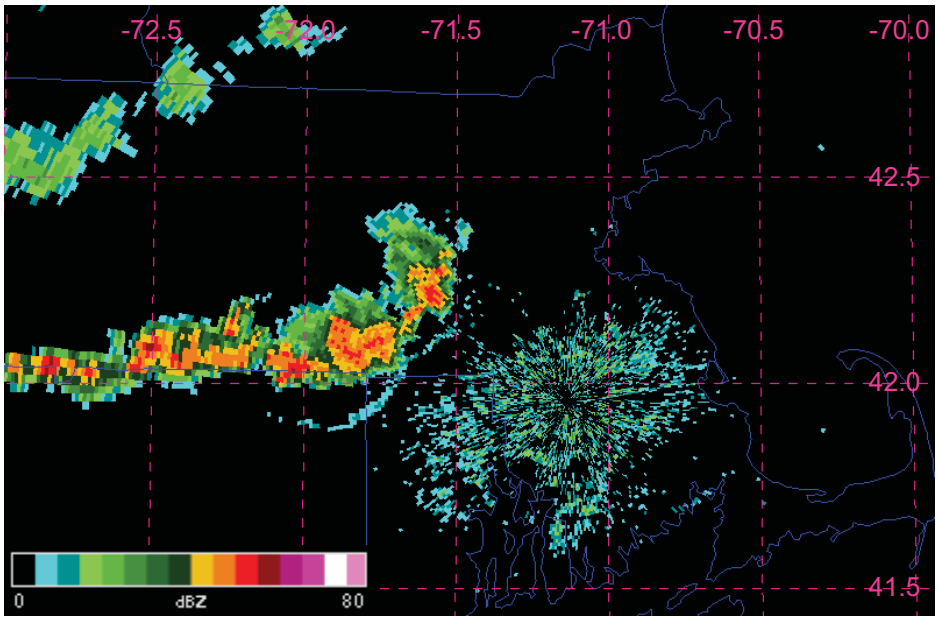

Figure 6.33: Base reflectivity at 2144 UTC from Taunton, MA (KBOX) radar on Aug. 2, 2006. Magenta dashed lines represent latitude and longitude (labeled in degrees N and E). The blue lines are state borders. Refer to legend at bottom-left for reflectivity values.

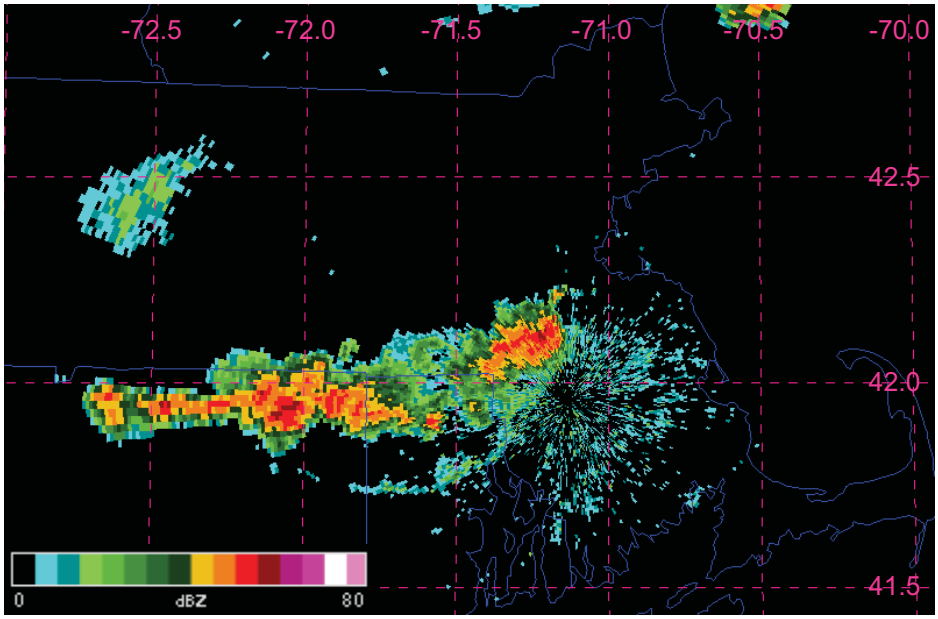

Figure 6.34: Same as Fig. 6.33 above except valid for 2214 UTC.

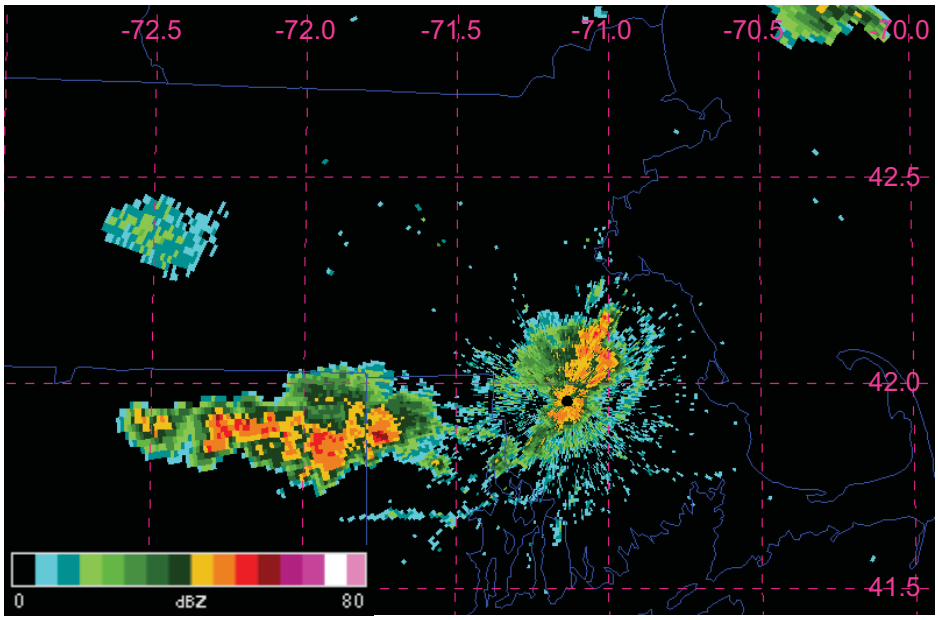

Figure 6.35: Same as Fig. 6.33 above except valid for 2231 UTC.

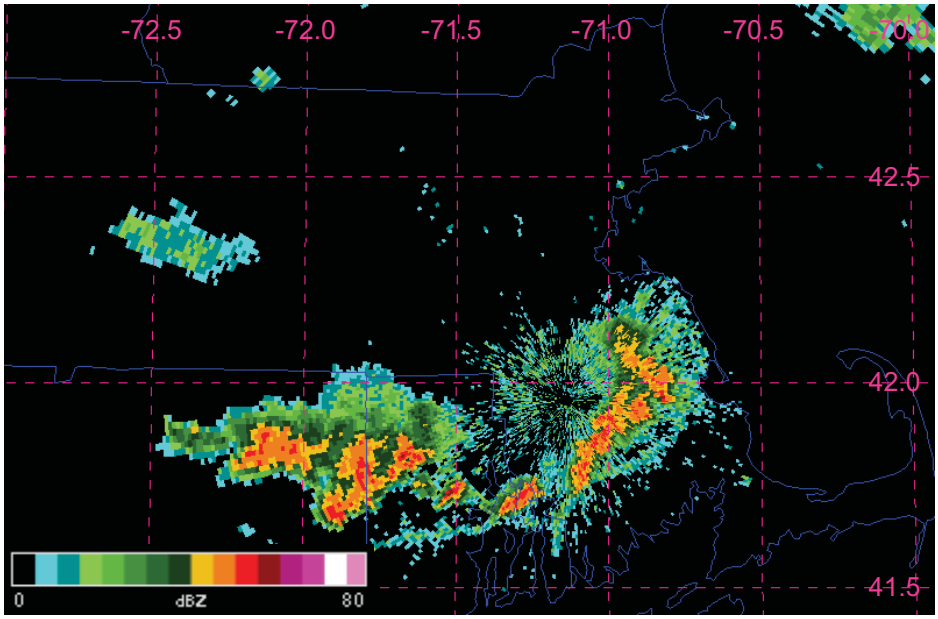

Figure 6.36: Same as Fig. 6.33 above except valid for 2243 UTC.

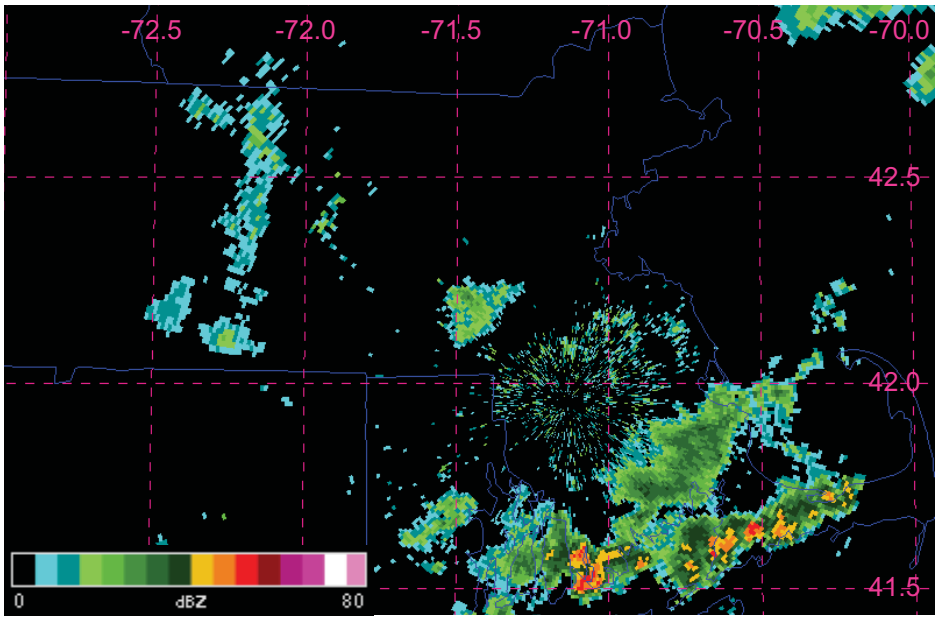

Figure 6.37: Same as Fig. 6.33 above except valid for 2334 UTC.

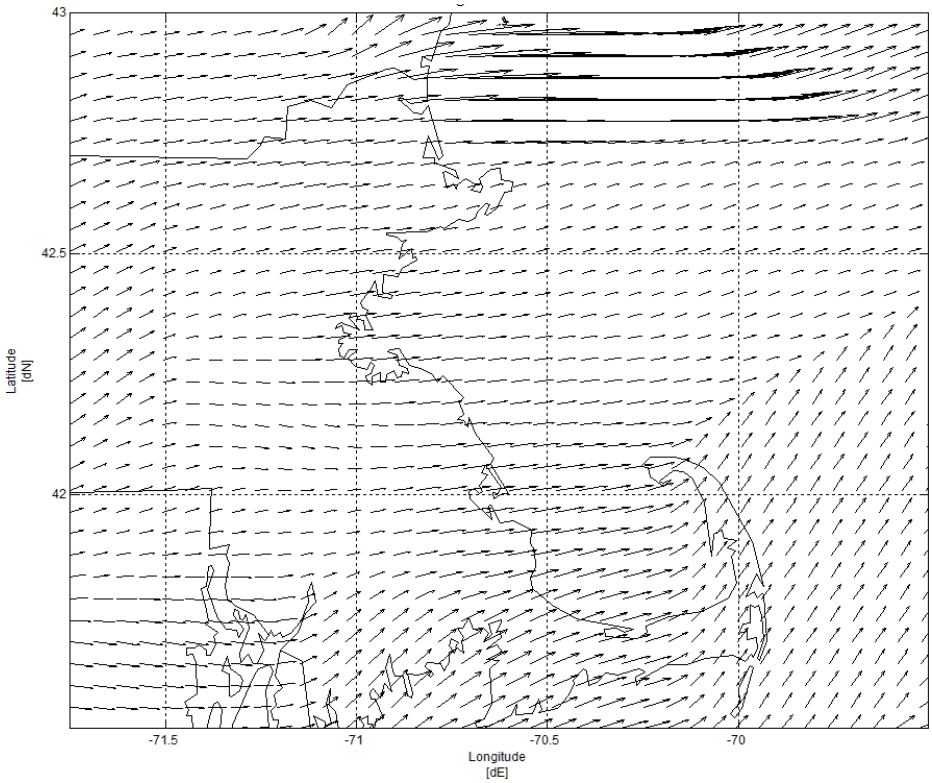

Figure 6.38: Wind vector plot for Aug. 2, 2006 at 2200 UTC.

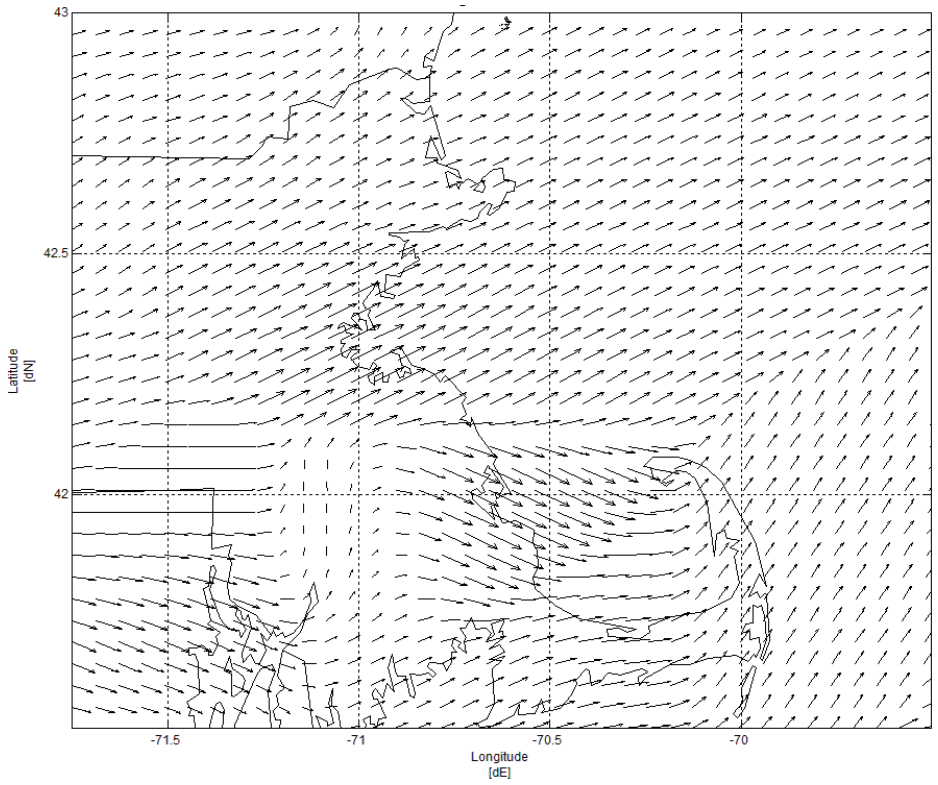

Figure 6.39: Same as Fig. 6.38 above except valid for 2300 UTC.

Both of these cases were non-sea breeze events. July 27, 2005 was identified as a synoptic class 5 event using the 1500 UTC surface analysis, which is characterized by post-frontal southwesterly flow (*See Appendix B*). By 2100 UTC, a secondary front has begun to move over Massachusetts causing pre-frontal precipitation in the area (Fig. 6.40). August 2, 2006 was classified as a synoptic class 7 and the precipitation was being caused by a trough passing through Massachusetts (Fig. 6.41).

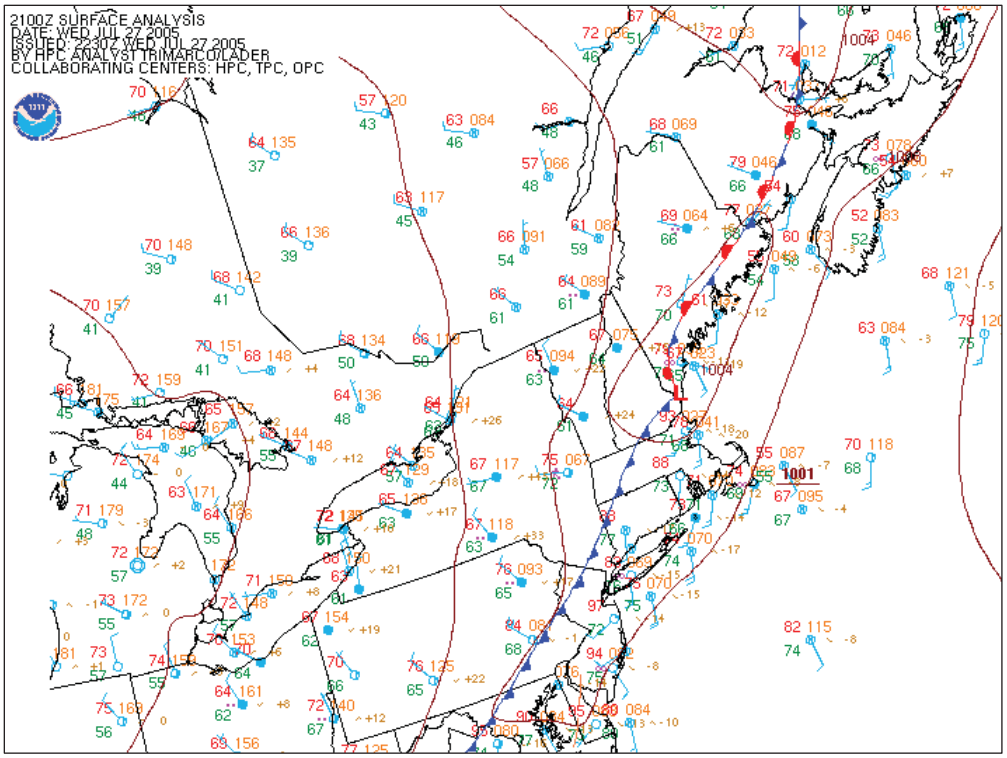

Figure 6.40: Surface analysis valid 2100 UTC July 27, 2005. Obtained from NESDIS (2008).

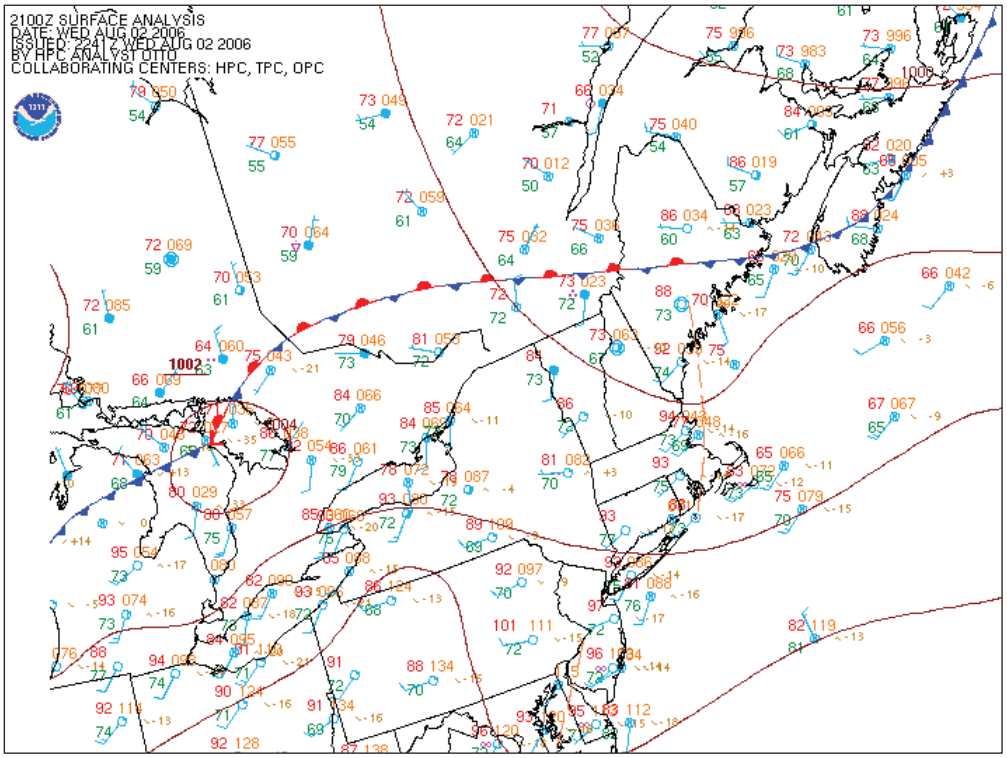

Figure 6.41: Surface analysis valid 2100 UTC Aug. 2, 2006. Obtained from NESDIS (2008).

Of a total of 562 events between 2002 and 2007, 24 events were selected for radar analysis. This analysis showed that the sea breeze was present for 14 of the 24 events. All of the 14 events showed an interaction between the sea breeze front and convection including some development. In the remaining 10 events the sea breeze was not present and convection developed or changed for 7 of these events; the other 3 events showed no changes in convection. The sample size of only 24 events is related to a bias created by the original methods used to define sea breeze events. The stipulations for cloud cover (no more than "broken" with a ceiling less than 18,000 ft) and precipitation (no precipitation within 6 hrs prior to or after the event) limited the number of thunderstorm days that could exist.

An important finding from this part of the study was that the sea breeze could occur at other locations along the coast even though in was a non-event day in Boston. More research is needed to determine what factors keep the sea breeze from penetrating into Boston on these non-event days.

CHAPTER 7

7. Summary & Conclusions

This study examined many different aspects of the Massachusetts sea breeze. A data set of events was created by determining if a sea breeze was possible and then categorizing the event as either a fast, slow, or marginal sea breeze event, or a non-sea breeze event. The data set was developed from nearly ten years (1998 to 2007) of METAR data from Logan Airport in Boston, Massachusetts (KBOS) and a total of 879 events were chosen. There were 171 fast sea breeze events, 60 slow sea breeze events, 78 marginal sea breeze events, and 570 non-sea breeze events.

The initial portion of study looked at basic characteristics such as time of onset and duration relative to Logan Airport in Boston, Massachusetts (KBOS). The data set was then classified using synoptic classes created by Miller and Keim (2003) and statistics were generated for these first three characteristics. The shape and depth of the inland penetration of the sea breeze air mass, relative to the entire Massachusetts coastline, was then analyzed as a function of synoptic class. Wind vector plots developed using surface observations and a Barnes analysis were used to create a mesoscale model of the sea breeze air mass and the sea breeze front was analyzed by windshift.

The mesoscale behavior of the sea breeze at KBOS was also investigated by using the cross-shore temperature gradient (dT/dx) and geostrophic wind component (u_G) at the surface. These two components were plotted to determine if there was a distinction between the balance of these two variables relative to sea breeze and non-sea breeze events. This was another method adapted from Miller and Keim (2003). A three

dimensional approach to this method was taken by incorporating a third variable, the 850 hPa geostrophic wind component, into the plot.

Lastly, the effect of the sea breeze on convection was examined using radar reflectivity data from the Taunton, Massachusetts radar (BOX). Events from 2002 to 2007 were studied using both the reflectivity data and wind vector plots to determine if a sea breeze was present during the event anywhere along the Massachusetts coastline and whether there was a change in convection.

a. Time of Onset and Event Duration

The time of onset showed variation not only by season, but by event type as well. The overall analysis of the time of onset stratified by event type revealed that slow sea breeze events begin the earliest and fast sea breeze events begin the latest. Marginal sea breeze events develop during a time between the fast and slow events. Seasonal variation showed that this scenario is not always true and in winter, marginal events occur a bit later than fast events; moreover, in spring marginal events occur slightly earlier than slow events. Winter and spring had the least number of marginal events of all the seasons so the sample size may be affecting the results. Events occurring in summer and fall followed the same time of onset pattern seen in the overall analysis. In regards to the time of onset itself, the latest time of onset of any sea breeze event was seen in winter when more time is needed for sufficient daytime heating to develop for the sea breeze to initiate.

The shortest duration of sea breeze events occurred during winter. This is attributed to the daytime heating issue discussed above with the time of onset. The longest duration for fast events occurred during spring, while that of slow and marginal

events occurred during summer. Slow events exhibited the longest duration overall which is related to the gradual transition of the wind direction into a strong sea breeze direction between 110° and 130°.

Future research for these aspects of the sea breeze could include breaking down the time of onset and event duration by synoptic class. This may lead to sample size issues which could be addressed by lengthening the data set. Increasing the sample size may also help with refining the time of onset for marginal events in winter and spring. Also, some of the variables that initiate the sea breeze could be investigated to determine the cause of the longest event duration for fast events occurring in spring versus that of the slow and marginal events occurring in fall.

b. Synoptic Classes

Synoptic classes were used to examine the effect of large scale flow on the occurrence or non-occurrence of the sea breeze. The classes were originally created by Miller and Keim (2003) for use in research of the sea breeze at Portsmouth, New Hampshire. This study improved upon these classes by creating composite analyses based on the synoptic classes. This provided unique classes for each event type. The composite analyses were used to examine the strength of the pressure gradient force over the study area and how much resistance there was to the initiation of the sea breeze. Non-events had the strongest pressure gradient for all of the synoptic classes, which is expected as this would stop the sea breeze from penetrating inland.

Statistics were generated to determine any seasonal patterns that might exist for the events based on the synoptic scale patterns. Plots were created to show the seasonal variation of each event type with a synoptic class. Synoptic classes 1, 2, and 3,

anticyclonic, neutral, and cyclonic northwesterly flow, respectively, behaved as if they were along one single spectrum of class. The minima and maxima of seasonal occurrence were most exaggerated with class 1, becoming less pronounced with synoptic class 2. Synoptic class 3 showed very little seasonal variation in occurrence. Non-events mirrored fast events with synoptic class 4, showing a non-event maximum when fast events were at a minimum and vice versa. Slow and marginal events reacted in the same way. With synoptic class 6, each event type showed its peak occurrence in a different season with slow and marginal events peaking in both summer and fall. The sample size of synoptic class 6 events for summer is only 8 events and for fall the sample size is 20 events. The summer peaks is not statistically significant. In fall, 50% of the synoptic class 6 events are slow transition sea breezes. Non-events peaked in the winter, which is expected due to a lack of sufficient daytime heating. The fast events peaked in the spring when a strong temperature difference between the land and ocean develops because the ocean is still rather cool from the winter.

c. Inland Penetration

Wind vector plots were created using a Barnes analysis and surface observations. The sea breeze front was analyzed based on changes in wind direction at the leading edge of the marine air mass. The mid-event average positions of the sea breeze front for each synoptic class were compared. Results showed that penetration was limited by the opposing synoptic scale flow. Of the northwesterly flow classes (1, 2, and 3), synoptic class 1 showed the deepest inland penetration towards the opposing northwest flow, which is related to the weaker anticyclonic winds associated with the class. Synoptic classes 2 and 3 did not penetrate as far inland. Synoptic class 4, southwesterly flow,

showed very limited inland penetration along the coastline south of Boston. The plot for synoptic class 6 (northeasterly flow) showed comparable penetration all along the coastline.

Further research can be done with this portion of the study. Only a limited number of events were used to create these plots. Increasing the sample size might improve the results. Also, only fast events were used in this analysis. A comparison of the effect of event type on inland penetration may produce interesting results.

d. Mesoscale Calculations

Mesoscale calculations were used to distinguish between the occurrence of a sea breeze event versus a non-sea breeze event. The cross-shore temperature gradient (dT/dx) and surface geostrophic wind component (u_G) were calculated and then plotted. Lines were analyzed between sea breeze and non-sea breeze events to identify the critical limits between the event types. The plot was then broken down by synoptic class to determine if a smaller transition area (area containing both sea breeze and non-sea breeze events) could be created. Classes 1, 2, and 3 again reacted as though they were along a single spectrum of class as they did with the statistics in the synoptic scale analysis. This break down proved successful in reducing the transition area size. A three dimensional plot was also created using the 850 hPa u_G component. There was a large transition area as with the two dimensional plot.

The three dimensional plot could be broken down by synoptic class just as with the two dimensional plot which may help reduce the size of the transition area. Also, changing the level of the third variable from 850 hPa to 925 hPa may show better results as it may be slightly deeper into the sea breeze circulation. Doppler VAD wind profile

(VWP) data could be used for low level wind data instead of the RAOB data from KCHH. Unfortunately, archived data only goes back to March 2009, so a new data set would need to be developed in order to employ it.

e. Radar Analysis of Convection

A radar analysis was done to determine if the sea breeze front along the Massachusetts coastline affected or caused convection. Events between 2002 and 2007 were examined for the occurrence of convection along the coastline in an area favorable for the sea breeze front. Out of the 562 events (both sea breeze and non-sea breeze events), convection only entered the favorable region 4% of the time (24 events). Of the 24 events, 14 events had convection affected or caused by the sea breeze front. During the remaining 10 events, the sea breeze did not occur in the area of convection. A total of 7 of these 10 events showed intensification or development of convection.

The methodology used to develop the overall data set has strict stipulations against precipitation and cloud cover. It is likely that convection reaches the coastline with the presence of a sea breeze front more often than this study shows. In order to avoid this bias, a future study could determine thunderstorm days first and then examine METAR data to determine if a sea breeze wind shift occurred, ignoring cloud cover and precipitation in the observations.

Future research could expand the dataset used to the length of the full data set (1998 to 2007) to create a larger sample size. This part of the study has shown that even though the sea breeze may not be occurring in Boston, it still can be occurring in other locations along the coastline. More research is needed to determine why the sea breeze does not occur evenly along the coastline in the case of the non-events with sea breezes.

Overall this study has uncovered many interesting details regarding the sea breeze both in Boston and along the Massachusetts coastline. There is ample room for further research on many of the different aspects discussed.

APPENDIX A

Convective Analysis in Maine

An investigation into thunderstorm interaction along the sea breeze front for the northern New England Coast yields interesting results. Nine sea breeze events, six contaminated sea breeze events, and nine non-sea breeze events were used in this study. A contaminated event is an event where all the criteria for a sea breeze event are met except for the cloud cover and precipitation stipulations. METAR data from the region as well as WSR-88D level II reflectivity data from Gray, Maine (KGYX) were used. The results showed four sea breeze events where thunderstorms developed or were enhanced along the sea breeze front. There were two contaminated events where enhancement was present. One contaminated event showed convection being weakened by the marine airmass. The overall conclusion from this study was that enhancement, development, and weakening of thunderstorms does occur along the northern New England coast. Further investigation needs to be done to identify the controlling factor for development versus enhancement. (Thorp, 2008)

APPENDIX B

Miller and Keim, (2003): Synoptic Classes

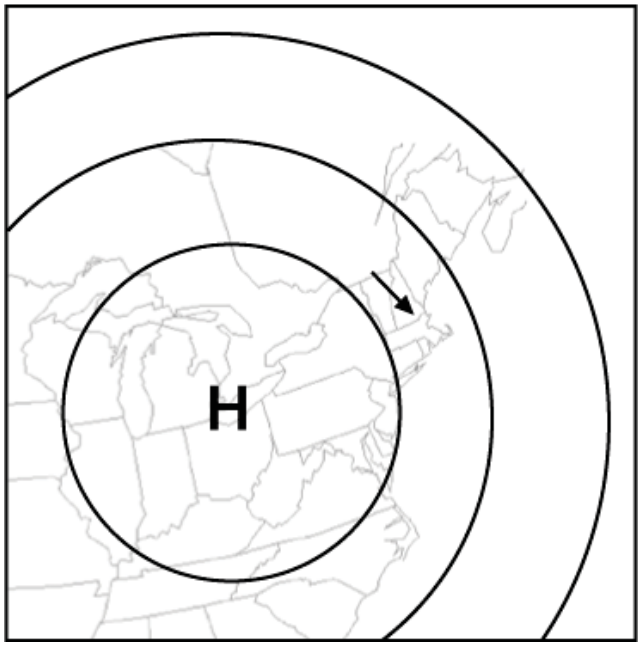

Figure A 1: Synoptic class 1, anticyclonic northwesterly boundary layer flow. Figure from Miller and Keim (2003).

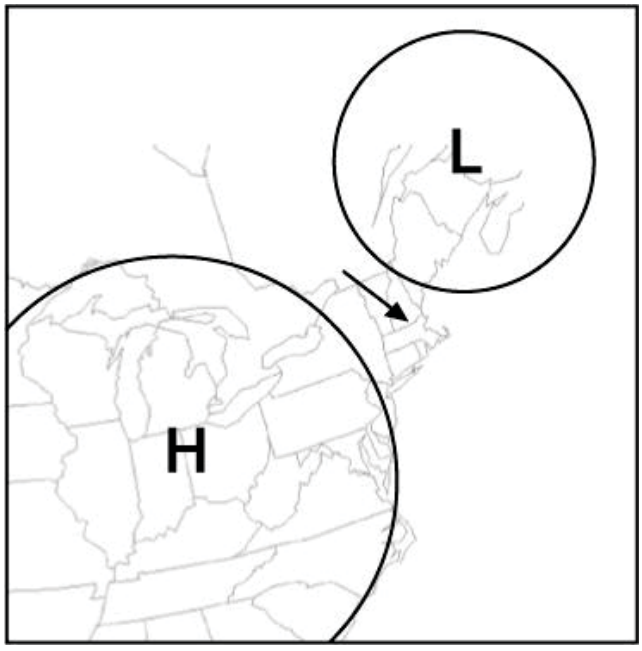

Figure A 2: Synoptic class 2, neutral northwesterly boundary layer flow. Figure from Miller and Keim (2003).

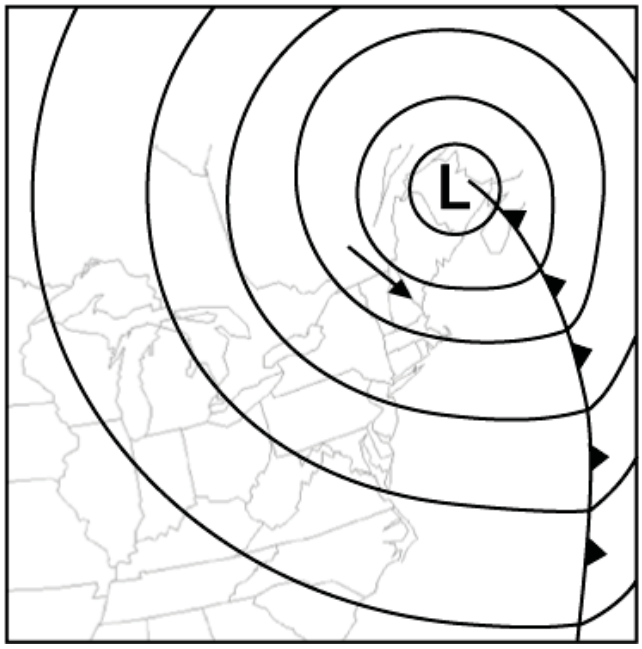

Figure A 3: Synoptic class 3, cyclonic northwesterly boundary layer flow. Figure from Miller and Keim (2003).

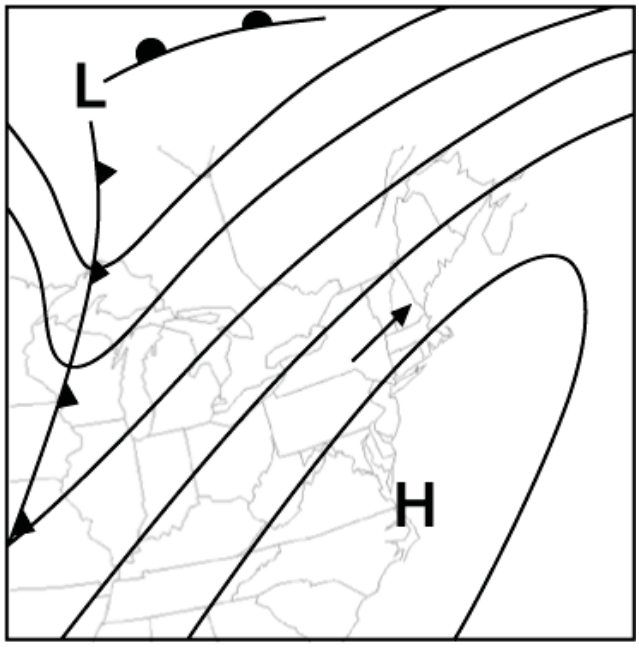

Figure A 4: Synoptic class 4, prefrontal southwesterly boundary layer flow. Figure from Miller and Keim (2003).

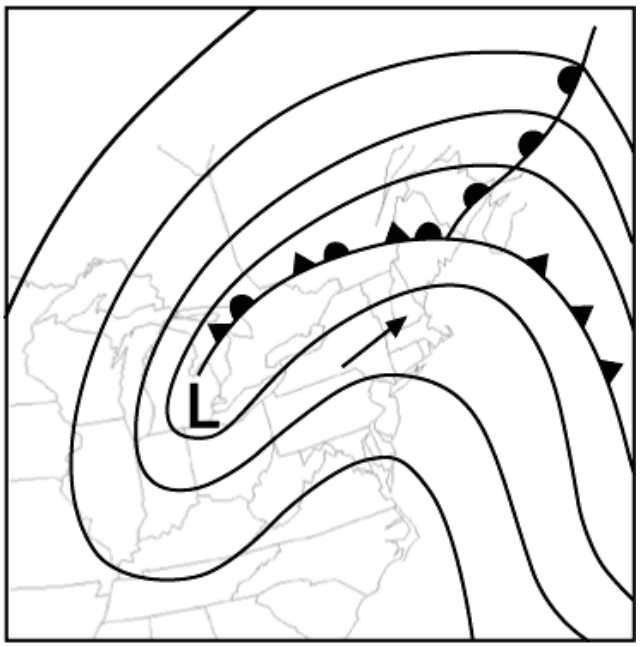

Figure A 5: Synoptic class 5, postfrontal southwesterly boundary layer flow. Figure from Miller and Keim (2003).

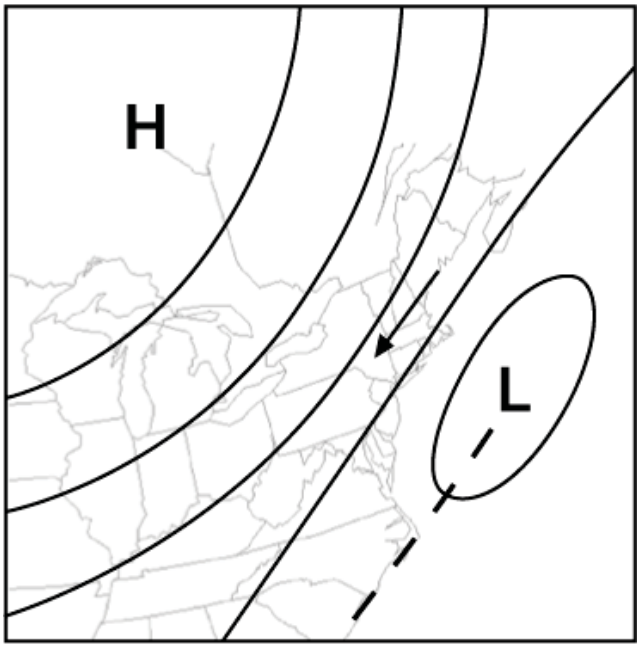

Figure A 6: Synoptic class 6, northeasterly boundary layer flow. Figure from Miller and Keim (2003).

Synoptic class 7 was reserved for boundary layer flow regimes that did not fall into classes 1 through 6.

APPENDIX C

Barnes Analysis (Barnes, 1964)

$$\widehat{wt}_n = \exp\left(-\frac{r^2}{a^2}\right)$$

$\widehat{wt}_n$ = unnormalized weight for observation point

r = distance (km) between observation and grid point

a = radius of influence (km). The radius of influence used for this study was 15 km.

$$wt_n = \sum_{i=0}^{n} \widehat{wt}_n$$

wt_n = normalized weight for observation point

$$x_{gridpoint} = \sum_{i=0}^{n} (x_n)(wt_n)$$

$x_{gridpoint}$ = interpolated value of gridpoint

x_n = observation value

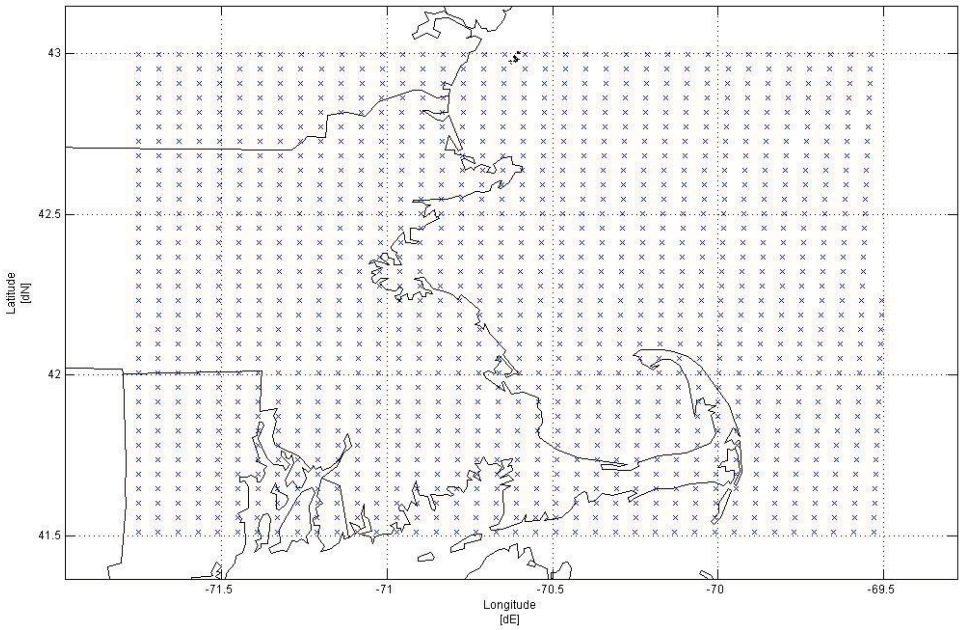

Figure B 1: Grid used for Barnes analysis.

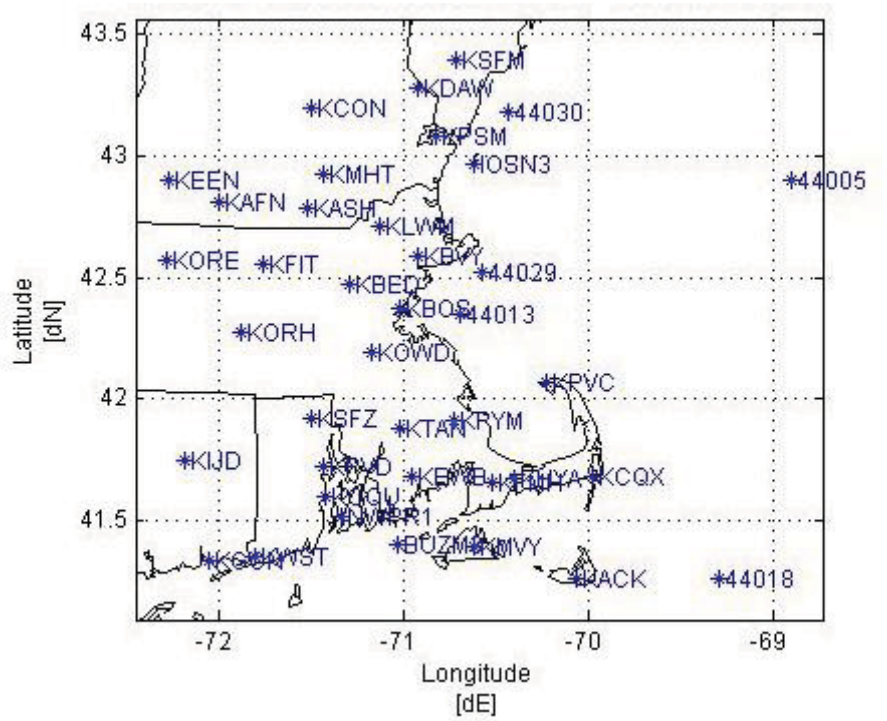

Figure B 2: Diagram of the weather stations used for Barnes analysis.

Table B 1: List of stations used in Barnes analysis.

Station Identity	Latitude (°N)	Longitude (°E)	Elevation (m above MSL)
KSFM	43.40	-70.72	74
KDAW	43.28	-70.92	100
44030	43.18	-70.43	0
KPSM	43.08	-70.82	31
KCON	43.20	-71.50	103
IOSN3	42.97	-70.62	0
KMHT	42.93	-71.44	81
KEEN	42.90	-72.27	149
KAFN	42.81	-72.00	313
KASH	42.78	-71.52	61
KLWM	42.71	-71.13	45
KBVY	42.58	-70.92	33
44029	42.52	-70.57	0
KORE	42.57	-72.28	169
KFIT	42.55	-71.76	106
KBED	42.47	-71.29	40
KBOS	42.37	-71.02	6
44013	42.35	-70.69	0
KORH	42.27	-71.87	307
KOWD	42.19	-71.17	15
KPYM	41.91	-70.73	45
KPVC	42.07	-70.22	2
KSFZ	41.92	-71.50	134
KIJD	41.74	-72.18	75
KPVD	41.72	-71.43	16
KOQU	41.60	-71.42	6
NWPR1	41.51	-71.33	4.5
KTAN	41.88	-71.02	13
KEWB	41.68	-70.96	24
KHYA	41.67	-70.40	15
KFMH	41.65	-70.52	40
KCQX	41.68	-69.98	20
KMVY	41.39	-70.62	20
KACK	41.25	-70.06	14
KWST	41.35	-71.80	24
KGON	41.33	-72.05	6
44018	41.26	-69.29	0
BUZM3	41.40	-71.03	0
44005	42.90	-68.90	0

APPENDIX D

Equations used in Mesoscale Calculations

Miller and Keim (2003) used cross shore components to examine the relationship between the forcing mechanism of the sea breeze and the flow resisting the inland penetration of the sea breeze. The cross shore potential temperature gradient represents the forcing mechanism that begins the sea breeze event and the cross shore surface geostrophic wind component represents the resistance to the inland penetration of the sea breeze. There was a lot missing pressure data for buoy 44013, so the cross shore temperature gradient was used instead the cross shore potential temperature gradient. The following equations were used in the mesoscale calculations.

Surface u_G equation

$$u_G = -\frac{1}{f\rho}\frac{dP}{dy} \quad \text{(C1)}$$

$$\frac{dP}{dy} = \frac{(P_{KLWM} - P_{KTAN})}{dy} \quad \text{(C2)}$$

u_G = surface geostrophic wind u-component (m s^{-1})

f = coriolis force (s^{-1})

ρ = density of air (approx. 1.25 kg m^{-3})

P_{KLWM} = Sea level pressure (Pa) at Lawrence, MA (KLWM)

P_{KTAN} = Sea level pressure (Pa) at Taunton, MA (KTAN)

dy = distance (m) between KLWM and KTAN

Surface dT/dx equation

$$\frac{dT}{dx} = \frac{(T_{44013} - T_{KORH})}{dx} \quad \text{(C3)}$$

T_{44013} = Temperature (°C) at buoy 44013

T_{KORH} = Temperature (°C) at Worcester, MA (KORH)

dx = distance (m) between 44013 and KORH

850 hPa u-component equation

$$u_{onset} = \left[\frac{(u_{00} - u_{12})}{12} \times t_{onset}\right] + u_{12} \quad \text{(C4)}$$

u_{onset} = 850 hPa interpolated wind u-component (m s^{-1}) for time of onset

u_{00} = 850 hPa wind u-component (m s^{-1}) at 00 UTC

u_{12} = 850 hPa wind u-component (m s^{-1}) at 12 UTC

t_{onset} = time of onset (UTC) of event

APPENDIX E

Miller and Keim, (2003): Mesoscale Calculations

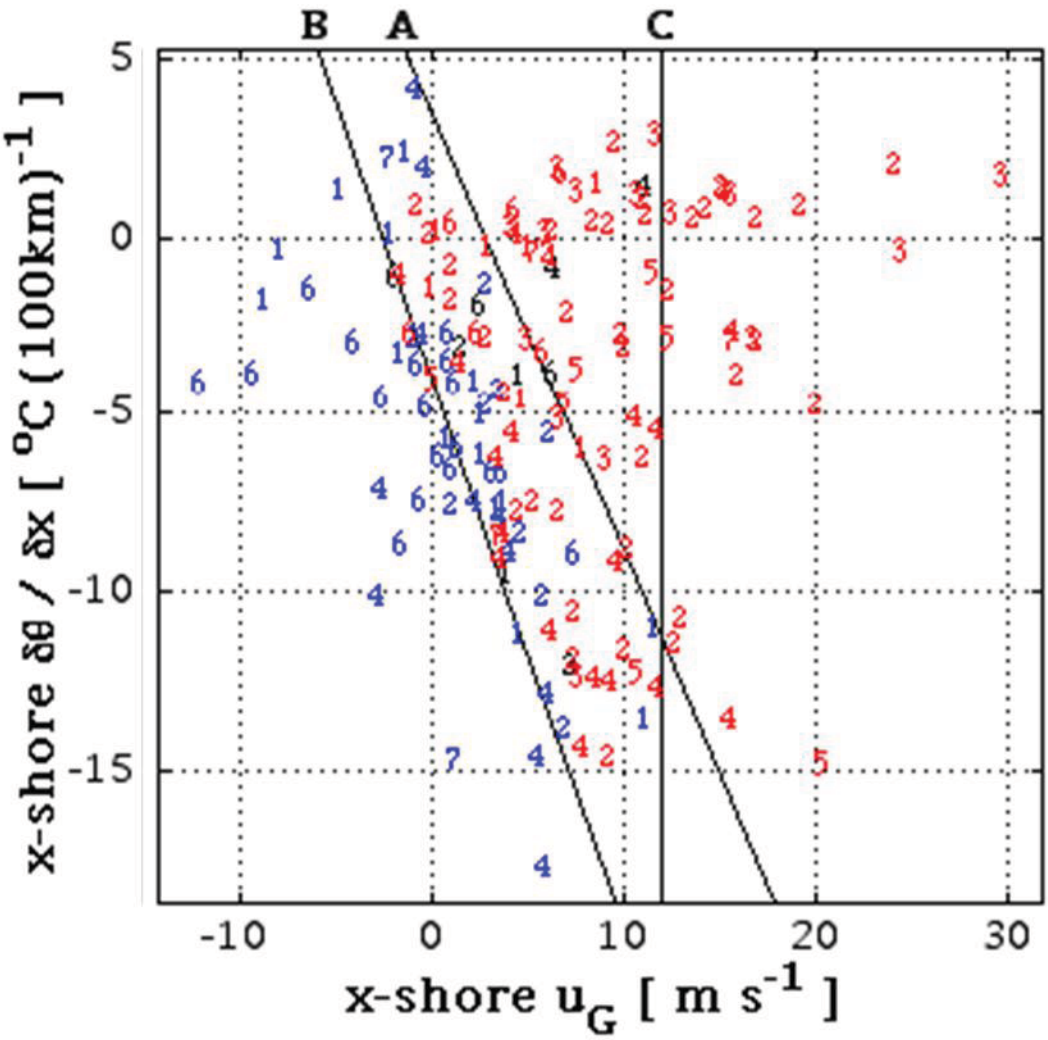

Figure D 1: All sea-breeze, marginal, and non-sea breeze events as a function of their associated cross-shore regional-scale temperature gradients and geostrophic wind components. The numbers represent the synoptic class of the event. Sea breezes are blue (●), marginal sea breezes are black (●), and non-sea breezes are red (●). Figure from Miller and Keim (2003).

REFERENCES

Barbato, J.P., 1978: Areal Parameters of the Sea Breeze and Its Vertical Structure in the Boston Basin. *Bull. Amer. Meteor. Soc.*, **59**, 1420–1431

Barnes, S.L., 1964: A Technique for Maximizing Details in Numerical Weather Map Analysis. *J. Appl. Meteor.*, **3**, 396–409.

Bedka, K. M., and J. M. Mecikalski, 2004: Nowcasting convective initiation and thunderstorm characteristics through the use of real-time geostationary satellite information. Preprints, *2004 EUMETSAT Met. Satellite Conf.,* Prague, Czech Republic, Czech Hydromet. Instit., P.41.

Colby, F.P., 2004: Simulation of the New England Sea Breeze: The Effect of Grid Spacing. *Wea. Forecasting*, **19**, 277–285.

ESRL PSD, 2008: 6-hourly NCEP/NCAR reanalysis data composites. Retrieved from http://www.cdc.noaa.gov/Composites/Hour/.

Estoque, M., 1961: A theoretical investigation of the sea breeze. *Quart. J. Roy. Meteor. Soc.*, **87**, 136-146.

Estoque, M., 1962: The sea breeze as a function of the prevailing synoptic situation. *J. Atmos. Sci.*, **19**, 244–250.

McPherson, R.D., 1970: A numerical study of the effect of a coastal irregularity on the sea breeze. *J. Appl. Meteor.*, **9**, 767–777.

Medlin, J.M., and P.J. Croft, 1998: A Preliminary Investigation and Diagnosis of Weak Shear Summertime Convective Initiation for Extreme Southwest Alabama. *Wea. Forecasting*, **13**, 717–728.

Miller, S.T.K., and B.D. Keim, 2003: Synoptic-Scale Controls on the Sea Breeze of the Central New England Coast. *Wea. Forecasting*, **18**, 236–248.

Miller, S.T.K., B.D. Keim, R.W. Talbot, and H. Mao, 2003: Sea breeze: Structure, forecasting, and impacts, Rev. Geophys., **41(3)**, 1011, doi:10.1029/2003RG000124.

NCDC, 2008: Radar data. Retrieved from http://www.ncdc.noaa.gov/oa/ncdc.html.

NESDIS, 2008: SRRS analysis and forecast charts. Retrieved from http://nomads.ncdc.noaa.gov/ncep/NCEP.

PSU Weather Center, 2008: METAR data. Retrieved from http://vortex.plymouth.edu.

Thorp, J., 2007: Improved sea breeze forecasting for Boston's General Edward Lawrence Logan International Airport. COMET Outreach Program. Retrieved from http://www.comet.ucar.edu/outreach/abstract_final/0658394_plymouth.pdf.

Thorp, J., 2008: Interaction of Thunderstorms and the Sea Breeze Front along the Northern New England Coast.

Suresh, R., 2007: Observation of Sea Breeze Front and its Induced Convection over Chennai in Southern Peninsular India Using Doppler Weather Radar. *Pure Appl. Geophys,* **164**, 1511-1525.